

SILVER NITRATE-DI(DD (ETHYLENE OXIDE) SURFACTANT  
... MESOPOROUS NANOCOMPOSITE FILMS AND MONOLITHS

A THESIS

SUBMITTED TO THE DEPARTMENT OF CHEMISTRY  
AND THE INSTITUTE OF ENGINEERING AND SCIENCES  
OF BILKENT UNIVERSITY

IN PARTIAL FULFILLMENT OF THE REQUIREMENTS  
FOR THE DEGREE OF  
MASTER IN SCIENCE

BY

OL'GA SAMARSKAYA

SEPTEMBER 2000

90  
137  
55  
526  
2000

SILVER NITRATE-OLIGO(ETHYLENE OXIDE) SURFACTANT  
MESOPOROUS NANOCOMPOSITE FILMS AND MONOLITHS

A THESIS

SUBMITTED TO THE DEPARTMENT OF CHEMISTRY  
AND THE INSTITUTE OF ENGINEERING AND SCIENCES  
OF BILKENT UNIVERSITY

IN PARTIAL FULFILLMENT OF THE REQUIREMENTS  
FOR THE DEGREE OF  
MASTER IN SCIENCE

By

OL'GA SAMARSKAYA

September 2000

QD

137

-S5

S26

2000

8053299

I certify that I have read this thesis and that in my opinion it is fully adequate, in scope and in quality, as a thesis of the degree of Master of Science



Asst. Prof. Dr. Ömer Dağ

I certify that I have read this thesis and that in my opinion it is fully adequate, in scope and in quality, as a thesis of the degree of Master of Science



Prof. Dr. Hüseyin Işçi

I certify that I have read this thesis and that in my opinion it is fully adequate, in scope and in quality, as a thesis of the degree of Master of Science



Asst. Prof. Dr. Serdar Özçelik

Approved for the Institute of Engineering and Sciences



Prof. Dr. Mehmet Baray

Director of Institute of Engineering and Science

## ABSTRACT

### SILVER NITRATE-OLIGO(ETHYLENE OXIDE) SURFACTANT MESOPOROUS NANOCOMPOSITE FILMS AND MONOLITHS

OL'GA SAMARSKAYA

M.S. in Chemistry

Supervisor: Asst. Prof. Dr. Ömer Dağ

September 2000

The purpose of this work is to improve and simplify the method of synthesis of metal functionalized mesoporous materials. This study has two particular goals. The first goal is to incorporate silver in its ionic form and to achieve its homogeneous distribution within the pores of meso-SiO<sub>2</sub>. The second goal is to establish the influence of concentration of silver present in the system on structure of the porous silica materials.

Silver nitrate salt dissolved in hexagonal mesophase of polyoxyethylene 10 lauryl ether (non-ionic PEO-type surfactant) was evenly distributed within silica framework which is tailored through liquid crystalline templating-sol-gel processing. In this approach, lyotropic liquid crystalline mixture containing silver ion and amphiphilic oligo(ethylene oxide) precursor organizes in hexagonal phase in the presence of nitric acid and water at room temperature. This preformed silver

containing LC mesophase is utilized as a template for subsequent condensation-polymerization reaction of  $\text{Si}(\text{OCH}_3)_4$  which results in formation of silicon oxide matrix as a direct cast of mesophase formed by the template.

The amount of silver nitrate homogeneously mixed in LC hexagonal phase of oligo-ethylene oxide/water system alters the mesophase. The template, lyotropic hexagonal mesophase made up by silver nitrate which is dissolved in PEO-type surfactant/water system in the certain concentration range, can be used to synthesize silver containing silica-based mesoporous materials.

It is determined that  $\text{C}_{12}\text{E}_{10}:\text{H}_2\text{O}(50 \text{ wt}\%):\text{HNO}_3$  system preserves its hexagonal LC phase in the presence of  $\text{Ag}^+$  ions up to 0.9 silver to surfactant molar ratios. Higher concentrations of  $\text{AgNO}_3$  in surfactant mesophase induce formation of white soft solid phase, which is assigned to the  $\text{Ag}^+/\text{surfactant}/\text{NO}_3^-$  complex. The template mixtures of 0.1-0.7  $\text{AgNO}_3$  to surfactant molar ratios yield silver containing 3D-hexagonal meso- $\text{SiO}_2$ . However, at higher  $\text{AgNO}_3$  concentration amorphous disordered materials form.

Homogeneously distributed  $\text{Ag}^+$  ions were successfully reduced to Ag nanoclusters on both internal and external surface of mesoporous silica materials by hydrazine in the gas phase.

Keywords: Mesoporous materials, lyotropic hexagonal mesophase, liquid crystalline templating-sol-gel processing, template, PEO-type surfactant, silver.

## ÖZET

### GÜMÜŞ NİTRAT-OLİGO(ETİLEN OKSİT) SÖRFEKTANT MEZOPORLU NANOKOMPOZİT FİMLER VE MONOLİTLER

OL'GA SAMARSKAYA

Kimya Bölümü Yüksek Lisans Tezi

Tez Yöneticisi: Asst. Prof. Dr. Ömer Dağ

Eylül 2000

Bu çalışmanın amacı, metal fonksiyonlu mezoporlu maddelerin sentez metodunu geliştirmek ve basitleştirmektir. Bu çalışmanın iki temel hedefi vardır. Birinci hedef, gümüşü iyonik halde ortama katmak ve daha sonra mezo-SiO<sub>2</sub> nin gözeneklerine homojen olarak dağılımını sağlamaktır. İkinci hedef, sistemde bulunan gümüşün derişiminin gözenekli silika maddelerin yapıları üzerindeki etkisini belirlemektir.

Polioksietilen 10 lauril eterin (iyonik olmayan PEO-tipi söfektant) altıgensel mezofazı içinde çözünmüş gümüş nitrat tuzu , sıvı kristal kalıplama-sol-jel işleme yöntemiyle oluşturulmuş silika yapısı içerisine homojen olarak dağıtıldı. Bu yaklaşımda, gümüş iyonu ve amfifilik oligo(etilen oksit) öncüsü içeren liyotropik sıvı kristal karışım, oda sıcaklığında nitrik asit ve su ortamında altıgensel faz şeklinde

organize olur. Öncelikle oluşturulmuş gümüş içeren LC mezofaz, daha sonraki  $\text{Si}(\text{OCH}_3)_4$  in yoğunlaşma-polimerleşme tepkimesi için bir kalıp olarak kullanılır ki bu tepkime kalıp tarafından oluşturulan mezofazın direkt dökümü olarak silikon oksit matrisin oluşumuyla sonuçlanır.

Oligo-etilen oksit/su sisteminin LC altıgensel fazında homojen olarak karıştırılmış gümüş nitratin miktarı mezofazı değiştirir. Kalıp, yani belirli derişim değerleri arasında bulunan PEO-tipi sörfektant/ su sisteminde, belirli derişim aralığında gümüş nitrat tarafından oluşturulan liyotropik altıgensel mezofaz, silika tabanlı mezogözenekli maddeler içeren gümüş sentezlenmesinde kullanılabilir.  $\text{C}_{12}\text{E}_{10}:\text{H}_2\text{O}:(50 \text{ wt}\%): \text{HNO}_3$  sisteminin altıgensel LC fazını  $\text{Ag}^+$  iyonları varlığında gümüş /sörfektant mol oranı 0.9 olana kadar koruduğu belirlenmiştir. Sörfektant mezofazdaki  $\text{AgNO}_3$  in daha yüksek derişimleri,  $\text{Ag}^+/\text{sörfektant}/\text{NO}_3^-$  kompleksi olduğu belirlenen beyaz, yumuşak, katı bir fazın oluşumuna sebep olur.  $\text{AgNO}_3/\text{sörfektant}$  mol oranları 0.1 ila 0.7 olan kalıp karışımlar, üç boyutlu-altıgensel mezo- $\text{SiO}_2$  içeren gümüş oluşturur. Ancak, daha yüksek  $\text{AgNO}_3$  derişimlerinde düzensiz amorf maddeler oluşur.

Homojen olarak dağıtılan  $\text{Ag}^+$  iyonları daha sonra basarılı bir şekilde, mezogözenekli silika malzemelemin hem iç hemde dış yüzeylerinde Ag nanoklastırlarına, gaz fazı hidrazin,  $\text{N}_2\text{H}_4$  molekülü kullanılarak indirgenmiştir.

Anahtar Kelimeler: Mezoporlu maddeler, liyotropik altıgensel mezofaz, sıvı kristal kalıplama-sol-jel işleme , kalıp, PEO-tipi sörfektant, gümüş.

## ACKNOWLEDGEMENTS

I would like to express my gratitude to Asst. Prof. Dr. Ömer Dağ for his supervision throughout my studies. I appreciate his patience and his giving me a chance to make the first small step in research.

I wish to thank Asst. Prof. Dr. Margarita Kantcheva, Asst. Prof. Dr. Ulrike Salzner and other members of Bilkent University Chemistry Department for their encouragement and help.

I am very thankful to Özgür Birir for all the help, kindness and support he has given me. I am grateful to my family for their inspiration and support.

I gratefully acknowledge the Scientific and Technical Research Council of Turkey (TUBITAK, project No TBAG1812) for funding this work.

## TABLE OF CONTENTS

<b>1. INTRODUCTION.....</b>	<b>1</b>
1.1. NANOWORLD .....	1
1.2. PURE SILICATE MESOPOROUS MATERIALS.....	3
1.2.1. Characterization and Structure Model.....	3
1.2.2. Nature of the MCM Internal Surface.....	5
1.3. SYNTHESIS OF SUPRAMOLECULAR-TEMPLATED MESOPOROUS MATERIALS.....	9
1.3.1. Surfactant Template.....	11
1.3.2. Tailoring of Surfactant/Inorganic Mesophase .....	15
1.3.3. Sol-Gel Processing .....	18
1.4. LC PHASE SYNTHESIS WITH PEO TYPE SURFACTANT.....	22
1.5. CHEMISTRY WITHIN HOST MESOPOROUS SILICATES .....	26
<b>2. EXPERIMENTAL. ....</b>	<b>32</b>
2.1. MATERIALS.....	32
2.2. SYNTHESIS.....	32
2.2.1. Preparation of LC Phases .....	32
2.2.2. Synthesis of Mesoporous Silica.....	33
2.2.3. Reduction of Ag <sup>+</sup> Ions in Mesoporous Silica .....	34
2.3. INSTRUMENTATION.....	35
2.3.1. FTIR Spectroscopy .....	35

2.3.2. Polarized Optical Microscopy .....	35
2.3.3. Powder X-ray Diffraction .....	36
2.3.4. UV-Vis Spectroscopy.....	36
<b>3. RESULTS AND DISCUSSION .....</b>	<b>37</b>
3.1. PHASE PROPERTIES OF AgNO <sub>3</sub> IN C <sub>12</sub> E <sub>10</sub> TYPE SURFACTANTS.....	38
3.1.1. Polarized Optical Microscopy Images.....	39
3.1.2. Mid-IR Spectral Studies .....	42
3.2. MESOPOROUS SILICA TEMPLATED BY AgNO <sub>3</sub> :C <sub>12</sub> E <sub>10</sub> :H <sub>2</sub> O.....	53
3.2.1. POM Images .....	56
3.2.2. PXRD Analysis .....	59
3.2.3. FTIR Spectroscopic Studies .....	66
3.2.4. UV-Vis Spectral Studies .....	72
<b>4. CONCLUSION.....</b>	<b>84</b>
<b>5. REFERENCES .....</b>	<b>87</b>

## LIST OF TABLES

1. PORE-SIZE REGIMES AND REPRESENTATIVE POROUS INORGANIC MATERIALS.....	1
2. MOLECULAR VIBRATION ASSIGNMENTS FOR THE OXYETHYLENE CHAIN OF PEG400, PEG400/(LiCl) <sub>x</sub> , PEO, Ag/PEO/NO <sub>3</sub> .....	50
3. CORRELATION BETWEEN CONTENT OF THE SYSTEM AND CORRESPONDING POM IMAGE AND IR SPECTRUM.....	52
4. PXRD DATA OF DIFFERENT PHASES OF MESOPOROUS MATERIALS.....	60
5. FT-IR ABSORPTION SPECTRA OF SILVER CONTAINING TEMPLATE.....	67
6. POSITIONS OF SPR ABSORPTION PEAK OF SILVER IN DIFFERENT REACTION MEDIUM.....	73

## LIST OF FIGURES

1. Illustration of M41S materials.....	4
2. Schematic representation of the three types of Si-OH groups of siliceous MCM-41 and their characteristics.....	6
3. Schematic representation of formation and dehydroxylation processes of SiOH groups in siliceous MCM-41.....	7
4. Representation of the silica network and polysilsesquioxane network.....	8
5. Schematic of the organic template approach to prepare nanoporous amorphous silica showing the incorporation and removal of the template.....	10
6. Phase sequence of surfactant-water binary system.....	12
7. Schematic of the liquid-crystal templating (LCT) mechanism via two possible pathways.....	15
8. Three structure types observed for silica-surfactant mesophases: (a) hexagonal; (b) cubic bicontinuous Ia3d; (c) lamellar.....	16
9. Phase diagram of the C <sub>12</sub> EO <sub>8</sub> /water system over the temperature range 0-100 °C.....	23
10. Grafting of monolayer of thiol functionalities in MCM pores. The coordination environment of absorbed mercury is shown.....	27
11. Schematic of fullerene inclusion and hydration at elevated temperature in the MCM channels.....	28

12. POM images between crossed polarizers of (A) fan texture, (B), (C) weakly anisotropic, (D) anisotropic phases.....	41
13. FT-IR absorption spectra of (a) pure $C_{12}E_{10}$ , (b) $C_{12}E_{10} \cdot H_2O(50 \text{ w/w}\%):HNO_3$ , (c) $0.1 \text{ AgNO}_3/C_{12}E_{10} \cdot H_2O(50 \text{ w/w}\%):HNO_3$ , (d) $0.5 \text{ AgNO}_3/ C_{12}E_{10} \cdot H_2O(50 \text{ w/w}\%):HNO_3$ , (e) $0.9 \text{ AgNO}_3/C_{12}E_{10} \cdot H_2O(50 \text{ w/w}\%):HNO_3$ .....	44
14. FT-IR absorption spectra for $AgNO_3/C_{12}E_{10} \cdot H_2O(50 \text{ w/w}\%):HNO_3$ - solid lines, $AgNO_3/C_{12}E_{10} \cdot H_2O:HNO_3$ - normal lines. The $Ag^+/C_{12}E_{10}$ molar ratios indicated along the spectra.....	45
15. FT-IR absorption spectra of aged $AgNO_3/C_{12}E_{10} \cdot H_2O(50 \text{ w/w}\%):HNO_3$ samples with different $Ag^+/C_{12}E_{10}$ molar ratios (a) $r = 0.9$ (gel), (b) $r = 0.9$ (film on the gel/air interface), (c) $r = 1.5$ (white precipitate), (d) $r = 1.5$ (gel), (e) $r = 2.0$ (white solid).....	46
16. FT-IR spectra recorded for $AgNO_3/C_{12}E_{10} \cdot H_2O:HNO_3$ ( $r = 0.9$ ) composite (a)-(d) upon water evaporation and (e)-(f) after aging in the frequency range $2000-500 \text{ cm}^{-1}$ .....	48
17. FT-IR absorption spectra of (a) pure $C_{12}E_{10}$ , (b) $r = 0.5 \text{ AgNO}_3/ C_{12}E_{10} \cdot H_2O(50 \text{ w/w}\%):HNO_3$ , (c) $r = 1.5$ precipitate, (d) $r = 1.5 \text{ AgNO}_3/ C_{12}E_{10} \cdot H_2O(50 \text{ w/w}\%):HNO_3$ gel, (e) $r = 2.0 \text{ AgNO}_3/ C_{12}E_{10} \cdot H_2O(50 \text{ w/w}\%):HNO_3$ .....	51
18. POM image of $AgNO_3/C_{12}E_{10} \cdot H_2O:HNO_3/TMOS$ fan-like texture.....	56
19. POM images between crossed polarizers of $AgNO_3/C_{12}E_{10} \cdot H_2O:HNO_3/TMOS$ with (A) 0.5, (B) 0.6, (C) 0.7, (D) 0.8 $Ag^+/C_{12}E_{10}$ molar ratios.....	57
20. Low-angle PXRD patterns for silver-surfactant-silica mesophases. $Ag^+/C_{12}E_{10}$ molar ratios are indicated along the spectra.....	61

21. Mid FT-IR absorption spectra of $\text{AgNO}_3/\text{C}_{12}\text{E}_{10}:\text{H}_2\text{O}:\text{HNO}_3/\text{TMOS}$ thin films. The $\text{Ag}^+/\text{C}_{12}\text{E}_{10}$ molar ratios are indicated along the spectra.....	64
22. FT-IR absorption spectra of thin films (A) 24 hours after preparation, (B) one month after preparation. In the frequency range $1600\text{-}1200\text{ cm}^{-1}$ .....	65
23. FT-IR spectra of $\text{AgNO}_3/\text{C}_{12}\text{E}_{10}:\text{H}_2\text{O}:\text{HNO}_3/\text{TMOS}$ at $r = 0.6$ (a) aged for 3 days, (b) aged for 24 hours, (c) pressed in KBr after 3 days aging; in the frequency range $1800\text{-}1200\text{ cm}^{-1}$ .....	70
24. POM image for $\text{KNO}_3/\text{C}_{12}\text{E}_{10}:\text{H}_2\text{O}:\text{HNO}_3/\text{TMOS}$ of 0.6 $\text{KNO}_3$ to surfactant molar ratio between crossed polars.....	71
25. UV-Vis spectra of thin porous silica films containing different amounts of silver before exposure to reducing agent. $\text{Ag}^+/\text{C}_{12}\text{E}_{10}$ molar ratios are indicated along the spectra. Samples were kept in open air in the dark.....	74
26. Absorption spectra of silver nanoparticles synthesized in $\text{C}_{12}\text{E}_{10}:\text{H}_2\text{O}:\text{HNO}_3$ in presence of meso- $\text{SiO}_2$ , $\text{Ag}^+/\text{C}_{12}\text{E}_{10}$ molar ratio is 0.2, with elapse expose to $\text{N}_2\text{H}_4$ 0-1) 0-15 min. 2) 30 min. 3) 45 min. 4) 60 min. 5) 90 min. 6) 105 min. 7) 120 min. 8) 120 min, after wiping .....	76
27. UV-Vis absorption spectra for (A) white and (B) brown meso- $\text{SiO}_2$ containing 0.9 $\text{Ag}^+/\text{C}_{12}\text{E}_{10}$ molar ratio upon reduction. Dashed line refers to the prolonged reduction after removing of silvery mirror surface layer.....	78
28. (A) UV-Vis and (B) FT-IR spectra of $\text{AgNO}_3/\text{C}_{12}\text{E}_{10}:\text{H}_2\text{O}:\text{HNO}_3/\text{TMOS}$ system with $r = 0.9$ during reduction. Time of reduction is mentioned along the spectra.....	80

29. Typical optical micrographs of meso-SiO <sub>2</sub> containing (A) 0.7, (B) 0.9 Ag <sup>+</sup> /C <sub>12</sub> E <sub>10</sub> molar ratios exposed to N <sub>2</sub> H <sub>4</sub> for 30 minutes .....	79
30. Optical micrographs of meso-SiO <sub>2</sub> containing reduced silver with Ag <sup>+</sup> /C <sub>12</sub> E <sub>10</sub> molar ratio (A) 0.7, (B) 0.8 between crossed polarizers.....	81
31. Optical micrographs of meso-SiO <sub>2</sub> containing 0.2 Ag <sup>+</sup> /C <sub>12</sub> E <sub>10</sub> (A) normal, (B) between crossed polarizers.....	82

# 1. INTRODUCTION

## 1.1. Nanoworld

Over last 20 years, there has been a particular interest of design, synthesis, characterization and evolution of properties of porous materials for catalysis, adsorption and separation, environmental pollution control etc. Three types of inorganic porous materials and their characteristic properties are listed in Table 1 [1].

Table 1. Pore-size regimes and representative porous inorganic materials

Pore-size regimes	Definition	Examples	Actual size range
Macroporous	$> 500 \text{ \AA}$	Glasses	$> 500 \text{ \AA}$
Mesoporous	$20\text{-}500 \text{ \AA}$	Aerogels	$> 100 \text{ \AA}$
		pillared layered clays	$10 \text{ \AA}, 100 \text{ \AA}$
		M41S	$16\text{-}100 \text{ \AA}$
microporous	$< 20 \text{ \AA}$	zeolites	$< 14.2 \text{ \AA}$

As we look toward the next millennium, we envision new technologies based on nanoscaled machines and devices. The realization of this task comes to simple efficient methods to organizing materials (molecules, molecular clusters, polymers or, generally speaking, building blocks) into precise, predetermined nanostructures that can be preserved in the robust engineering form. That is why tailor made pore size and shape materials have attracted the attention of chemists and material scientists. Inorganic hollow tubes that have been fabricated at the very beginning are those composed of carbon [2,3], boron nitride [4], silica, and vanadium oxide [5]. Apart from vanadium oxide, these inorganic nanotubes have been synthesized under high temperature reaction conditions. For example, carbon nanotubes are produced by arc-discharge evaporation of carbon [6]. On the other hand, recent advances in molecular biology have shown molecular self-assembly to construct microstructure of biomaterials [7]. The bio-inspired method is another important route to the fabrication of nanotubes [7]. For example, the biomineralization has been explored to prepare ceramic materials [8-9]. In 1990's the researches at Mobil-Oil-Corporation used long-chained alkyl-ammonium ions in an attempt to increase the pore size of zeolites [10]. They observed honeycomb like arrays of 4nm pores and, based on analogies of hexagonal liquid crystal systems, proposed a supramolecular liquid crystalline templating mechanism.

The discovery of tailor made mesoporous molecular sieves brought about a revolution in materials research at the interface of polymer (organic) and inorganic materials chemistry. Explorations at the boundary between two major

sub-disciplines of chemistry are now being integrated in new classes of polymer inorganic hybrid materials with structures and compositions unparalleled in materials science [11-14]. These new synthetic methods provides an approach to nanocomposite materials in which interface between polymer and inorganic constituents is under molecular control. The new materials occurring at the boundary of polymer/oligomer and inorganic materials can exploit new chemical and physical properties. Polymer/inorganic composite displays unique behavior not available to the polymer and inorganic parts alone [15]. The amalgamation of structures and length scales typically associated with polymers and inorganics to create functional hybrid materials with hierarchical architectures that are unprecedented in material science. The combination of polymeric and inorganic building units in a self-assembly processes provide control over interfaces at the molecular scale [12,15-16].

## **1.2. Pure Silicate Mesoporous Materials**

### **1.2.1. Characterization and Structure Model**

Mesoporous molecular sieves (MMS) which is discovered by Mobil scientists (very often in the literature referred to MCM (Mobile-Corporation-Meter) type materials) are condensed forms of unit cylindrical structures and possess unusual textural characteristics: uniform pore size in a range of 2-50 nm, surface area of 1000 m<sup>2</sup>g<sup>-1</sup> or higher, high adsorption capacities, long range ordering of packing of pores.

Mesoporous materials (MM) are typically amorphous solids, such as silicas or transitional aluminas or modified layered materials such as pillared clays and silicates. MCM-41 denoted for hexagonal mesoporous silica material is thermally stable with high acid resistance but hydrothermally unstable and with low base tolerance [17]. The study of mechanical stability on the basis of nitrogen adsorption and small angle X-ray diffraction were carried out. These results revealed that drastically altered structure of MCM-41 powder was observed upon applying an external pressure of 8.6 Mpa. It is essentially destroyed at pressures of 224 MPa, completely amorphized at 1200 MPa [18]. Mechanical stability depends on pore walls thickness. On the basis of both the  $\text{NH}_3$ -TPD [19] and the pyridine adsorption data [20], MCM-41 possesses only some weak and middle strength acid sites. According to arrangement of pores, there are three types of ordered materials: MCM-41 has hexagonal structure, MCM-48 refers to cubic arrays of pores and MCM-50 symbolizes for lamellar structure type, Figure1 [21].

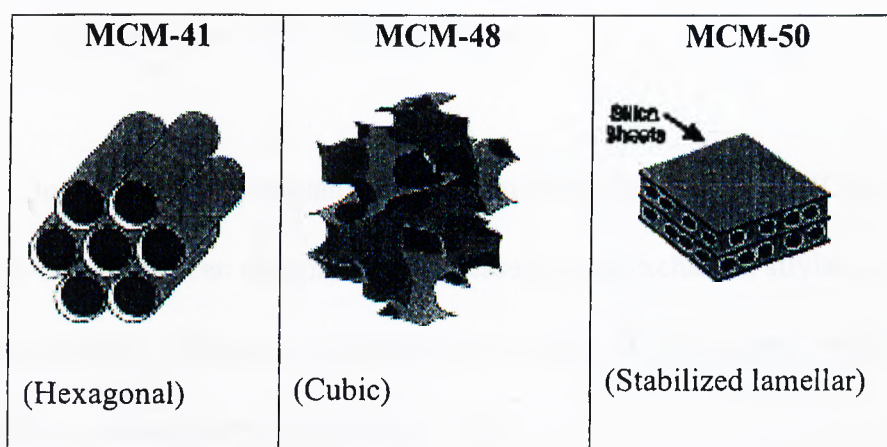


Figure 1. Illustration of M41S materials

Ordered mesoporous materials (OMM) can be obtained in wide variety of topological constructions, such as monoliths, fibers, dispersed powders, thin films. Isomorphous substitution of T atom (T = Si, Al) by other elements can generate a new hybrid atom molecular sieve to improve properties of OMM and increase their scale of utilization. Although the concentration of metal dopents, other than aluminar, into amorphous silicate framework is very low the stability of the material is highly affected. The most successful attempts to obtain metal doped MCM-41 type materials were achieved with Zr, Mn [22], B, Ga [23], Fe [24], Nb [1].

Thermally stable ordered large-pore (up to 140 Å) mesoporous materials have been synthesized with non-silica oxides of Ti, Zr, Al, Nb, Ta, W, Ga, Ge, V, Zn, Cd, In, Sb, Mo, Re, Ru, Fe, Ni, Cr, Mn, Cu employed as inorganic precursors [14,25].

### 1.2.2. Nature of the MCM Internal Surface

Qualitative and quantitative investigations of the surface of MCM in terms of its Si-OH groups can elucidate the processes of ion exchange, silylation, chemical deposition etc. There are three types of surface Si-OH groups, which have the following characteristics, see Figure 2 [26]:

- 1) single  $\text{O}_3\text{Si-OH}$  group with an IR absorption band at  $3738\text{ cm}^{-1}$  and  $^{29}\text{Si}$  magic angle spinning nuclear magnetic resonance (MAS-NMR) signal at  $-101\text{ ppm}$  with respect to tetramethylsilane (TMS) and denoted as  $\text{Q}_3$
- 2) hydrogen-bonded  $\text{O}_3\text{Si-OH}$  groups with IR absorption band at  $3200\text{-}3600\text{ cm}^{-1}$  and  $^{29}\text{Si}$  MAS-NMR peak at  $-101\text{ ppm}$
- 3) geminal  $\text{O}_2\text{Si(OH)}_2$  groups with IR absorption band at  $3738\text{ cm}^{-1}$  and  $^{29}\text{Si}$  MAS-NMR peak at  $-92\text{ ppm}$ , denoted as  $\text{Q}_2$ .

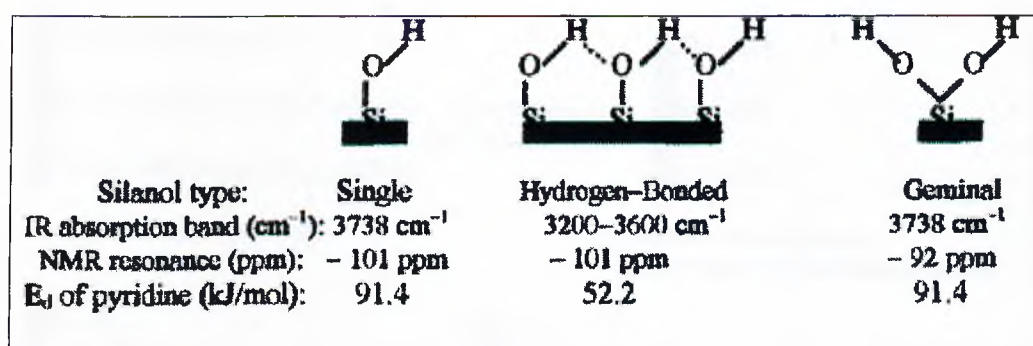


Figure 2. Schematic representation of the three types of Si-OH groups in siliceous MCM-41 and their characteristics.  $E_d$  is the activation energy of the desorption sites.

Existence of internal Si-OH groups is related to formation process of MCM. The dehydroxylation reactions of hydrogen bonded and geminal Si-OH groups take place to form siloxane bonds and simultaneously more free Si-OH groups are generated, see Figure 3 [26]. However, dehydroxylation of single Si-OH groups is considered to be not very probable, since they are too far apart from each other and such a process would necessarily involve the unfavorable formation of highly strained linked structures. Dehydroxylation from geminal groups could also be difficult since silicon does not form any siloxane links ( $=\text{Si}=\text{O}$ ) [27].

The population of silanol groups and the number of adsorbed water molecules on the mesoporous silica surface greatly affect reactivity of the surface, for example, formation of functionalized organic monolayers within pores which affects the efficiency of removing heavy metal ions from aqueous and nonaqueous blends [28].

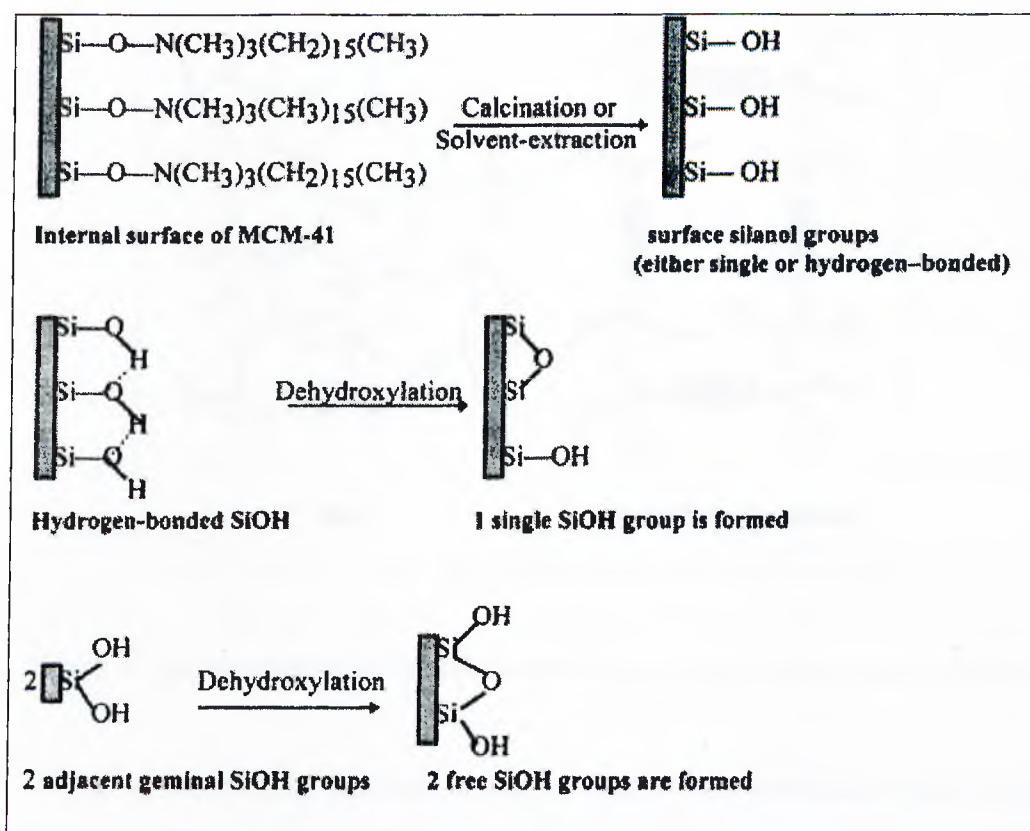


Figure 3. Schematic representation of formation and dehydroxylation processes of SiOH groups in siliceous MCM-41

Using homogeneous, molecularly defined hybrid network in which the temporary organic groups are covalently bonded to the silicon atom through the Si-C bond can modify the physical and chemical properties of the amorphous silica. Porous materials implied non-hydrolyzable silicon-carbon bond like  $R'Si(OR)_3$  or polysilylated  $(RO)_3Si-Y-Si(OR)_3$  organo-silicon compounds were synthesized and studied [29-31]. These bridged polysilsesquioxanes are three dimensional network materials, as shown on Figure 4 [30].

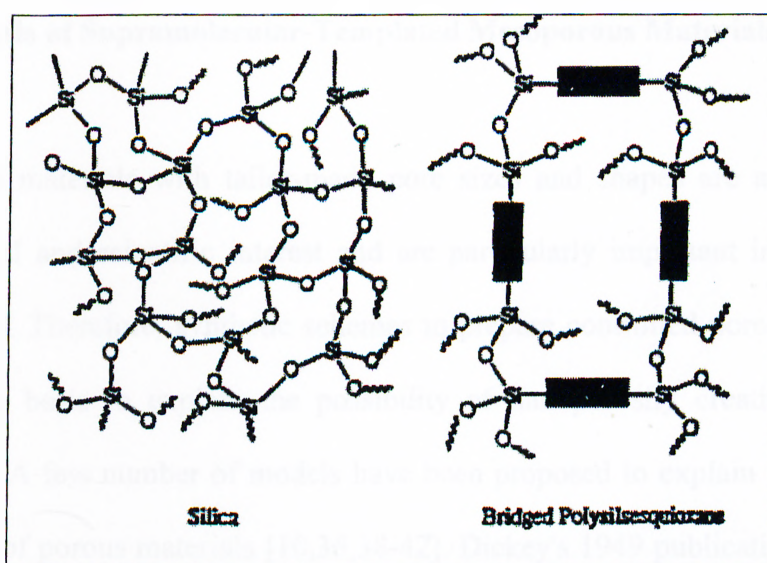


Figure 4. Representation of the silica network and polysilsesquioxane network

The trialkoxysilane terminated organic spacers can introduce a wide variety of organic functionality, such as arylene, alkylene, alkenylene, acetylene groups into the final network materials [32]. The hybrid materials, mentioned above, are amorphous silicates and have random network with broad pore-size distributions although they display unique properties. The synthesis of novel organic/inorganic hybrid mesoporous materials with a homogenous distribution of organic

fragments and inorganic oxide within the framework, rather than end-grafted, exhibiting a highly ordered structure of uniform pores. Periodic mesoporous organosilica containing bridge-bonded ethen [33], ethane, methylene, phenylene [34] groups and ability to incorporate a variety of bridging organic and organometallic species [35] develop the chemistry of nanoscaled channel hosts and inspire generation of materials with new properties.

### **1.3. Synthesis of Supramolecular-Templated Mesoporous Materials**

The materials with tailor-made pore sizes and shapes are a new area of technological and scientific interest and are particularly important in applications [1,21,36-37]. Therefore, synthetic schemes to prepare controlled porosity materials and rational basis to explain the possibility of nanoporosity creation are to be understood. A few number of models have been proposed to explain the formation mechanism of porous materials [10,36,38-42]. Dickey's 1949 publication appears to be a first documented demonstration of molecular "imprinting" or "templating" to control pore size and shape [43] and concerned to be a common step in the preparation of amorphous, nanoporous silica materials. A template may be defined as a central structure about which a network forms in such a way that removal of the template creates a cavity with morphological and/or stereochemical features related to those of the template [44]. A general templating mechanism is illustrated in the Fig. 5 [37] where primary structural units are crystallized around the molecular template. The initial ordered species might consist of aggregates of water molecules or silicate moieties. Subsequent growth proceeds because nucleation by this initial

structure or assembly of number of such structures, but crystal growth is the result of the initial silicate organization. The fidelity of the imprint created by template removal depends on several factors: (1) nature of the interaction between the template and embedding matrix; (2) ability of the matrix to conform to the template; (3) relative size of the template and the primary units used to construct the matrix.

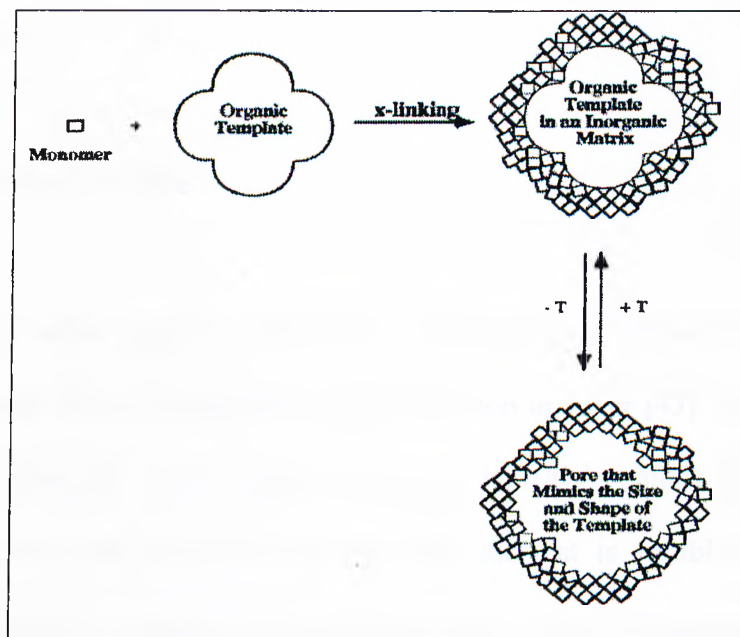


Figure 5. Schematic of the organic template approach to prepare nanoporous amorphous silica showing the incorporation and removal of the template

Thus, how inorganic precursor interacts with template is the issue whereby the models diverge; the type of interaction between template and inorganic precursor will be seen as a significant difference among the various synthetic routes, formation models, and the resulting classes of mesoporous materials.

The ordered mesoporous molecular silicas can be formed by surfactant molecules and/or supramolecular surfactant assemblies where the nature of the

surfactant matrix interaction is via noncovalent bonding mechanisms such as electrostatic interactions, van der Waals contact and hydrogen bonding or can be based on organic ligands and polymers covalently bonded to the siloxane network.

Before one can understand how to engineer the pore sizes and shapes it is necessary to understand the components that make up the mesophase and how they are assembled.

### 1.3.1. Surfactant Template

Surface active agents (surfactants) are molecules that may have a binary character, which allows them to alter surface tension in water [43]. A dual property within one molecular entity composed of a polar (hydrophilic) head, which is soluble in water, and nonpolar (hydrophobic) tail that is soluble in oil makes surfactant unique for various interfacial interactions. These amphiphilic surfactant molecules or polymers composed of hydrophobic and hydrophilic parts can self-assemble in solvents. Self-assembly is a spontaneous organization of materials through noncovalent interactions (hydrogen bonding, van der Waals forces, electrostatic forces,  $\pi$ - $\pi$  interactions, etc.) with no external intervention. Self-assembly typically employs asymmetric molecules that are preprogrammed to organize into well-defined supramolecular assemblies. In a simple binary system of surfactant-water, surfactant molecules manifested themselves as very active components with increasing concentrations, as schematically shown in Figure 6 [17]. At very low concentrations, they energetically exist as molecules. With increasing the concentration, surfactant molecules aggregate together to form

micelles in order to keep the system entropy low. The amphiphilic aggregates maintain the hydrophilic parts of molecules in contact with water while shielding hydrophilic parts inside the micelle interior.

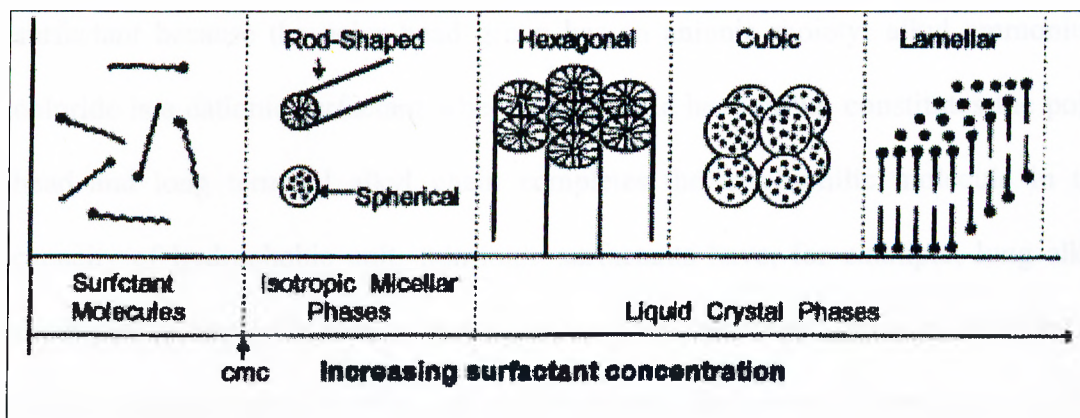


Figure 6. Phase sequence of surfactant-water binary system

The initial threshold concentration at which molecules aggregate to form micelles is called CMC (critical micellization concentration). As the aggregation process continues, hexagonal close packed arrays appear, producing hexagonal phases. The final step in the process (highest surfactant concentration) is the coalescence of adjacent, mutually parallel cylinders to produce the lamellar phase. In some cases the cubic phase also appears prior to the lamellar phase [17]. The cubic phase is generally believed to consist of complex, interwoven networks of rod-shaped aggregates. The architectural phase make up usually depends on surfactant concentration in solvent as well as on the nature itself (length of the hydrophobic carbon chain, hydrophilic head group and counter ion) and the environmental parameters (pH, temperature, ionic strength, and other additives). These supramolecular aggregates generate liquid crystalline mesophases. The liquid crystal (LC) is called lyotropic, if the type of liquid crystal phase is dictated by the

concentration of material in the solvent. There are several different types of lyotropic liquid crystalline phase structures. Each of these types has a different extent of molecular ordering within the solvent matrix. Anionic, cationic, nonionic surfactants exhibit lyotropic LC phases. Alkyl sulfate, for instance, is anionic surfactant because the polar head group has an anionic moiety; alkyl ammonium chloride is a cationic surfactant where the cationic head group constitutes the polar head and long terminal alkyl chain completes the amphiphilic molecule in the capacity of hydrophobic unit; non-ionic surfactants have, for example, long alkyl chain as a hydrophobic section and the hydrophilic polar head group constructed of several ethylene glycol units, poly(oxyethylene) alkyl ether system is a typical example. The structure of micelles is determined by the nature of solvent. In the water-oil mixture, above CMC, spherical micelles are formed. Reverse micelles formation occurs in the oil-water mixture where the nonpolar chains radiate away from the centrally aggregated head groups that surround the water molecules. Further increase in micellar concentration provides formation of larger structures and generates the formation of lyotropic LC phases. On adding more water lyotropic liquid crystal phase would eventually "dissolve" to give a micellar solution. As temperature increases the lyotropic liquid crystalline phases exist until the melting point of the neat surfactant is reached. At low temperatures the molecules become rigid and a crystalline structure results (solid phase). Upon increasing temperature, first LC phase is reached and then melting into liquid phase takes places. Phase diagrams are used to specify the temperature and concentrations at which various structures exist at equilibrium. Three different lyotropic LC phase structures are widely recognized. These are the lamellar, the hexagonal and the cubic phases Figure 6 [17].

The lamellar LC structure consists of layered arrangement of amphiphilic molecules. Self-assembly process results intertwining nonpolar chains from oppositely directed molecules, where the polar head group is separated by the layer of water molecules. Water layer thickness is in between 1 to 10 nm, if water content is in between 10 and 50% by weight in the surfactant/water binary phase. Typically, below 50% surfactant/water ratio, the lamellar phase give rise to hexagonal lyotropic LC phases or an isotropic micellar solution. Lamellar lyotropic LC phase is less viscous than the hexagonal LC phase because of their parallel layers flexibility [45]. Hexagonal lyotropic LC phases have molecular aggregate ordering which corresponds to a hexagonal arrangement. There are two structures of hexagonal LC phase, the hexagonal phase ( $H_1$ ) and the reversed hexagonal phase ( $H_2$ ). The hexagonal phase consists of micellar cylinders of indefinite length packed in hexagonal arrangement. The spacing between cylinders varies enormously between 1 and 5nm depending upon the relative amounts of water and surfactant. This phase is very viscous. Cubic lyotropic liquid crystal phases are not as common as lamellar or hexagonal phases and are not structurally well characterized. The most well known cubic phase consists of a cubic arrangement of molecular aggregates. This phase is even more viscous than the hexagonal phase. The high viscosity results from the lack of shear planes within the structure that would allow the sliding [46].

### 1.3.2. Tailoring of Surfactant/Inorganic Mesophase

To synthesize periodic mesoporous silica, four reagents are generally required: water, a surfactant, a silica source, and a catalyst. Water, surfactant and catalyst are first combined to form homogeneous micellar solution. To this micellar solution the molecular alkoxide, such as tetramethylortosilicate (TMOS) or tetraethylorthosilicate (TEOS) is added. The mesophase is generally formed in seconds to minutes at room temperatures. A cosolvent such as methanol can be added to precursor solution to ensure homogeneity and to maximize product yield [37]. The synthetic route described above is called liquid crystalline templating (LCT) mechanism and can be depicted as in Figure 7 [17], where the formation of hexagonal nanostructure is shown.

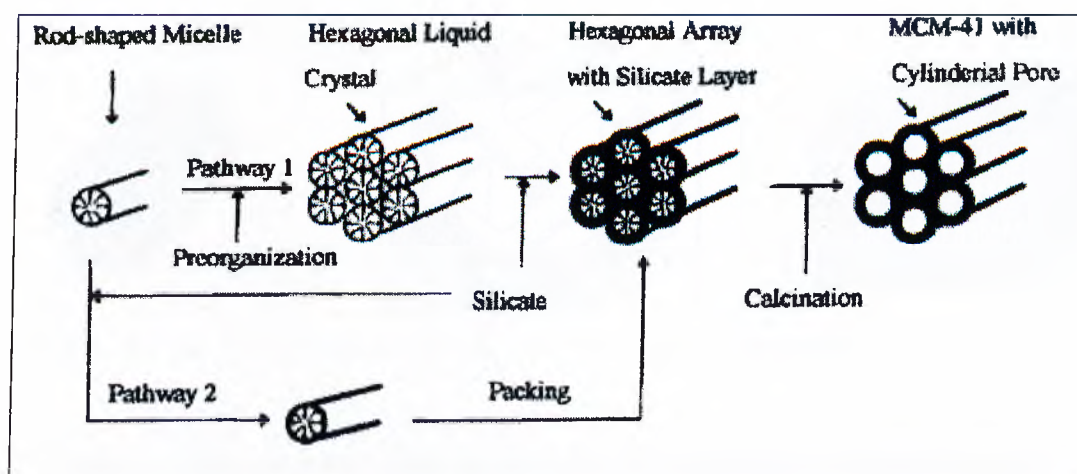


Figure 7. Schematic of the liquid-crystal templating (LCT) mechanism via two possible pathways

Thus, two features dictate the formation mechanism of mesoporous molecular sieve family. The first is the dynamic of surfactant molecules to form molecular assemblies, which lead to liquid crystal formation. The second is the

testing different synthesis pathways based on different structure-directing agents or reaction mechanisms [12-13,36,38,42,47-50]. A formation mechanism based on specific type of electrostatic interaction between a given inorganic precursor **I** and surfactant head group **S** has been proposed by Huo and co-workers [42,48]. This so-called charge density matching approach describes the synthesis of periodic mesophase at the surfactant/inorganic interface under a range of pH conditions. The MCM-41 periodic porous silica can be obtained under basic conditions ( $\text{pH} > 9$ ) by the self-assembly of the anionic silicates  $\text{I}^-$  and cationic surfactant molecules  $\text{S}^+$  [48]. This synthetic route is called direct pathway and can be abbreviated as  $\text{I}^-\text{S}^+$ . In the case of cationic silica species  $\text{I}^+$  ( $\text{pH} < 2$ ) and cationic surfactant  $\text{S}^+$  present the formation of MCM-41 material proceeds through mediated pathway denoted as  $\text{S}^+\text{X}^-\text{I}^+$ . Halide counteranion ( $\text{X}^-$ ) became involved in the synthesis to buffer the repulsion between  $\text{I}^+$  and  $\text{S}^+$  by means of hydrogen bonding forces. The electrostatic charge matching between long chain quaternary ammonium cation surfactant ( $\text{S}^+$ ) and anionic inorganic precursor ( $\text{I}^-$ ) was found as especially effective in generating mesostructures with hexagonal, cubic, lamellar symmetry [10,36]. Stucky and co-workers [48] have extended the electrostatic templating concept to include a charge-reversed  $\text{S}^-\text{I}^+$  pathway between anionic surfactants such as sulfonates, phosphonates and carboxylates, and cationic precursor. They also demonstrated counterion mediated  $\text{S}^+\text{X}^-\text{I}^+$  ( $\text{X}^- = \text{halide}$ ) and  $\text{S}^-\text{M}^+\text{I}^+$  ( $\text{M}^+ = \text{alkali metal ion}$ ) pathways.

Tanev and Pinavaia recently demonstrated [51] that the assembly of hexagonal mesoporous metal oxides also can be achieved by hydrogen bonding between neutral amine surfactant ( $\text{S}^0$ ) and neutral inorganic precursor ( $\text{I}^0$ ). They worked on mesoporous molecular sieves by alkyl nonionic polyethylene oxide

surfactants ( $N^0$ ) of the type  $C_{11-15}H_{23-31}(OCH_2CH_2)_mOH$  as a template in which  $n$  is number of ethyleneoxide (EO) units through  $N^0I^0$  strategy [52-53]. Nonionic etoxylated sorbitan esters as a templates were used to assembly mesoporous silica sieves by charge density matching mechanism between neutral TEOS and nonionic poly(ethylene oxide) entities [54]. The synthesis of micelle-templated structures (MTS) which are assembled from poly(ethylene oxide) (PEO) surfactants are accomplished by first dissolution of hydrophobic tetraethyl ortosilicate molecules (TEOS,  $Si(OC_2H_5)_4$ ) into the outer hydrophilic volume of lyotropic liquid crystal phase of long-chain poly(ethylene oxide) shell. Followed by sol-gel synthesis of monomer is confined within the aqueous domains of microphase separated medium which acts as a template [55].

### 1.3.3. Sol-Gel Processing

The sol-gel process is a chemical synthesis method initially used for the preparation of organic materials such as glasses and ceramics. Its low temperature-processing characteristic also provides unique opportunity to make pure and well-controlled composition organic/inorganic hybrid through incorporation of low molecular weight oligomeric/polymeric organic molecules with appropriate inorganic moieties at temperatures under which the organic can survive.

Organic/inorganic hybrid materials prepared by the sol-gel process can be generated using different synthetic techniques by incorporating various starting inorganic and organic components with varied molecular structures:

- (1) Hybrid networks can be synthesized by using low molecular weight organoalkoxysilanes as one or more of the precursors for the sol-gel reaction in which organic groups are introduced within an inorganic network through the =Si-C- bond [56-57].
- (2) Organic/inorganic hybrid network materials can also be formed via the co-condensation of functionalized oligomers or polymers with metal alkoxides in which chemical bonding is established between inorganic and organic phases [58].
- (3) A hybrid material can also be synthesized through the in-situ formation species within a polymer matrix [59-60]. Specifically, inorganic species, generally in the form of particles with a characteristic size of a few hundred angstroms, can be generated in situ within the polymers.
- (4) Organic/inorganic composites can be obtained by either the infiltration of previously formed oxide gels with polymerizable organic monomers or the mixing of polymers with a single or mixture of metal alkoxides in a common solvent. In a first approach the impregnation of porous oxide gels with organics is followed by an in-situ polymerization initiated by thermal or irradiation methods. In the second approach, polymers can be trapped within the oxide gel network if the hydrolysis and condensation metal alkoxide are carried out in the presence of preformed polymers [61].
- (5) Organics can also be simply impregnated or entrapped as a guest within inorganic gel matrix (as a host) [62-63].
- (6) Hybrid networks can also be formed by interpenetrating networks and simultaneous formation of inorganic and organic phases. By using triethoxysilane  $R'Si(OR)_3$  as a precursor with  $R'$  being a polymerizable group



Initial hydrolysis of silicon alkoxide (1) results in partially hydrolyzed molecules. These can react with each other or with silicon alkoxide through condensation reaction (2-3). Both hydrolysis and condensation occur by nucleophilic substitution ( $S_N$ ) mechanisms which involve three steps: nucleophilic addition ( $A_N$ ), proton transfer within the transition states, and removal of the protonated species as either alcohol or water. The structure and the morphology of the resulting network strongly depend on the pH of the reaction.

The acid catalysis promotes the development of more linear or polymer-like molecules in the initial stages. Base catalysis results in a higher condensation rate to produce denser, colloidal particulate structures [21,29,65]. Mesoporosity arises from larger primary silica particles formed during the early stages of sol-gel polymerization reactions. The size of alkoxy group can also influence the hydrolysis and condensation reactions through a steric or leaving group stability. For example, species such as TMOS tends to be more reactive than TEOS. Lam and co-workers [65] noticed that the final morphology of the cured hybrid materials was the result of competition between the kinetics of polymerization and kinetics of (microphase) organic phase separation. Low pH conditions (pH = 2.5) reveals rapid hydrolysis and slow condensation. Thus the entire surfactant phase separation had enough time to take place. As hydrolysis and condensation-polymerization reactions continue, viscosity increases until the solution ceases to flow. This sol-gel transition is irreversible, and at this stage the one-phase liquid is transformed to a two phases system. At this point of gelation significant concentration of soluble silicates are still present in the liquid phase. In the next stage of sol-gel processing, gel aging, these species become attached to gel network, leading to an increase in rigidity [21,29,66-

67] Condensation can still occur within the gel network resulting in stiffening and contraction. Longer aging can reduce the rigidity of the silica network [21,37]. Once gel aging is completed drying of the gel takes place. It occurs through remove of liquid phase from the solid gel framework. Shrinkage in pore volume and a corresponding reduction in the pore size are involved in this stage.

Additives are generally introduced to the sol-gel material at the sol stage, and thus they are usually dissolved and remain in the liquid phases of the gel. It provides mobility and desorption of the additive materials in the matrix and gives them possibility to perform their functions [21,66].

#### **1.4. L C Phase Synthesis with PEO Type Surfactant**

An alternative route towards ordered mesoporous ceramic nanostructures is utilization of lyotropic liquid crystalline phases as structure directing media [50]. The normal hexagonal, lamellar, "bicontinuous" cubic structures of lyotropic mesophases are known for non-ionic poly(ethylene)alkyl ether  $[C_nH_{2n+1}(OCH_2CH_2)_mOH, C_nE_m]$  [68]. Intramicellar forces determined the micellar shape just above the CMC. Intermicellar forces are responsible for mesophase structure. Hydrogen-bonding of water to hydrophilic oligo(ethylene oxide)  $(CH_2CH_2O)_m$  head groups determines the conformation of head group, while the surfactant:water ratio indicates the mesophase formation [68-69]. Thus, competition

between head group (EO)/water and head group/head group (EO/EO) interactions establishes the type of mesostructure and their sequence upon length of the alkyl chain of  $C_nE_m$ , temperature, and composition of binary aqueous amphiphil solutions.

The phase behavior of non-ionic surfactant decaethylene glycol monododecile ether  $CH_3C_{11}H_{22}(OCH_2CH_2)_{10}OH$ , denoted as  $C_{12}E_{10}$ , which was used, is similar to the phase diagram shown on the Figure 9 [68] for  $C_{12}EO_8$  surfactant.

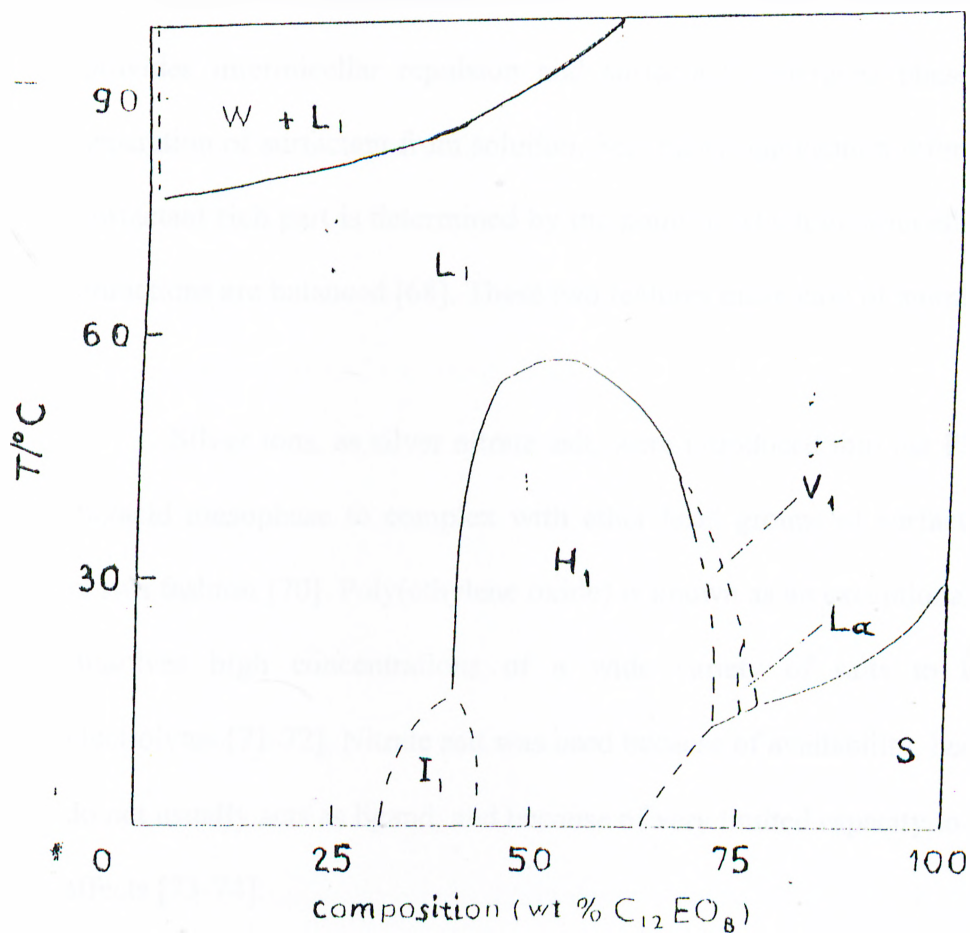


Figure 9. Phase diagram of the  $C_{12}EO_8$ /water system over the temperature range 0-100 °C. ( $I_1$ , close-packed spherical micelle cubic phase;  $H_1$ , normal hexagonal phase;  $V_1$ , normal "bicontinuous" cubic phase;  $L_\alpha$ , lamellar phase)

$C_{12}E_{10}$  displays hexagonal liquid crystalline phase in the wide region of surfactant concentration (70-40%) up to 60 °C, and cubic phase followed by narrow region of lamellar phase at high concentration (70-90%) of non-ionic surfactant.

Other characteristics of the poly(ethylene oxide) PEO type surfactants which justifies their choice as a template for the developing of inorganic mesostructure are to be mentioned. These are cloud point and second aggregation. At cloud point (CP) the hydrogen bonding interactions between water and EO units are disrupted what provides intermicellar repulsion and surfactant undergoes phase transition with separation of surfactant from solution. Secondary aggregation refers to separation of surfactant rich part is determined by the point in which intermicellar repulsions and attractions are balanced [68]. These two features make ease of template recovery.

Silver ions, as silver nitrate salt, were introduced into the PEO/water (50 wt %)/acid mesophase to complex with ether head groups of surfactant in a pseudo crown fashion [70]. Poly(ethylene oxide) is known as an exceptional polymer which dissolves high concentrations of a wide variety of salts to form polymeric electrolytes [71-72]. Nitrate salt was used because of availability, because nitrate ion do not usually acts as ligand, and because of very limited capacity to salting in or out affects [73-74].

The ordered bulk hexagonal silver containing liquid crystalline mesophase of  $C_{12}E_{10}$  is preliminary and very important step in synthesis of metal-surfactant-mesoporous silica nanocomposite materials.

Prehydrolyzed tetramethylortosilicate (TMOS) was added to form nanostructure within aqueous domains of a microphase separated media through sol-gel processing and results in formation of solid transparent film. Non-ionic PEO-type surfactant and neutral inorganic precursor form framework assembly through hydrogen bonding between the hydrophilic (EO)<sub>m</sub> segments and the silanol groups of the alkoxide precursor. Prereaction of inorganic precursor yields a family of low weight oligosilicates, which serves as building blocks for further polymerization and formation of inorganic walls between ordered surfactant micelles [21]. Prehydrolysis promotes low temperature nucleation of inorganic network [75] and leads to formation thicker silica walls [52]. The subsequent stages of sol-gel processing (gelation, aging and drying) are overlapped in the case of film formation. Preferential alcohol evaporation occurs during the deposition, leaving a film increasingly enriched in water content [21,66-67]. This is potentially important feature, since the water content in the pores influences the capillary forces which affect densification. Changes in solvent composition were correlated with the film thickness [66].

Synthetic approach of formation mesoporous molecular sieves (MMS) is that inorganic oligomers and surfactant molecules co-organize or subsequently organize in aqueous media to form composite structures resembling lyotropic liquid crystalline mesophases with inorganic constituents located adjacent to the hydrophilic head groups of the surfactant [50]. It was modified for MMS films formation and is that exceeding of critical micelle concentration of a bulk silica surfactant solution results in formation of hexagonal mesophases by interfacial self-assembly [76-77].

The last approach was extended to obtain metal containing MMS films is that metal ion is associated with head groups of non-ionic PEO type surfactant assembly that is imbibed within the channels of hexagonal mesoporous silica, [meso-SiO<sub>2</sub>-C<sub>n</sub>E<sub>m</sub>-Met<sup>+</sup>] [78].

The latest one was successfully used for preparation silver containing MMS films. Here silver with a help of C<sub>12</sub>E<sub>10</sub> non-ionic surfactant was evenly distributed within silica mesopores tailored through liquid crystalline-sol-gel processing. The hexagonal lyotropic liquid crystalline phase of C<sub>12</sub>E<sub>10</sub> is the simultaneous template for synthesis of nanoscaled silver particles and nanostructure of porous silica. Separated investigation of silver containing template system Ag<sup>+</sup>/C<sub>12</sub>E<sub>10</sub>/H<sub>2</sub>O/HNO<sub>3</sub> might elucidate an effect of added silver nitrate on behavior of bulk hexagonal LC phase of non-ionic surfactant used. This investigation can contribute into the two vibrating scientific directions. One is preparation of MMS films containing nanosized metal particles, which, in turn, develop catalysis, photography, surface enhanced Raman spectroscopy [79]. The second group comprises preparation and studies of particles itself.

### **1.5. Chemistry within Host Mesoporous Silicates**

Mesoporous molecular sieve, MCM-41 (member of M41S family) possesses hexagonally arranged uniform porous structure. The important characteristics of this new material are its large surface area, high porosity, controllable and

narrowly distributed pore size, large pore openings, mild acidity, high thermal stability [1,10,28,36,80]. These make it attractive for various industrial applications, as well as, an excellent reference material for study of functional interfacial process by a variety of physicochemical methods [80].

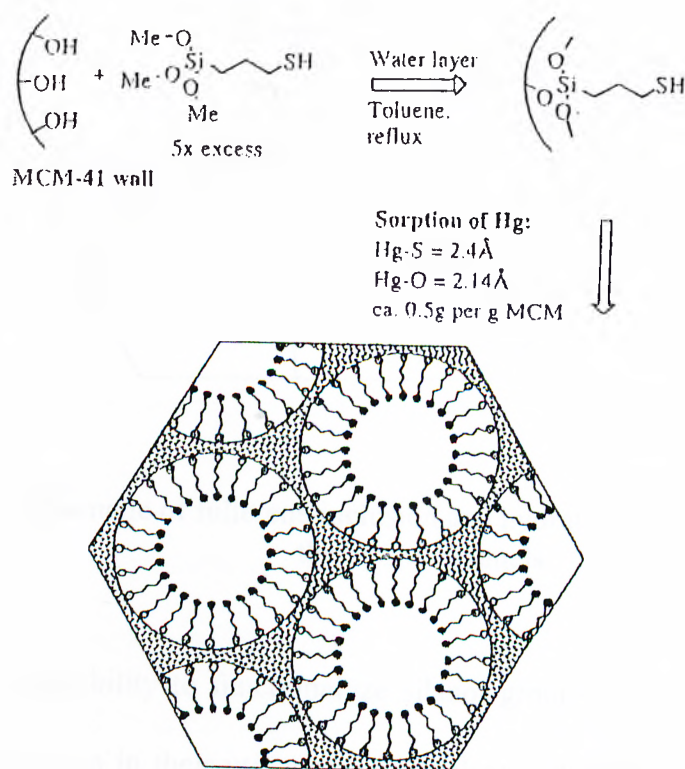


Figure 10. Grafting of monolayer of thiol functionalities in MCM pores. The coordination environment of absorbed mercury is shown

A rich field of inclusion chemistry has been explored in context of ordered mesoporous materials, including sorption and phase transition in confined spaces [81-82], ion exchange [83-84], imbibition followed by reduction [85], grafting of materials of different nature, Figure 10 [80], shapes and sizes from small metal oxides to bulky bimetallic complexes [86] and fullerene [87], Figure 11 [80], polymerization in the channels [88-89], cocondensation of the reactive species during the synthesis of mesoporous materials [49].

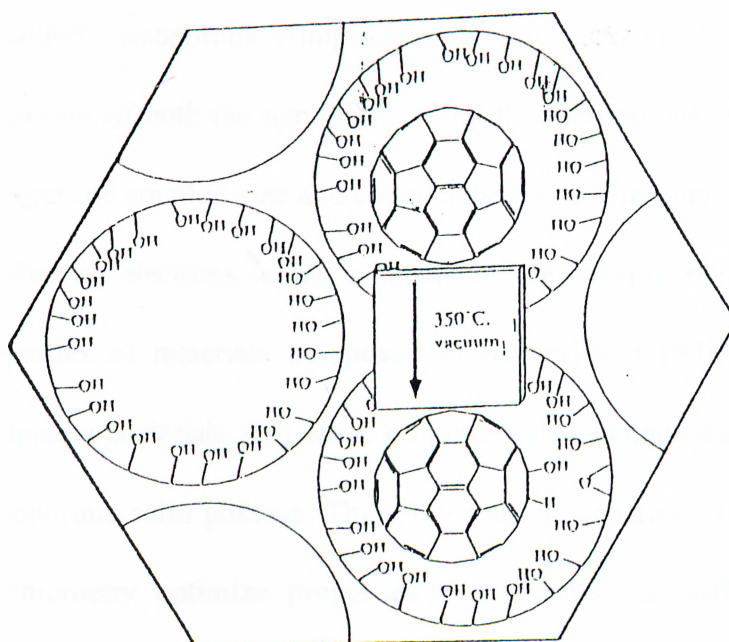


Figure 11. Schematic of fullerene inclusion and hydration at elevated temperature in the MCM channels

The possibility to functionalize silanol groups on the surface of materials opens new area in their utilization as catalysts [20,28,89-92], catalytic supports [28,89-90,92-93], chromatographic resins [93-94], sensors [28], membranes [94], low dielectric coatings, optical communications [95]. For instance, mesoporous fibers are important in biology as a remote chemical/biological sensors or fibrous catalyst supports [47]. Hollow nanotubes find the application in optics, electronics, energy storage/conversion, can be designed to mimic biological channels [6]. Materials with tailor made pore size and shape are potentially useful as nano- or subnanosized vessels, composites or hosts to assembly semiconductor clusters [83-84], organic molecules [94], molecular wires [1,80], in general, building blocks in their inner spaces [80,90]. If one assembles the nanoscaled particles (semiconductors, compounds or metals) into the pores of mesoporous

solids a new material will be obtained. This nanoparticle loaded mesoporous solid is called mesoporous composite and will undoubtedly possess some unique properties of both the nanoparticle and the mesoporous solid. The nanoparticles in pores are small in size and chemically active. Confinement and quantization of conduction electrons within a small volume enhance the optical and electronic properties of materials composed of nanocrystals [97]. So this new type of composite materials will have properties that neither the nanoparticle nor the mesoporous solid possess. Thus, interparticle separations, particle size, particle stoichiometry optimize properties of materials may offer the possibility for observing new collective physical phenomena and produce novel devices [15,97].

Materials which contain metal nanoclusters have been prepared by a variety of chemical and physical methods including hydrosol formation [98], impregnation of a solid support [99], inert gas evaporation [100], vacuum evaporation [101], vacuum evaporation with organic matrix isolation [102], cremate formation [100], pressure impregnation of a porous host, or cluster nucleation by irradiation [103-104]. Vast literature exists on the preparation of heterogeneous catalysts by the deposition or formation of solid particles on the solid support of high-surface area [100]. Protected or persisted metal colloids have been prepared in which metal nanoparticles are coated with synthetic polymers [98-99,111], surfactants [80,105-109], or surface-bound ligands [107-110]. Membrane-based synthesis of nanomaterials entails formation species of desired size and shape within the pores of a nanoporous membrane [113].

Nanosized silver particles [97,112,114] and  $\text{Ag}_x\text{Au}_{1-x}$  ( $0.2 < x < 0.8$ ) alloy particles [115] were synthesized into pores of monolithic mesoporous silica by soaking and annealing method. Regular and oriented silver nanocrystal arrays were impregnated onto the surface of MCM-48 by deposition and thermal decomposition of  $\text{AgNO}_3$ . The different silver nanocrystal arrays may be formed through reorganization superfine silver particles at a suitable temperature range [101]. Synthetic layered silicate, laponite has been used as an inorganic protective specie for preparation of Au and Ag nanoparticles [99,116]. Silica shells were formed on the core silver particles by a modified Stöber process [117]. Metal/silica xerogels nanocomposites containing nanoclusters of Ag, Cu, Os, Pd, Pt, Re, Ru are prepared in three-stage strategy. First of all, metal salts, containing thiolate ligands in the case of silver, were prepared. The second step is incorporation of this complex into a formed silica xerogel matrix. Third one is a formation of silica-metal nanocomposites by thermal treatment [118].

Despite of all of these methods of creating nanoscaled metal, there are no techniques, which has been developed for directing of self-assembly of nanocrystals into ordered aggregates dispersed throughout host matrix. The understanding of chemical activity of nanostructured particles and the behavior of chemically active species in this environment require preparation and studies of the particles itself and development of advanced nanostructured materials.

In the first part of this work the phase properties of  $\text{AgNO}_3/\text{C}_{12}\text{E}_{10} \cdot \text{H}_2\text{O}$  (50 w/w%): $\text{HNO}_3$  (template) upon addition of silver nitrate were investigated. The

boundaries of hexagonal LC phase of the template were determined by Polarized Optical Microscopy (POM) and FTIR spectroscopy. In the second part of the study the silver containing porous silica films were synthesized through Liquid Crystalline-Templating-Sol-Gel mechanism. The structure of silver-surfactant-silica films was studied by Powder X-ray Diffraction (PXRD) and POM. FTIR spectroscopy was used for investigation the behavior of the template in the presence of meso-SiO<sub>2</sub>. The processes of generation and growth of silver metal particles in film samples were monitored by UV-Vis spectroscopy.

## 2. EXPERIMENTAL

### 2.1. Materials

All chemicals and solvents were reagent grade and used as received without any pretreatment.

Homogeneous polyoxyethylene 10 lauryl ether (C<sub>12</sub>E<sub>10</sub>) is commercially available from Sigma, Germany. Tetramethyl orthosilicate (Si(OCH<sub>3</sub>)<sub>4</sub>, TMOS) 98% pure was obtained from Fluka. Silver nitrate salt was purchased from Turkey. Methanol (99%) was obtained from Riedel-deHaën, Germany. Nitric acid (65 wt %) and hydrazine hydrate were obtained from Carlo Erba Reagenti, Italy.

### 2.2. Synthesis

#### 2.2.1. Preparation of LC Phases

The melted surfactant at 40 °C was mixed with water in the presence of nitric acid to form a transparent gel with 50:50 wt % surfactant to water ratio. The

mixture was heated at 70-75 °C for 15-20 minutes with periodical shaking and then slowly cooled to room temperature. This cooling-heating cycle was repeated three times to attain homogeneity. Resulting transparent gel was kept in the tightly closed bottle.

Set of blends with  $0 \leq r \leq 2$  silver nitrate/surfactant molar ratios were prepared by mixing certain amount of silver nitrate salt dissolved in 2-3 drops of distilled water with stock gel mixture. Blends were kept in oven at 60-70 °C for 10-15 minutes and shaken until obtaining completely homogenized samples. The mixtures were kept in sealed vials in the dark for three days. The absence of changes between cross polars under POM suggest no change on the homogeneity of  $\text{AgNO}_3/\text{C}_{12}\text{E}_{10}:\text{H}_2\text{O}(50 \text{ wt}\%):\text{HNO}_3$  systems. The measurements were repeated for several systems after a week of storage, which showed good reproducibility, and stability of the system.

### 2.2.2. Synthesis of Mesoporous Silica

Silver nitrate ( $\text{AgNO}_3$ ) in amount of 0.0-0.25 g was dissolved in 0.7 g of distilled water and 0.2 g of nitric acid. 1 g of poly(ethylene oxide) non-ionic surfactant,  $\text{CH}_3\text{C}_{11}\text{H}_{22}(\text{CH}_2\text{CH}_2\text{O})_{10}\text{OH}$  was added to above solution. The homogeneous transparent dense blends were obtained while heating at 40-50 °C in the oven for 20 minutes followed by cooling to ambient temperature. The characteristic optical birefringence texture of each sample sealed between two glass slides was revealed by POM. 1.47 g of tetramethylorthosilicate (TMOS) was prehydrolyzed in an acidic solution of 0.22 g of water and 0.02 g of nitric acid and cooled to room temperature.

This mixture was added to above homogenous mixture of silver nitrate containing surfactant mesophase, which was dissolved in 5 g of methanol.

Clear, isotropic liquid mixture was poured on a glass slide to dry in open air at ambient conditions. The densification of the film takes place upon methanol evaporation. Characteristic fan-like birefringence texture was observed in POM over silicification period of 10-60 min. Appearance of a particular POM image signals about regaining of entirely formed hexagonal LC phase of silver nitrate containing template, but now it is rigidified in the form of hexagonal mesoporous silica film. The samples were kept in the dark for three days before investigation. Preserved fan-like optical texture was observed under POM during the curing of silica network. In this work three different substrates were used for three different purposes; silicon, Si(100) was used to make thin films for FT-IR measurements, glass slides for POM and quartz windows for UV-Vis spectroscopic measurements.

### 2.2.3. Reduction of $\text{Ag}^+$ Ions in Mesoporous Silica

0.0225 gram (1 drop) of hydrazine,  $\text{N}_2\text{H}_4$  was diluted with one drop of distilled water was placed at the bottom of the tightly closed container to obtain  $\text{N}_2\text{H}_4$  atmosphere at room temperature, (RT). Thin, silver containing porous silica films were exposed to hydrazine vapor. Silver ions, which are in contact with hydrazine, undergo reduction. The samples kept at low  $\text{N}_2\text{H}_4$  atmosphere for 15 minutes were examined by UV-Vis spectroscopy, FTIR spectroscopy and POM and this procedure was repeated every 15 minutes of hydrazine exposure until no changes were recorded, approximately 2 hours.

## 2.3. Instrumentation

### 2.3.1. FTIR Spectroscopy

The transmission IR spectra were recorded with a Bomem Hartman MB-102 model FTIR spectrometer. A standard DTGS detector was used and with a resolution of  $4\text{ cm}^{-1}$  and 64 scans for  $\text{AgNO}_3/\text{C}_{12}\text{E}_{10}:\text{H}_2\text{O}(50\text{ wt}\%):\text{HNO}_3$  samples sandwiched between two Si(100) wafers. Thin films of meso- $\text{SiO}_2$  deposited onto Si(100) wafers and as KBr pellets were analyzed with a resolution of  $2\text{ cm}^{-1}$ , and 64 scans. FT-IR spectra of these materials were recorded in the range of  $200\text{-}4000\text{ cm}^{-1}$  for silicon samples and in the range of  $250\text{-}4000\text{ cm}^{-1}$  for samples pressed with KBr.

### 2.3.2. Polarized Optical Microscopy

POM was applied to characterize the mesomorphic phases formed in  $\text{AgNO}_3/\text{C}_{12}\text{E}_{10}:\text{H}_2\text{O}(50\text{ wt}\%):\text{HNO}_3$  mixtures sealed between two microscopic glass slides and meso- $\text{SiO}_2$  thin films containing  $\text{AgNO}_3/\text{C}_{12}\text{E}_{10}:\text{H}_2\text{O}:\text{HNO}_3$  deposited on microscopic glass or quartz.

The POM textures were obtained in transmittance mode on a Meije Techno ML9400 series Polarizing Microscope with reflected and transmitted light illumination and using convergent white light between parallel and crossed polarizers. Two polarizers were used for visual observation in order to examine optical property. Stereo microscope Stemi 2000 from Carl Zeiss Jena GmbH with halogen lamp 6V10W equipped for bright field and phase contrast was used for

visual sample observations and to shoot the micrograph images. Power of the objective was 10x/0.25.

### 2.3.3. Powder X-ray Diffraction.

PXRD spectra were acquired on a Siemens D 5000 diffractometer using a high power Cu-K $\alpha$  source operating at 50kV/35mA. PXRD patterns were recorded to determine the structure type of different amounts of AgNO<sub>3</sub> containing porous silica materials.

### 2.3.4. UV-Vis Spectroscopy

UV-Vis spectroscopy was used to investigate optical properties of silver mixed with C<sub>12</sub>E<sub>10</sub>:H<sub>2</sub>O:HNO<sub>3</sub> in the presence of silica network as an evolution of surface plasmon resonance absorption band. The UV-Vis spectra were recorded with a Varian Cary 5 double beam spectrophotometer with 30 nm/min speed at a resolution of 2 nm over the wavelength range from 1400 to 250 nm. The measurements were performed over equal periods of time of sample exposure to reducing agent.

### 3. RESULTS AND DISCUSSION

#### **The Phase Properties of AgNO<sub>3</sub> in Oligo (ethylene oxide) Type Surfactants and Synthesis of Mesoporous Silica Materials Functionalized with Ag<sup>+</sup> Ions and Ag Clusters**

The synthesis paradigm, employed here, confirms formation and preservation of liquid crystalline (LC) phase of a template as the first and crucial step in tailoring mesoporous silica matrix. In order to find out the optimum conditions for synthesis of silver functionalised mesoporous silica, this work has been broken into two parts. In the first part, the properties of the AgNO<sub>3</sub>/C<sub>12</sub>E<sub>10</sub>:H<sub>2</sub>O(50 w/w%):HNO<sub>3</sub> system were studied, the second part is devoted to tailoring the silica network by the help of the same system investigated in the first step. In C<sub>12</sub>E<sub>10</sub>/water system, the sequence of mesophases is changed as hexagonal (H<sub>1</sub>) → cubic (V) → lamellar (L<sub>α</sub>) with increasing of surfactant concentration, see Figure 9 [68] at 25 °C. This study is limited to hexagonal phase with a C<sub>12</sub>E<sub>10</sub>:H<sub>2</sub>O(50 w/w%). However, hexagonal LC phase is stable and appears in a wide range of surfactant concentrations (40-70%).

The hexagonal LC phase of C<sub>12</sub>E<sub>10</sub>:H<sub>2</sub>O(50 w/w%) binary mixture was determined by POM. The primary identification of liquid crystalline phase involves a magnified view of a thin sample of a mesogenic material placed between crossed

polarisers. The arrangement of molecules was identified by the microscopic texture. Since the polarisers are crossed the isotropic disordered phase and cubic mesophase remain polarised, the light is unaffected (i.e. no light passes through the analyser, second, upper polariser). However, when an anisotropic birefringence medium is present the light is not extinguished and an optical texture appears that gives information about alignment of molecules within the medium. Hexagonal LC phase displays fan optical birefringence texture between crossed polarisers [45,69,113], Figure 12(A). One can see alternation of bright and dark regions.  $H_1$  LC phase consists of hexagonally packed rod-like surfactant aggregates and solvent molecules between them. Thus, blackness reveals isotropic disordered medium i.e. solvent reach regions, while brightness anisotropy i.e. ordered aggregates.

### **3.1. Phase Properties of $AgNO_3$ in $C_{12}E_{10}$ Type Surfactants**

Poly(ethylene oxide) (PEO)-type surfactants found their utilization in industry daily life and science. PEO based polymer electrolytes with inorganic fillers and high molecular weight polymers are polymer ionic conductors [68-69, 72-73]. It was found that conductivity is highly dependent on the concentration of inorganic salt (used as filler) and often is limited to the narrow salt concentration range [69-70]. Nonionic surfactants have been used as both reductants and stabilizers preventing aggregation of nanoscaled particles in different media. However high polydispersity and stability of the nanoparticles as well as accurate control of the size and fabrication of the ordered arrays of nanoscaled metals were not completely achieved. Lyotropic liquid crystalline phase of  $C_nE_m$  type surfactants revealed

themselves as good templates for synthesis of mesoporous silica and nanoscaled metal particles [50,108].

An obvious conclusion comes out of the above mentioned studies which are based on PEO-type surfactants. The particular property of the  $C_nE_m$  surfactants can be "improved" by additives and/or changes in surrounding media but these are efficient as long as initial property of surfactant does not change.

The properties of  $C_{12}E_{10}:H_2O(50 \text{ w/w\%}):HNO_3$  will be studied in conditions where the system may suffer during the synthesis of silver containing mesoporous silica films. The first part of the work is devoted to the investigation of the effect of added salt and solvent evaporation on the LC phase of  $C_{12}E_{10}:H_2O(50 \text{ w/w\%}):HNO_3$  system. In particular, how much of silver nitrate can be introduced into hexagonal mesophase of  $C_{12}E_{10}:H_2O(50 \text{ w/w\%}):HNO_3$  without a change in the preformed mesostructure.

### 3.1.1. Polarized Optical Microscopy Images

The phase properties of  $C_{12}E_{10}:H_2O(50 \text{ w/w\%}):HNO_3$  upon addition of silver nitrate can be revealed by phase diagram built up as a function of salt concentration. To create a phase diagram samples with the range of  $0.0 = r = 2.0$  where  $r$  is  $Ag^+/C_{12}E_{10}$  molar ratios were analyzed. The mixture was pressed between glass

plates where the glass surface generally imposes an additional order on the liquid crystalline domains. Randomly oriented cylinders will be ordered with the cylinders axes parallel to the glass surface in the hexagonal phase, whereas lamellar phases acquire an orientation where lamellae are parallel to the glass plates. In order to visualize the structure of the mesophases, the heated samples were observed under POM. Upon cooling down the isotropic liquid (heated samples are always isotropic, melting) natural texture of the sample results. So the orientation of the sandwiched sample along the glass surface could only be achieved when preformed liquid crystalline material was applied. POM is reliable and appropriate technique to study phase behavior of anisotropic phases.

The system to begin with  $\text{AgNO}_3/\text{C}_{12}\text{E}_{10}:\text{H}_2\text{O}(50 \text{ w/w\%}):\text{HNO}_3$  with  $r=0.0$   $\text{Ag}^+/\text{C}_{12}\text{E}_{10}$  molar ratio which displays fan optical birefringent texture. The clear, transparent, dense gels with  $0.0 \leq r \leq 0.6$  where  $r$  is  $\text{Ag}^+/\text{C}_{12}\text{E}_{10}$  molar ratios and weakly opaque gels with  $0.6 < r \leq 0.8$   $\text{Ag}^+/\text{C}_{12}\text{E}_{10}$  molar ratios display well resolved optical fan texture, Figure 12(A). The liquid-like samples of higher ratio ( $0.8 < r \leq 1.2$ ) are weakly anisotropic and/or do not display birefringent fan texture between crossed polars, Figure 12(B), and 12(C). POM images of solid-like high  $\text{AgNO}_3$  containing samples ( $1.5 \leq r \leq 2.0$ ) are anisotropic but do not have a fan optical texture, Figure 12(C), and 12(D). The samples sandwiched between glass slides were monitored under POM with time. The samples with  $\text{Ag}^+/\text{C}_{12}\text{E}_{10}$  molar ratios below 0.7 became isotropic after  $\sim 10$  hours upon aging under ambient conditions. Random optically birefringent formations of different shapes and forms were observed for mixtures with  $0.7 \leq r \leq 0.9$ . The POM image of aged sample with  $r =$

1.2 appeared anisotropic and displayed in Figure 12(D). The samples of  $1.5 \leq r < 2.0$  preserve their initially formed optical textures during aging.

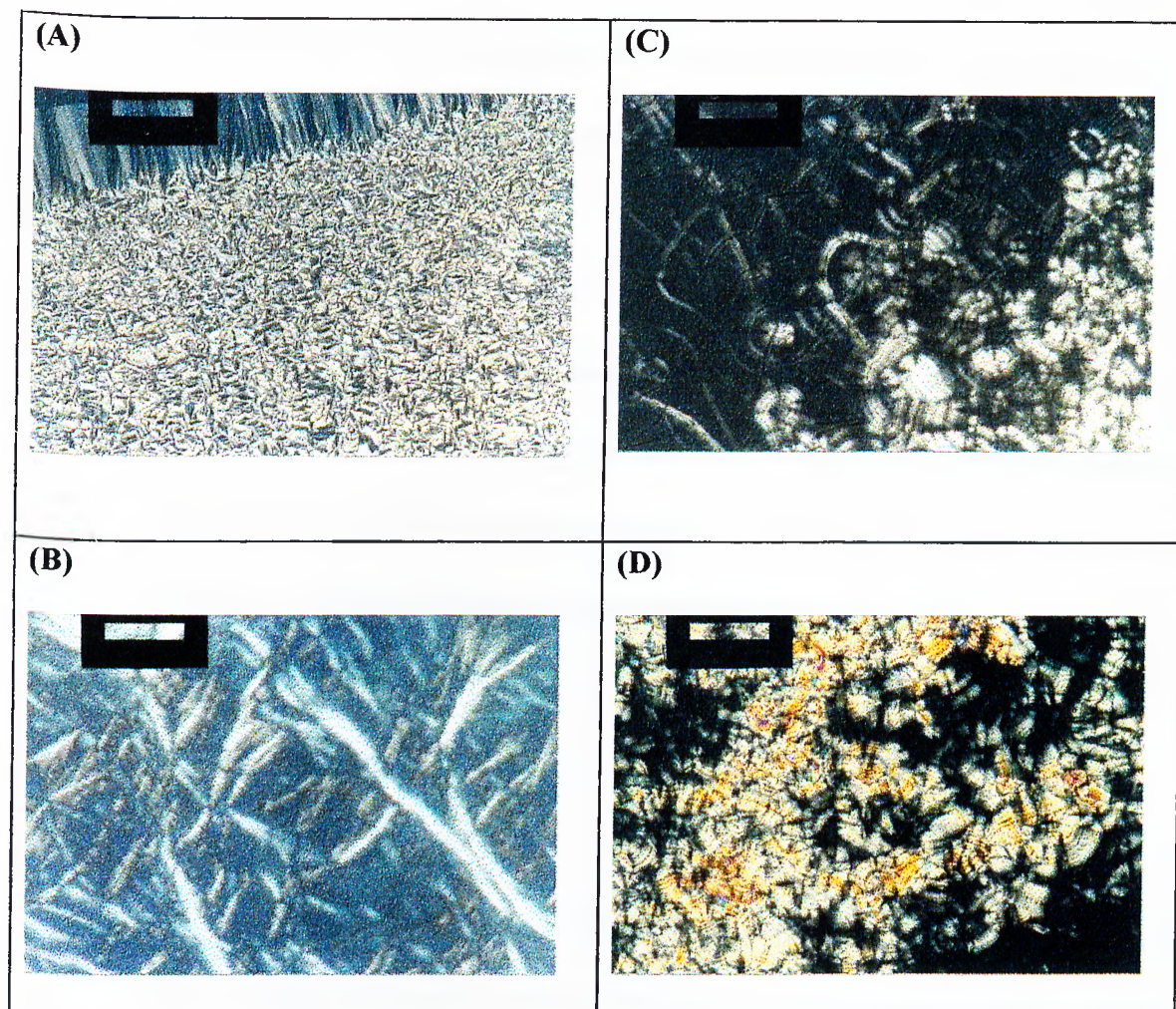


Figure 12. POM images between crossed polarizers of (A) fan texture, (B), (C) weakly anisotropic, (D) anisotropic phases

The samples, which are sealed in vials and kept in the dark, undergo changes. The aged mixtures with  $\text{Ag}^+/\text{C}_{12}\text{E}_{10}$  molar ratios up to 0.8 remained unchanged. However, white solid has formed over transparent gel, from  $r = 0.9$ , and

gray gel-like, from  $r = 1.2$ , mixtures upon aging. Figure 12(C) shows the optical texture of white solid layer, while gels displayed fan texture, which remains with time. The mixture with  $r = 1.5$  has two phases: white solid at the bottom of the vial and transparent gel, the upper part. The POM image of gel is anisotropic and displays fan texture, resembling the hexagonal mesophase. The optical birefringent texture of most concentrated sample does not change by aging.

In contrast to well detected optical birefringent texture of  $H_1$  mesophase, POM images of V mesophase and another LC phases as well as boundary regions between mesophases are not easy to determine using POM. Therefore other methods are required to build neat phase diagrams. FT-IR spectroscopy was used in an attempt to study the behavior of template during the processing.

### 3.1.2. Mid-IR Spectral Studies

The properties of  $C_{12}E_{10}:H_2O(50 \text{ w/w\%}):HNO_3$  system containing silver nitrate is highly dependent on the structural order of surfactant-water phase. The geometry of lyotropic liquid crystals, LLC, is influenced by the structure and functionality of the amphiphile used, the concentration of additives or solvents, and the temperature of the system. According to experimental conditions the temperature was kept as ambient and solvent content was unchanged. Thus the phase formed by LLC is altered by either changing the structure of hydrophobic portion of the surfactant or by altering of hydrophilic head groups.

It has been concerned that the hexagonal LC phase of binary PEO type surfactant-water system consists of amphiphile molecules micellized as cylinders containing fluid hydrocarbon interior with the polar groups on the surface. Within local uniform domains the cylindrical micelles disposed in a regular two-dimensional hexagonal array with intervening water [68-69]. It is believed that a rather strong interaction acts between the hydrophilic poly(ethylene oxide) chain and water in fluid phase and plays an important role in determining the solution properties and mesomorphic phase behavior [122-124].

The studies dealing with PEO surfactant-salt systems suggest in formation of weak bonds between metal ions and oxygen PEO head groups. Metal-to-oxygen bonding imparts the slight cationic character to the head groups [70-71,74,119]. Thus we expect to trace the effect of salt added to the  $C_{12}E_{10} \cdot H_2O(50 \text{ w/w}\%):HNO_3$  system by investigation of ethylene oxide  $(EO)_m$  units.

FT-IR spectroscopy was extensively used as a technique sensitive for the presence of hydrogen bonds, conformation of molecules, phase changes of materials. The behavior of PEO-type surfactants in the aqueous medium has been widely investigated [122-123]. It was found that hydrogen bonding between water and POE chain of the surfactant becomes stronger in the order liquid < mesophase < solid [122-123]. The detailed studies of carbon-hydrogen stretching ( $\nu\text{-CH}_2$ ) modes and carbon-hydrogen bending ( $\delta\text{-CH}_2$ ) modes in the regions between 2960 and 2820  $\text{cm}^{-1}$ , and 1500 and 1220  $\text{cm}^{-1}$ , respectively provide information about surfactant poly(ethylene oxide) chain with respect to the environment.

The IR spectra of freshly prepared, homogeneous  $\text{AgNO}_3/\text{C}_{12}\text{E}_{10}\cdot\text{H}_2\text{O}(50 \text{ w/w\%}):\text{HNO}_3$  mixtures with different  $\text{Ag}^+/\text{C}_{12}\text{E}_{10}$  molar ratios ( $r$ ) and pure surfactant are shown in Figure 13.

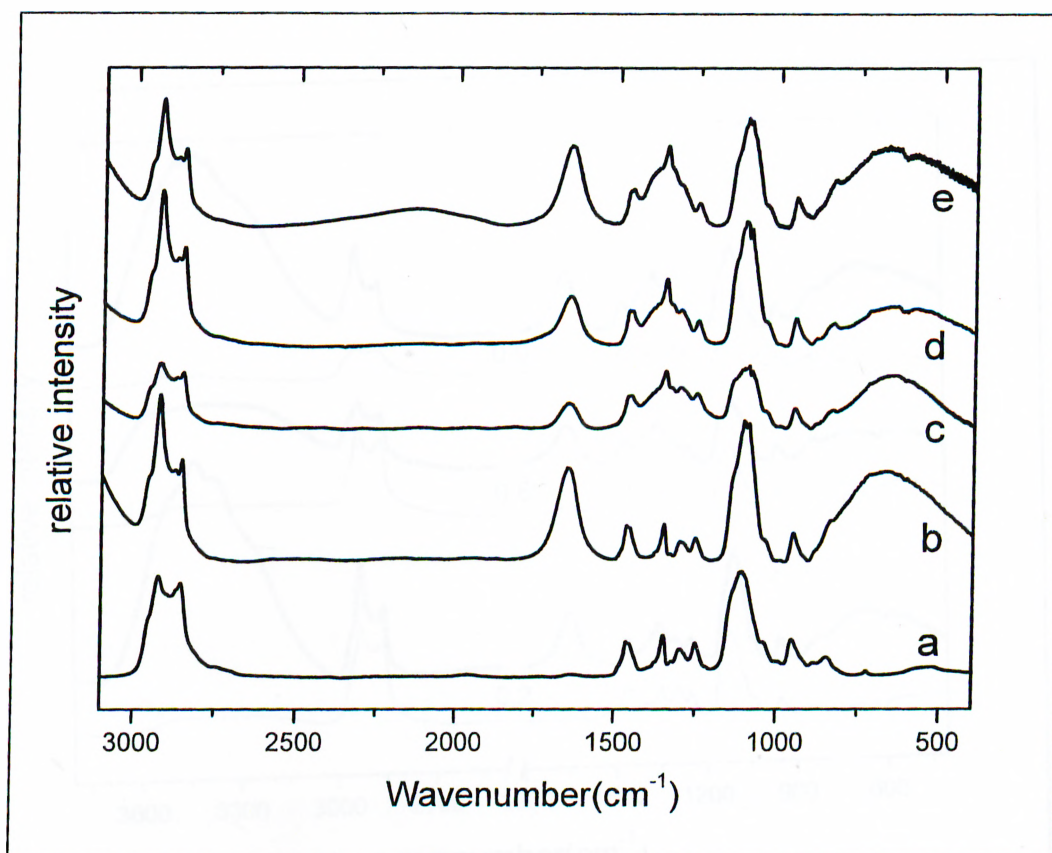


Figure 13. FT-IR absorption spectra of (a) pure  $\text{C}_{12}\text{E}_{10}$ , (b)  $\text{C}_{12}\text{E}_{10}\cdot\text{H}_2\text{O}(50 \text{ w/w\%}):\text{HNO}_3$ , (c)  $0.1 \text{ AgNO}_3/\text{C}_{12}\text{E}_{10}\cdot\text{H}_2\text{O}(50 \text{ w/w\%}):\text{HNO}_3$ , (d)  $0.5 \text{ AgNO}_3/\text{C}_{12}\text{E}_{10}\cdot\text{H}_2\text{O}(50 \text{ w/w\%}):\text{HNO}_3$ , (e)  $0.9 \text{ AgNO}_3/\text{C}_{12}\text{E}_{10}\cdot\text{H}_2\text{O}(50 \text{ w/w\%}):\text{HNO}_3$

The  $\delta\text{-CH}_2$  bending vibration modes become difficult to analyze because of the broadening of the bands due to increasing of nitrate concentration. The changes are drastic after solvent evaporation in samples with  $r > 0.4$  as well as with aging of

samples with  $r > 0.8$ . The IR peaks of the samples with low ( $0.1 = r < 0.5$ )  $\text{Ag}^+$ /surfactant molar ratios do not shift but become sharper and better resolved as solvent is evaporated, see Figure 14. The significant changes are traced on comparison of IR spectra of solution with  $r = 0.5$  before and after water evaporation.

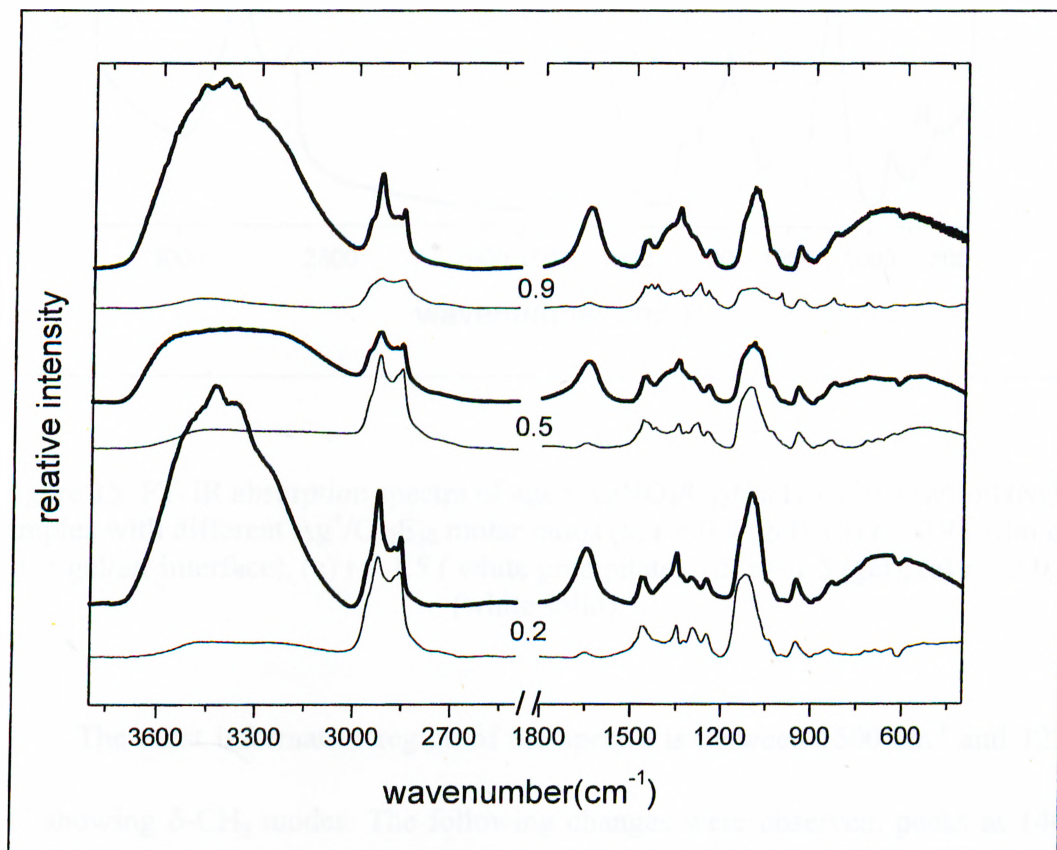


Figure 14. FT-IR absorption spectra for  $\text{AgNO}_3/\text{C}_{12}\text{E}_{10}:\text{H}_2\text{O}(50 \text{ w/w}\%):\text{HNO}_3$  -solid lines,  $\text{AgNO}_3/\text{C}_{12}\text{E}_{10}:\text{H}_2\text{O}:\text{HNO}_3$  - normal lines. The  $\text{Ag}^+/\text{C}_{12}\text{E}_{10}$  molar ratios indicated along the spectra

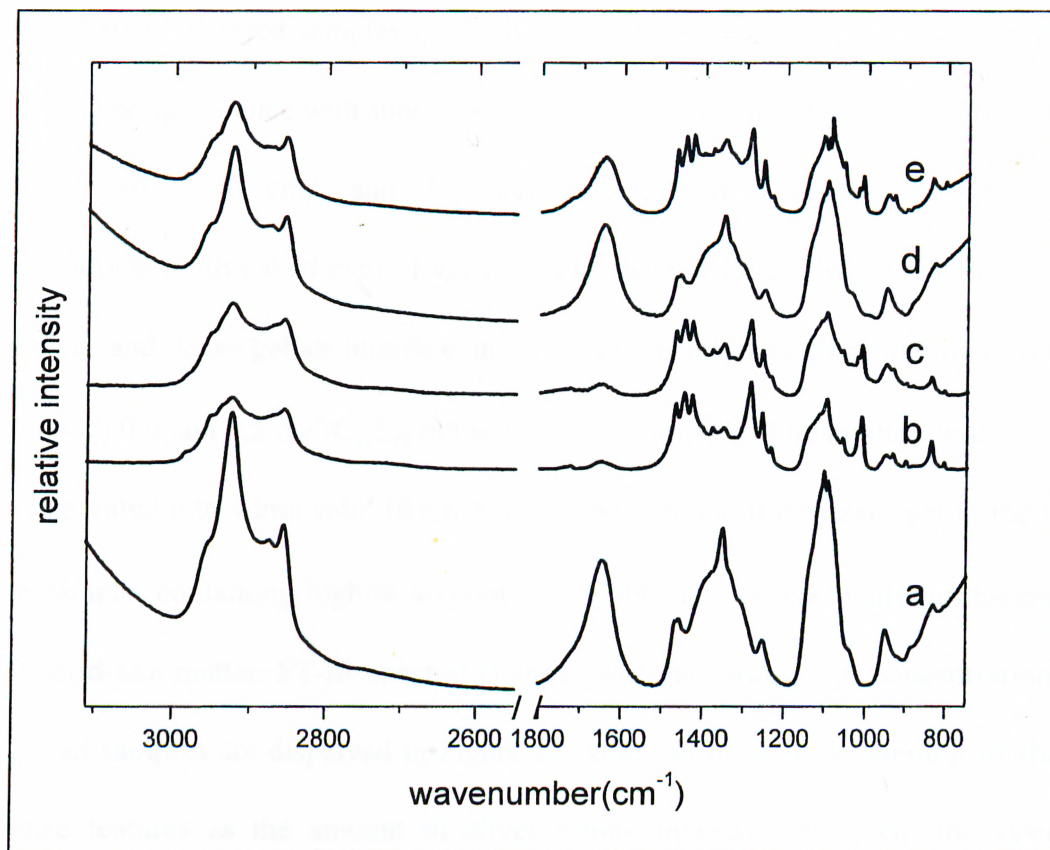


Figure 15. FT-IR absorption spectra of aged  $\text{AgNO}_3/\text{C}_{12}\text{E}_{10}:\text{H}_2\text{O}(50 \text{ w/w}\%):\text{HNO}_3$  samples with different  $\text{Ag}^+/\text{C}_{12}\text{E}_{10}$  molar ratios (a)  $r = 0.9$  (gel), (b)  $r = 0.9$  ( film on the gel/air interface), (c)  $r = 1.5$  ( white precipitate), (d)  $r = 1.5$  (gel), (e)  $r = 2.0$  (white solid)

The most informative region of the spectra is between  $1500 \text{ cm}^{-1}$  and  $1220 \text{ cm}^{-1}$  showing  $\delta\text{-CH}_2$  modes. The following changes were observed: peaks at  $1467 \text{ cm}^{-1}$  and  $1446 \text{ cm}^{-1}$  become sharper and more intense, a new peak appears at  $1427 \text{ cm}^{-1}$ , the peak at  $1305 \text{ cm}^{-1}$  shifts to lower wavenumber by  $\Delta\nu \cong 20 \text{ cm}^{-1}$ , the peak at  $1250 \text{ cm}^{-1}$  slightly shifts and appears as a sharper peak at  $1256 \text{ cm}^{-1}$ . The correlation between spectra of solutions with  $r > 0.5$  before and after water evaporation respectively resembles those at  $r \cong 0.5$ . So the addition of  $\text{AgNO}_3$  causes broadening of the bands in the region of  $\delta\text{-CH}_2$  in solutions with  $\text{C}_{12}\text{E}_{10}:\text{H}_2\text{O}(50 \text{ w/w}\%):\text{HNO}_3$  while sharp intense peaks appear in the spectra of dried samples. By following the

spectral trend of dried samples from low concentrations of silver nitrate to higher, one can see appearance with subsequent increase in intensity of peaks at 1467, 1446, 1427, 1286, 1256  $\text{cm}^{-1}$ , and the peak at 1350  $\text{cm}^{-1}$  becomes broader. The observations (with naked eye) of aged samples revealed that a white film forms on the clear and dense gel/air interface and gray gel/air interface of sealed mixtures in vials with 0.9 and 1.2  $\text{Ag}^+/\text{C}_{12}\text{E}_{10}$  molar ratios, respectively. The mixture with  $r \cong 1.5$  has separated into white solid-like part at the bottom and transparent gel at the top. The sample, containing highest amount of  $\text{AgNO}_3$  ( $r \cong 2$ ) was white homogenous soft solid-like matter. FT-IR spectral changes with increasing  $\text{Ag}^+$  concentration in the aged samples are displayed in Figure 15. One can observe developing of sharp intense features as the amount of silver nitrate increases. As well, the system undergoes phase separation into gel and solid matter. The peaks at 1467, 1446, 1350, 1305 and 1250  $\text{cm}^{-1}$  dominate in the  $\delta\text{-CH}_2$  spectral region of samples in the gel phase. The intense and sharp peaks at 1467, 1446, 1427, 1286, 1256 and 1234  $\text{cm}^{-1}$  indicate white solid-like phase in the samples. So similar changes take place in the system upon increase of salinity and/or solvent evaporation. The effect of silver nitrate on the properties of  $\text{C}_{12}\text{E}_{10}:\text{H}_2\text{O}(50 \text{ w/w\%}):\text{HNO}_3$  system can be clarified by detailed analysis of IR spectra of system with  $r = 0.9$  under different conditions, see Figure 16. The spectral region between 1500 and 1220  $\text{cm}^{-1}$  can be divided into three parts with respect to carbon-hydrogen vibration modes.

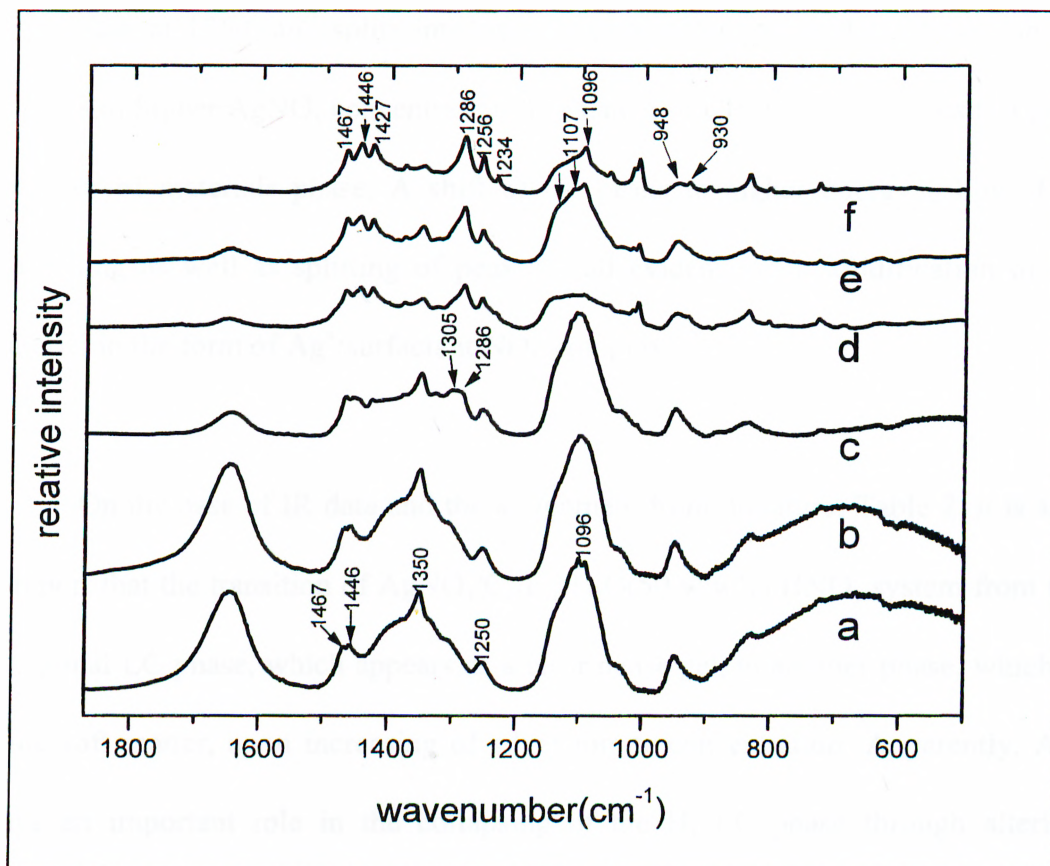


Figure 16. FT-IR spectra recorded for  $\text{AgNO}_3:\text{C}_{12}\text{E}_{10}:\text{H}_2\text{O}:\text{HNO}_3$  ( $r = 0.9$ ) composite (a)-(d) upon water evaporation and (e)-(f) after aging in the frequency range  $2000\text{-}500\text{ cm}^{-1}$

The peaks at  $1467\text{ cm}^{-1}$  and  $1446\text{ cm}^{-1}$  belong to  $\text{CH}_2$  scissoring vibration mode known to be sensitive to the environment. Sharpening and intensification of these peaks indicate intermolecular constrain of  $(\text{EO})_m$  units. A new peak at  $1427\text{ cm}^{-1}$  appears upon drying and/or aging. The band at  $1350\text{ cm}^{-1}$  was observed at all conditions employed. It refers to  $\text{CH}_2$  wagging mode which appears in the gauche conformation of the  $\text{O}-(\text{CH}_2)_2\text{-O}$  unit [16,121]. The broadening and decreasing the intensity of this band and then splitting into a new peak at  $1349\text{ cm}^{-1}$  and a shoulder at  $1363\text{ cm}^{-1}$  suggests conformation change of PEO chain. The peak at  $1305\text{ cm}^{-1}$  shifts to higher energy by  $\Delta\nu \cong 20\text{ cm}^{-1}$  upon loss of small quantity of water. The

broad peak at  $1250\text{ cm}^{-1}$  splits into two peaks at  $1256\text{ cm}^{-1}$  and  $1234\text{ cm}^{-1}$  in the samples of higher  $\text{AgNO}_3$  concentration. The nature of  $\text{CH}_2$  twisting modes is a good indicator of materials phase. A shift of the peaks to higher energy followed by sharpening as well as splitting of peak are all evidences for solidification of the material in the form of  $\text{Ag}^+/\text{surfactant}/\text{NO}_3^-$  complex.

On the base of IR data and the assignment from literature, Table 2, it is safe to report that the transition of  $\text{AgNO}_3/\text{C}_{12}\text{E}_{10}:\text{H}_2\text{O}(50\text{ w/w\%}):\text{HNO}_3$  system from the hexagonal LC phase, which appears as a clear dense gel, to another phase, which is white soft matter, upon increasing of silver nitrate concentration. Apparently,  $\text{Ag}^+$  plays an important role in the collapsing of the  $\text{H}_1$  LC phase through altering hydrophilicity of PEO head groups. If this is true, one would expect a down-shift of the maximum of C-O-C stretching mode from the value  $1116\text{ cm}^{-1}$  recorded for the amorphous pure polyether phase [119]. A broad single peak, centered at  $1096\text{ cm}^{-1}$ , Figure 16, confirms interactions between PEO and salt leading to the formation of transient cross-links, which weaken the C-O polyether bonds. Appearance of the triplet peak at  $1130, 1096, 1078\text{ cm}^{-1}$  in C-O-C stretching vibration region, instead of single peak, suggest that silver ions interact with (EO) unit with a different strength and stiffens PEO chain and thereby induces phase transition.

Thus, the effect of silver nitrate additives on the properties of the  $\text{C}_{12}\text{E}_{10}:\text{H}_2\text{O}(50\text{ w/w\%}):\text{HNO}_3$  system was discovered as an initiator for the phase transition, through formation of  $\text{Ag}^+/\text{C}_{12}\text{E}_{10}/\text{NO}_3^-$  complex.

Table 2. Molecular vibration assignments for the oxyethylene chain of PEG400<sup>[125]</sup>,  
 PEG400/(LiCl)<sub>x</sub><sup>[121],a</sup>, PEO<sup>[126]</sup>, Ag<sup>+</sup>/PEO/NO<sub>3</sub><sup>a</sup>

Wavenumber(cm <sup>-1</sup> )					
PEG400 <sup>[125]</sup> liquid	PEG400/(LiCl) <sub>x</sub> <sup>[121]</sup>	PEO <sup>[126]</sup> cryst.	PEO <sup>[126]</sup> molten	Ag <sup>+</sup> /PEO/NO <sub>3</sub> solid	Assignments
1475	1473(m)	1466		1467(m)	CH <sub>2</sub>
1453	1455(m)	1454	1457	1454(sh)	scissoring
	1360(sh)	1360		1363(sh)	CH <sub>2</sub>
	1350(m)	1342	1349	1349(m)	wagging
1303				1305(sh)	
1286	1294(m)	1281	1297	1286(vs)	CH <sub>2</sub>
1244	1248(m)	1241	1251	1256(s)	twisting
		1234		1234(sh)	
1147	1148(w)	1148	1140	1130(sh)	
	1123(vs)	1116		1095(vs)	CO
1105		1110	1107	1107(sh)	stretching
1064	1031(w)			1078(sh)	
		961			CH <sub>2</sub>
	953(m)	947	947	948(m)	rocking
				930(w)	

<sup>a</sup>Relative intensities are reported in parenthesis; vs: very strong, s: strong, m: medium, w: weak, sh: shoulder.

This white soft solid is detected by the appearance of strong IR peaks at 1467, 1446, 1427, 1286, 1256, and 1234  $\text{cm}^{-1}$  in the carbon-hydrogen deformation vibration region between 1500 and 1220  $\text{cm}^{-1}$ .

FT-IR spectroscopy was used in an attempt to find out whether it is possible to establish the mesophase through IR spectral changes of  $\nu\text{-CH}_2$  known to be very sensitive to the environment. The appearance of series of carbon-hydrogen stretching bands between 2980 and 2700  $\text{cm}^{-1}$  support interactions between polar molecules.

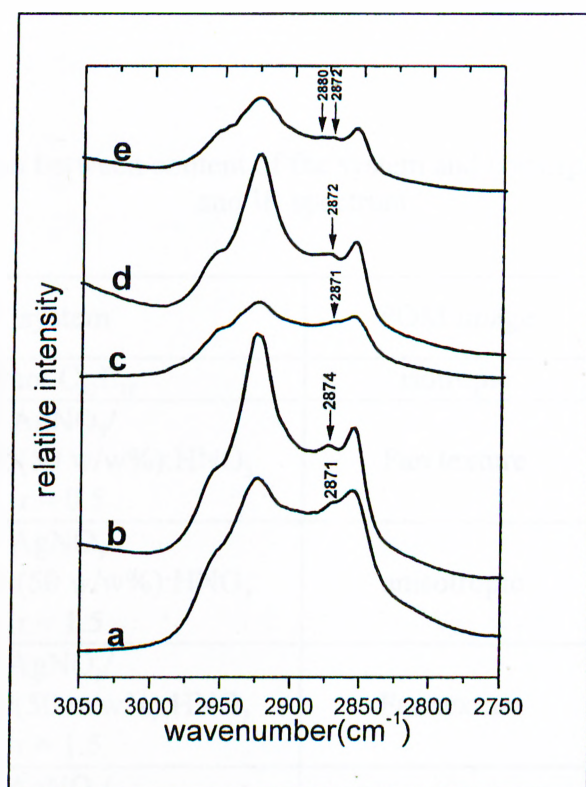


Figure 17. FT-IR absorption spectra of (a) pure  $\text{C}_{12}\text{E}_{10}$ , (b)  $r = 0.5$   $\text{AgNO}_3/\text{C}_{12}\text{E}_{10}:\text{H}_2\text{O}(50 \text{ w/w}\%):\text{HNO}_3$ , (c)  $r = 1.5$   $\text{AgNO}_3/\text{C}_{12}\text{E}_{10}:\text{H}_2\text{O}(50 \text{ w/w}\%):\text{HNO}_3$  precipitate, (d)  $r = 1.5$   $\text{AgNO}_3/\text{C}_{12}\text{E}_{10}:\text{H}_2\text{O}(50 \text{ w/w}\%):\text{HNO}_3$  gel, (e)  $r = 2.0$   $\text{AgNO}_3/\text{C}_{12}\text{E}_{10}:\text{H}_2\text{O}(50 \text{ w/w}\%):\text{HNO}_3$

The IR spectra of  $C_{12}E_{10}$  surfactant in different surrounding media are plotted in Figure 17. Spectra **b** and **d** show intense, sharp, well-resolved peaks and thereby support high structural order of surfactant self-assembly. Spectra **a** and **c** can be assigned to disordered materials. The existence of two peaks at 2880 and 2872  $\text{cm}^{-1}$  in carbon-hydrogen stretching region of ethoxy methylenes, spectrum **e**, may suggest an increase in crystallinity of EO chain of the surfactant. If one combines this straightforward analysis of IR spectra and content of the samples from which particular spectrum was taken along with POM images, it will give a correlation between mesophase and extent of order of surfactant self-assembly. These are summarized in Table 3.

Table 3. Correlation between content of the system and corresponding POM image and IR spectrum

spec tra	system	POM image	remarks
<b>a</b>	Pure $C_{12}E_{10}$	isotropic	
<b>b</b>	$\text{AgNO}_3/$ $C_{12}E_{10}:\text{H}_2\text{O}(50 \text{ w/w}\%):\text{HNO}_3$ $r = 0.5$	Fan texture	Freshly prepared
<b>c</b>	$\text{AgNO}_3/$ $C_{12}E_{10}:\text{H}_2\text{O}(50 \text{ w/w}\%):\text{HNO}_3$ $r = 1.5$	anisotropic	White precipitate
<b>d</b>	$\text{AgNO}_3/$ $C_{12}E_{10}:\text{H}_2\text{O}(50 \text{ w/w}\%):\text{HNO}_3$ $r = 1.5$	Fan texture	Dense, clear gel
<b>e</b>	$\text{AgNO}_3/$ $C_{12}E_{10}:\text{H}_2\text{O}(50 \text{ w/w}\%):\text{HNO}_3$ $r = 2.0$	anisotropic	

On the basis of the information presented in the Table 3, it is clear that hexagonal LC phase is the most ordered phase of the surfactant, which displays intense, sharp features in  $\nu$ -CH<sub>2</sub> stretching region. Hydrogen bonding provides just small shifts towards lower energy, as mentioned along the spectra in Figure 17, and can not be used for determination of the physical state of the system.

### **3.2. Mesoporous Silica Templated by AgNO<sub>3</sub>:C<sub>12</sub>E<sub>10</sub>:H<sub>2</sub>O**

A lot of efforts have been devoted to developing a simple route to tailor mesoporous materials and to understand the role of starting materials and synthetic conditions to create resulting material with desirable size, shape, and order of the pores. It has been concerned that inorganic material with dimensions ranging from angstrom to micrometers can be synthesized through sol-gel reaction of alkoxides in the presence of molecular assemblies of surfactant or related structure-directing agents [48,50,52,76-77,95]. Surfactant can organize silica in several geometries depending on structure and functionality of amphiphile used through the mediation of electrostatic, hydrogen-bonding, covalent and van der Waals interactions.

Initially formed mesophase of surfactant and solvent mixture at fixed temperature and composition undergoes structural changes during the generation and condensation of silica network. So inorganic framework and surfactant arrays affect and control one another in cooperative fashion. Suitable reaction conditions and

starting materials can be chosen to control surfactant molecular packing in order to obtain the expected mesophase product.

Loading of mesoporous silica with different additives can modify and/or induce new properties to silicates, thus expanding an already wide scope of its application. The presence of metals promotes applications involving electron transfer or magnetic interactions as well as improves ability of mesoporous ceramics as catalysts, sorbents, and functional supports. Methods to incorporate metals into pores MCM-41 materials are incipient wetness impregnation, ion exchange or direct introduction during the synthesis of mesoporous materials. The last procedure ensures uniform deposition of metal ions or complexes inside the mesoporous silica. This synthetic route has been used to incorporate lithium [78], platinum [128], and transition metal [55] ions.

In this part of the work, method of incorporation of metal ions or complexes into pores of mesoporous silica by mixing salt of the metal with PEO-type nonionic surfactant, applied for lithium triflate [78], was tested for silver. PEO-type surfactant, denoted as  $C_{12}E_{10}$ , has proven successful to form bulk hexagonal LC phase in long range surfactant-to-water concentrations at room temperature. These properties of the surfactant along with the subsequent formation reactions of inorganic network provide:

- A high degree of control over the structure because the resulting ceramic oxide is a direct cast of the liquid crystalline template.
- The formation of hexagonal array of pores which prompt easy access to silver.

- The possibility of synthesising materials with desirable properties and high yield at room temperature and atmospheric pressure.
- The ability to obtain transparent monoliths, which, once a template is removed, could be suitable for separation process.

The interactions in the systems of silver nitrate-surfactant and [silver nitrate-surfactant]meso-SiO<sub>2</sub> are not well understood yet.

Our purpose was to synthesise mesoporous materials containing silver ions evenly distributed within hexagonally arranged pores. A broad range of AgNO<sub>3</sub>/C<sub>12</sub>E<sub>10</sub>:H<sub>2</sub>O(50 w/w%):HNO<sub>3</sub>/TMOS sample compositions was narrowed down to a range, Ag<sup>+</sup>/C<sub>12</sub>E<sub>10</sub> molar ratios between 0.0 < r < 0.9, where AgNO<sub>3</sub>/C<sub>12</sub>E<sub>10</sub>:H<sub>2</sub>O(50 w/w%):HNO<sub>3</sub> preserves the hexagonal LC phase. AgNO<sub>3</sub>/C<sub>12</sub>E<sub>10</sub>:H<sub>2</sub>O(50 w/w%):HNO<sub>3</sub> system will respond to any changes, which occur during formation of silica network. So the investigation of template behavior can give clues to understand how size, shape, order of pores can be tuned by gradual modification of supramolecular surfactant self-assembly by changing concentration of silver nitrate.

The thin films deposited on microscopic glass slide were observed by POM, relatively thinner films on the Si(100) wafer were examined by FT-IR spectroscopy, the films on the quartz were analyzed by UV-Vis spectroscopy.

### 3.2.1. POM Images

Investigation of silica matrix formation during sol-gel processing was based on POM images, which can directly be correlated with structure type. POM reveals unaltered optical texture during the progress of reaction, leading to the formation of rigid films. The freshly prepared films have transparent crack-free smooth surfaces and appear birefringent between crossed polars. The microscopic image, Figure 18, displays so-called fan-like texture that is an alternation of bright and dark regions but now darkness is caused by amorphous disordered silica network.

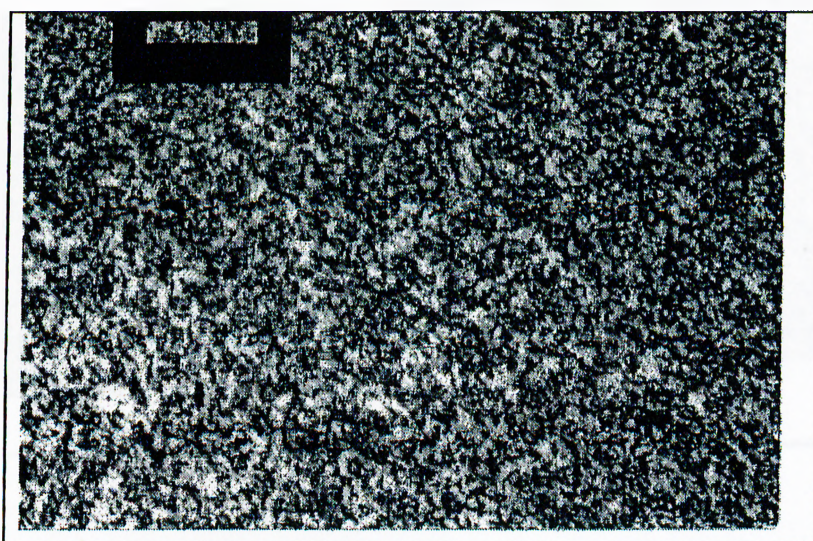


Figure 18. POM image of  $\text{AgNO}_3/\text{C}_{12}\text{E}_{10}:\text{H}_2\text{O}:\text{HNO}_3/\text{TMOS}$  fan-like texture

The POM images of the samples aged for 3 days showed significant changes. The surface of the films with  $\text{Ag}^+/\text{C}_{12}\text{E}_{10}$  molar ratios above 0.5 became white in color. Instead of previously observed fan-like texture, birefringent brushes of indefinite shapes and sizes were observed from white samples containing  $0.5 < r \leq$

0.8, Figure 19. The fan-like optical texture remains unchanged for transparent films with  $\text{Ag}^+/\text{C}_{12}\text{E}_{10}$  molar ratios below 0.5 and white films with  $r$  above 0.8.

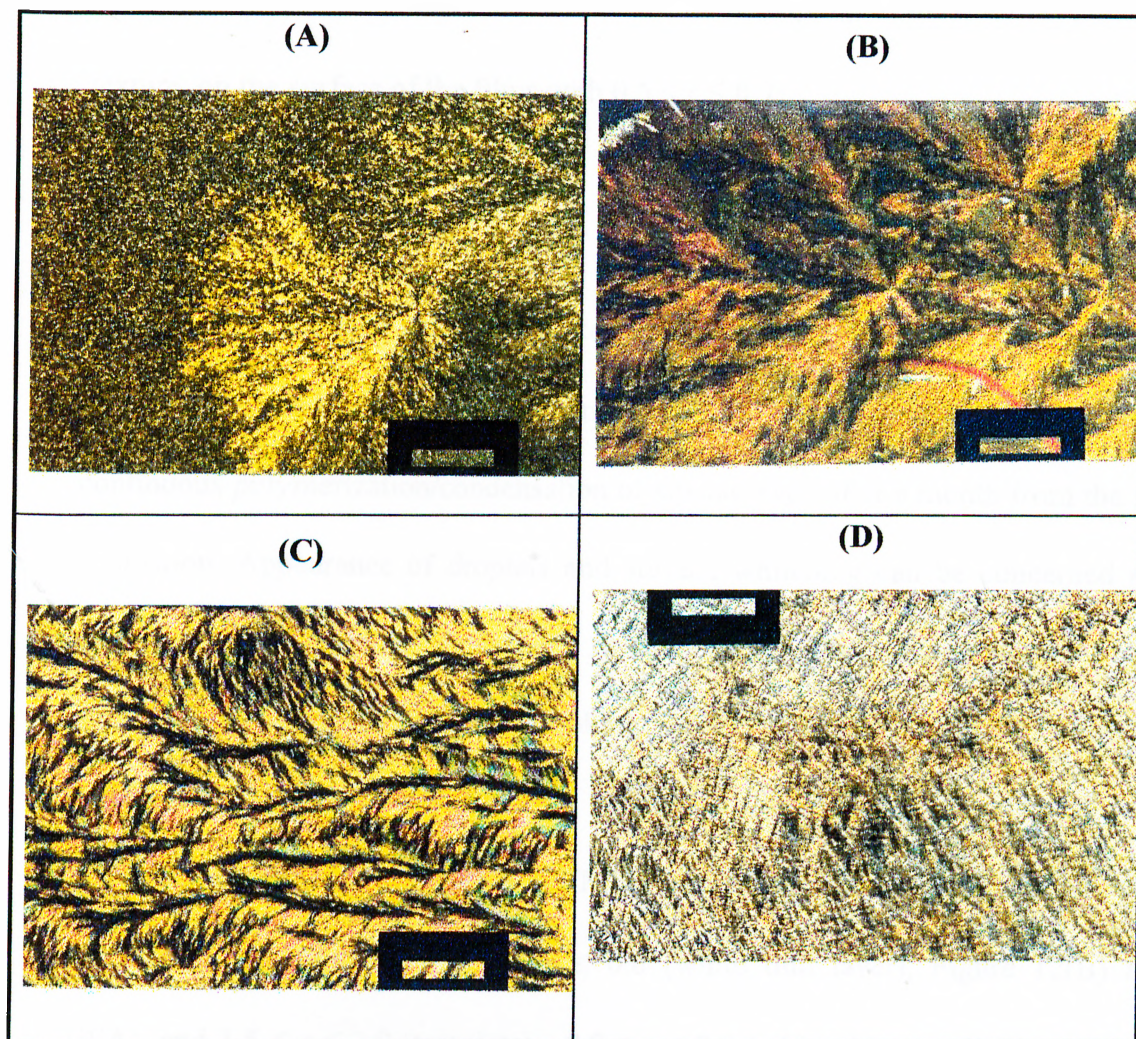


Figure 19. POM images between crossed polarizers of  $\text{AgNO}_3/\text{C}_{12}\text{E}_{10}:\text{H}_2\text{O}:\text{HNO}_3/\text{TMOS}$  with (A) 0.5, (B) 0.6, (C) 0.7, (D) 0.8  $\text{Ag}^+/\text{C}_{12}\text{E}_{10}$  molar ratios

The samples exposed to air for a month crack. The transparent films with  $0.0 < r \leq 0.3$  display droplets over fan-like texture when viewed under microscope. A brownish color covers a white thin layer on the film/air interface and becomes more

intense as concentration of silver nitrate increases from  $r = 0.6$  to  $0.9$ . The white thin layer can be easily wiped out, leaving behind a transparent film. The fan-like birefringent optical texture was observed after wiping, instead of a brush-like texture, on the surface of the films with  $0.5 < r \leq 0.7$ .

The similarity of the optical textures before and after addition of silica precursor (i.e. between fan and fan-like textures) predetermines hexagonal arrays of pores in the solid materials. The changes in POM images, taken in time, suggest continuous polymerization/condensation of silicate even after a month from the film deposition. Appearance of droplets and surface whitening can be concerned as a squeezed out of template, surfactants from the pores, during contraction of silica matrix due to polymerization and shrinking. The similarity of POM images between  $\text{AgNO}_3/\text{C}_{12}\text{E}_{10}:\text{H}_2\text{O}(50 \text{ w/w}\%):\text{HNO}_3$  template and white thin layer over  $\text{AgNO}_3/\text{C}_{12}\text{E}_{10}:\text{H}_2\text{O}(50 \text{ w/w}\%):\text{HNO}_3/\text{TMOS}$  film samples of  $\text{Ag}^+/\text{C}_{12}\text{E}_{10}$  molar ratios  $0.8 < r \leq 1.2$  (template) -  $0.5 < r \leq 0.8$  (white thin layer), Figure 12(B) and 19(A), and  $1.5 \leq r \leq 2.0$  (template) -  $0.8 \leq r \leq 0.9$  (white thin layer), Figure 12(D) and 19(D), is an evidence of identical nature of brushes formation before and after addition of TMOS. The brushes, which adorn the film surface by forming white thin layer, are optically active and have structures dependent on  $\text{Ag}^+/\text{C}_{12}\text{E}_{10}$  molar ratio. Notice that small amounts of silver nitrate in the template do not induce brushes formation.

### 3.2.2. PXRD Analysis

The powder x-ray diffraction, PXRD, has been used to investigate a microscopic structure of the materials synthesized in this work. It is one of the most powerful technique which provides information on structural ordering, structure type, quality and crystallinity of the materials. The method is based on Bragg's diffraction equation given below:

$$\lambda = d \sin(2\Theta),$$

where  $\lambda$  is wavelength of the radiation,  $d$  is the spacing between the repeating planes of crystalline or partially crystalline materials (in this work, mesoporous silica materials),  $\Theta$  is angle of incidence and "reflection" of the x-ray beam. The intensity and resolution of the reflections in mesoporous silica materials is based solely on the degree of ordering of 3-dimensional diffraction planes and arises from the electron density gradient between the silica walls and pores (surfactant in the uncalcined samples) [96]. A typical PXRD pattern of hexagonal mesoporous silica consists of three to five well-resolved diffraction lines [129]. The nature of diffraction lines, namely position, intensity, width and resolution are all related to the structure and the crystallinity of the materials. The materials studied in this work, however usually have single diffraction lines at low angles. This makes the assignment of the structure type hard to determine. At least three diffraction lines are required to determine the structure type. There are many publications in the literature of this type of materials on PXRD for all types of structure [13,16-17,55,127,129]. However, if the synthesis conditions are not properly established, there may be more than one phase (like mixture of hexagonal, lamella and cubic) in the samples. The

Tunneling Electron Microscopy, TEM, is usually the complimentary technique to determine the pore size and structure type. Table 4 lists PXRD diffraction data and unit cell parameters of lamellar, hexagonal and cubic phases of mesoporous silica materials with our data.

Table 4. PXRD data of different phases of mesoporous materials

Materials	Unit cell parameters (Å)	d-spacing (Å)	Mesophase
MCM-41 <sup>16</sup>	a=54.4	47.3(d <sub>100</sub> )	2d-hexagonal (p6m)
MCM-48 <sup>16</sup>	a=92.0	79.7(d <sub>100</sub> )	cubic (Ia3d)
MCM-50 <sup>16</sup>	a=37.9	32.8(d <sub>100</sub> )	lamellar
SBA-1 <sup>a, 16</sup>	a=97.0	84.0(d <sub>100</sub> )	cubic (Pm3n)
SBA-15 <sup>136</sup>	a=110.5	95.7(d <sub>100</sub> )	cubic (Ia3d)
SBA-2 <sup>a, 96</sup>	c/a= 1.61-1.63		
SBA-2 <sup>16</sup>	a=54.4, c=87.4 c/a=1.62	47.11(d <sub>100</sub> )	3d-hexagonal (P6 <sub>3</sub> /mmc)
SBA-3 <sup>a, 16</sup>	a=72.5	63.0(d <sub>100</sub> )	2d-hexagonal (p6m)
Ag <sup>+</sup> -MCM	a=55.8, c=90.2 c/a=1.62	48.3(d <sub>100</sub> ) 45.1(d <sub>002</sub> ) 42.2(d <sub>101</sub> )	3d-hexagonal (P6 <sub>3</sub> /mmc)

<sup>a</sup>silica-based mesoporous materials synthesized at low surfactant concentrations and low temperatures

In this study, PXRD was used to evaluate the structure type and d-spacing in our materials presented so far. PXRD patterns were recorded for samples with different  $\text{AgNO}_3$  concentrations. The patterns of samples with  $\text{Ag}^+/\text{C}_{12}\text{E}_{10}$  molar ratios up to 0.7 showed three diffraction lines at 42.2, 45.1, and 48.3 Å d-spacing Figure 20.

The inspection of PXRD patterns of samples with different  $\text{AgNO}_3$  contents reveals existence of sharp, narrow, intense diffraction lines at low angles for sample with 0.7  $\text{Ag}^+/\text{C}_{12}\text{E}_{10}$  molar ratio.

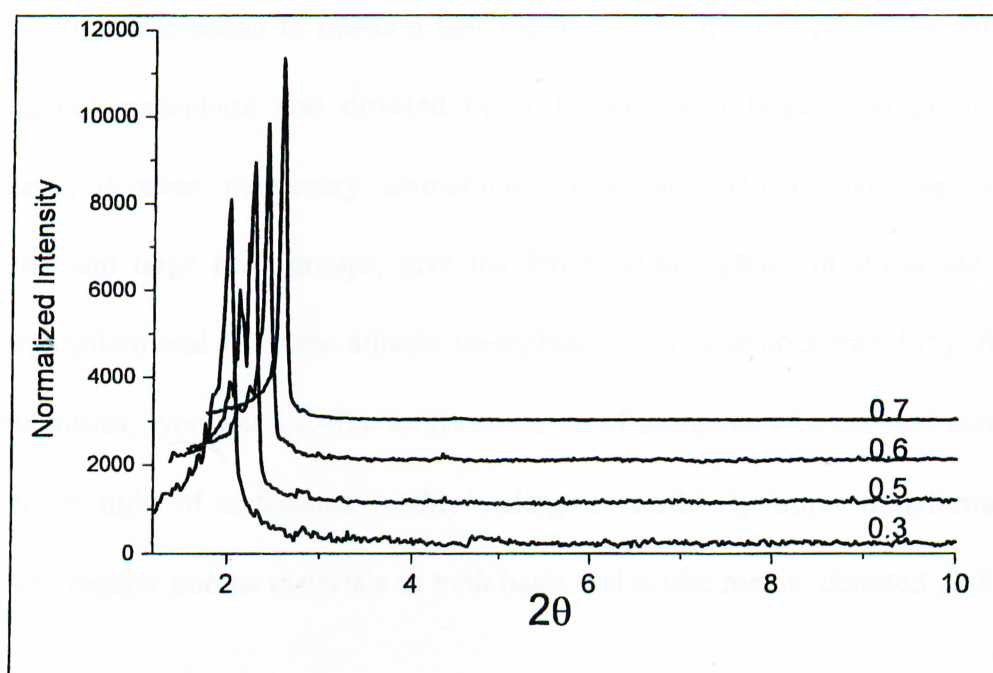


Figure 20. Low-angle PXRD patterns for silver-surfactant-silica mesophases.  $\text{Ag}^+/\text{C}_{12}\text{E}_{10}$  molar ratios are indicated along the spectra

This particular sample exhibits the highest structural order among the other reported samples, Figure 20. The presence of low angle diffraction lines and absence of high angle lines is a good indication of short-range order in these materials.

The PXRD patterns with  $r > 0.7$  display very broad peak at  $20^\circ 2\theta$  (the amorphous silica usually display very broad diffraction around this value) without low angle lines, overall, this indicates amorphous nature of silica. The materials synthesized in this work with  $r \leq 0.7$  can be indexed to 3-D hexagonal crystal structure type with a space group  $P6_3/mmc$  [55,128].

It is interesting to mention that the formation of silica materials with 3D-hexagonal mesophase was directed by surfactants with large head groups. For instance, divalent quaternary ammonium surfactants, which have high charge density and large head groups, give the  $Pm\bar{3}n$  (cubic) phase in surfactant water binary system and  $P6_3/mmc$  silicate mesophase at room temperature [55]. At low temperatures, lyotropic LC-like arrays made up of inorganic clusters and inorganic molecular units of surfactants, readily undergo reversible lyotropic transformations to form regular porous materials in both basic and acidic media, denoted as SBA-2 [16].

Regular porous silica materials with large inner surface area can be dimensionally tailored by  $\text{AgNO}_3/\text{C}_{12}\text{E}_{10}:\text{H}_2\text{O}:\text{HNO}_3$  template of  $0 \leq r \leq 0.7$   $\text{AgNO}_3$  to surfactant molar ratios.

### 3.2.3. FT-IR Spectroscopic Studies

The dimensional resolution of optical microscopy is limited by the wavelength of the light and also requires an optical contrast between phases. In contrast, IR absorption spectroscopy is sensitive to the environment on a scale of nanometer. The nature of IR transition implies that polar functionalities will have intense IR absorption bands. Understanding the nature of surfactant-solvent-salt system in the hexagonal LLC phase during tailoring of the mesoporous materials, it is possible to elucidate the process of formation of mesoporous molecular sieves through studying the template using FT-IR spectroscopy. The carbon-hydrogen vibration modes of the surfactant can be used to determine the head group (ethoxy group of the surfactant) ordering and hydrophobic interaction within the developing mesophase.

The FT-IR absorption spectra recorded for freshly prepared  $\text{AgNO}_3/\text{C}_{12}\text{E}_{10}:\text{H}_2\text{O}$  (50 w/w%): $\text{HNO}_3/\text{TMOS}$  thin films with  $0.0 < r \leq 0.9$   $\text{Ag}^+/\text{C}_{12}\text{E}_{10}$  molar ratios are depicted in the Figure 21.

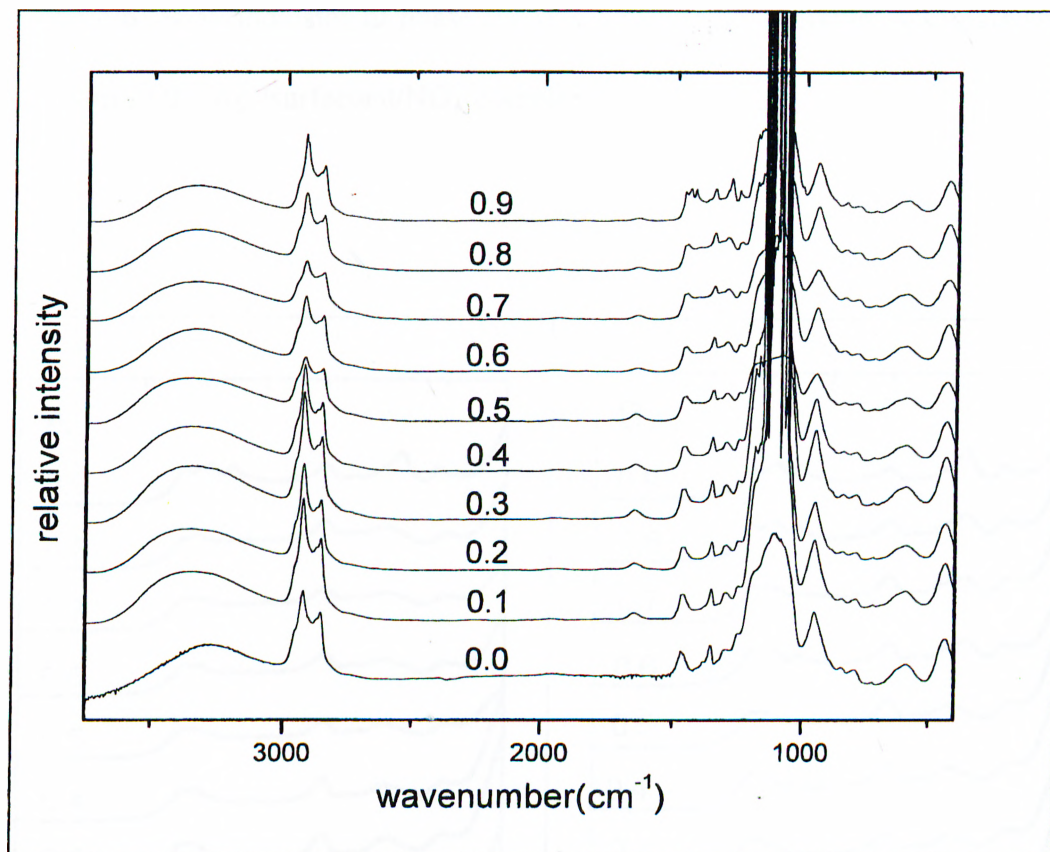


Figure 21. Mid FT-IR absorption spectra of  $\text{AgNO}_3/\text{C}_{12}\text{E}_{10}:\text{H}_2\text{O}:\text{HNO}_3/\text{TMOS}$  thin films. The  $\text{Ag}^+/\text{C}_{12}\text{E}_{10}$  molar ratios are indicated along the spectra

The frequency range  $1500\text{-}1220\text{ cm}^{-1}$  consists of  $\delta\text{-CH}_2$  deformation vibration modes of surfactant as well as nitrate ion. There are no significant changes in the spectra of silica samples with  $0.1 \leq r < 0.9$   $\text{Ag}^+/\text{C}_{12}\text{E}_{10}$  molar ratios, Figure 21. However, appearance of sharp well-resolved features at  $1467$ ,  $1446$ ,  $1427$ ,  $1286$ , and  $1256\text{ cm}^{-1}$  were detected by FT-IR for sample with highest silver content ( $r = 0.9\text{ Ag}^+/\text{C}_{12}\text{E}_{10}$

molar ratio) is an indicator of phase transition of template mixture associated with formation of the  $\text{Ag}^+/\text{surfactant}/\text{NO}_3^-$  complex.

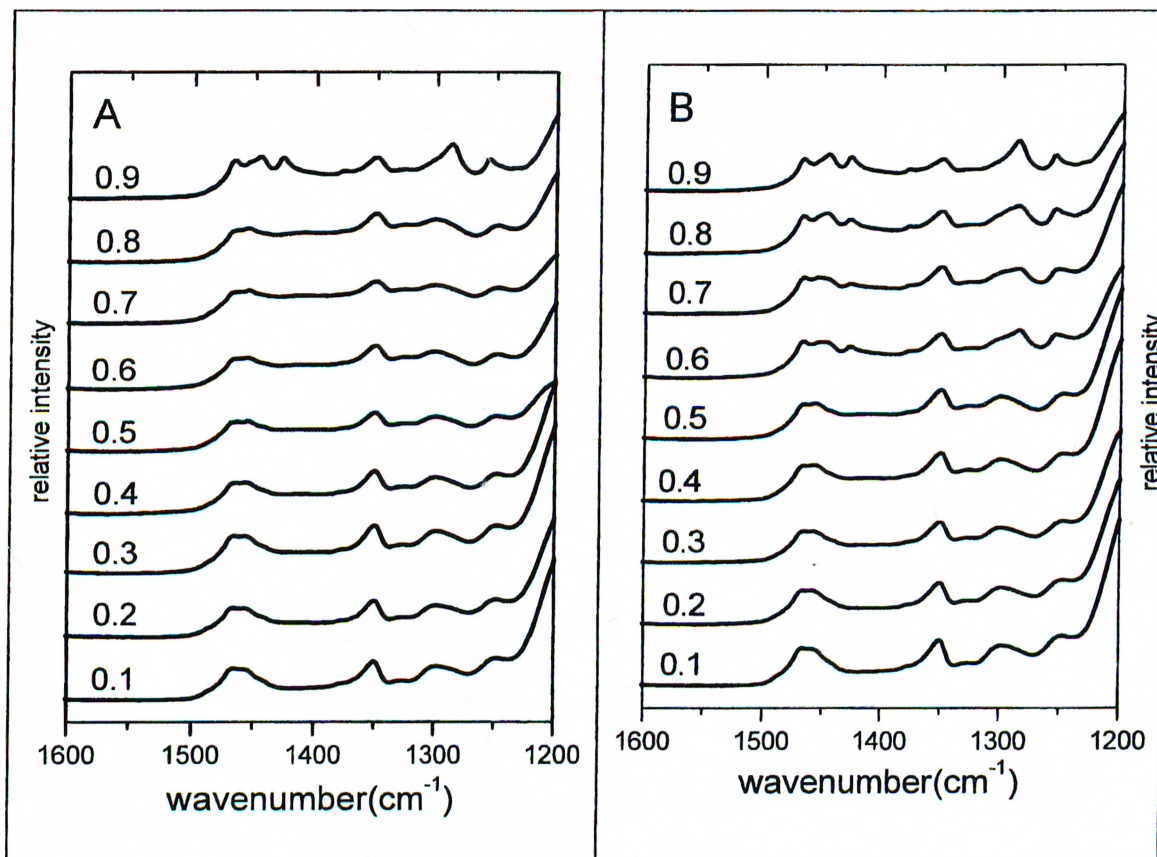


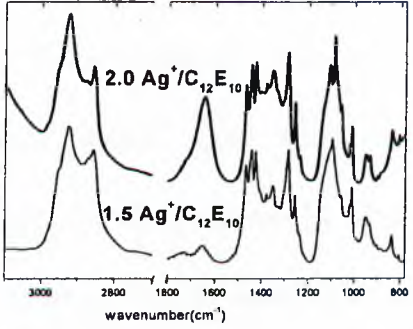
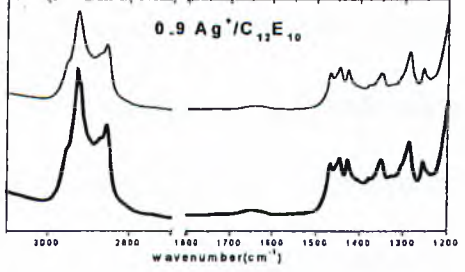
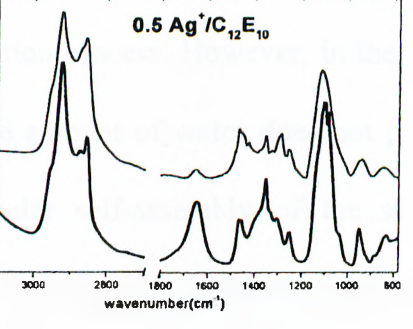
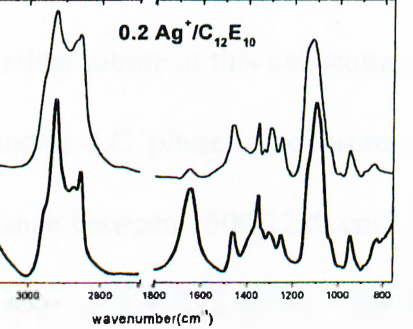
Figure 22. FT-IR absorption spectra of thin films (A) 24 hours after preparation, (B) one month after preparation. In the frequency range  $1600\text{-}1200\text{ cm}^{-1}$

The films, aged in closed containers in the dark were also analyzed by FT-IR spectroscopy after a month of the preparation, Figure 22(B). The spectra of aged samples with  $\text{Ag}^+/\text{C}_{12}\text{E}_{10}$  molar ratios below  $r = 0.6$  resemble one another, Figure 22. However, the spectra of aged samples with  $\text{Ag}^+/\text{C}_{12}\text{E}_{10}$  molar ratios between  $r = 0.6$  and  $0.8$  show series of changes compared to corresponding fresh samples; the peaks

at 1467 and 1446  $\text{cm}^{-1}$  became sharper and more intense, a new peak appeared at 1427  $\text{cm}^{-1}$ , the peak at 1350  $\text{cm}^{-1}$  broadened, the  $\text{CH}_2$  twisting mode observed at 1305  $\text{cm}^{-1}$  shifted by  $\Delta\nu \approx 20 \text{ cm}^{-1}$  to higher energy and the peak at 1256  $\text{cm}^{-1}$  increased in intensity, Figure 22. The spectrum of aged film sample with  $r = 0.9$  did not change upon aging, see Figure 22. The trend in the spectra of samples from  $r = 0.1$  to  $r = 0.9$  clearly shows that peaks at 1467, 1446, 1427, 1286, and 1256  $\text{cm}^{-1}$  gradually increase in intensity, become sharper and dominate in the spectra, Figure 22.

It is interesting to compare the behavior of  $\text{AgNO}_3/\text{C}_{12}\text{E}_{10}:\text{H}_2\text{O}(50 \text{ w/w}\%):\text{HNO}_3$  system before and after the addition of silica source. The samples containing different amounts of silver nitrate can be divided in three groups with respect to changes observed in FT-IR spectra, Table 5. The first group consists of samples with low  $\text{Ag}^+/\text{C}_{12}\text{E}_{10}$  molar ratios. The FT-IR spectra of these do not show significant changes upon solvent evaporation. The second group comprises of samples, the FT-IR spectra of which detect appearance of characteristic features. The high salt containing samples, which display strong sharp peaks in the spectra belong to third group. The similar changes take place in the  $\delta\text{-CH}_2$  deformation region of surfactant in both columns, namely peaks at 1467, 1446, 1427, 1286, 1256  $\text{cm}^{-1}$  increase in intensity while following the spectral trend from first group through second to third, Table 5, due to saturation of the system with silver nitrate.

Table 5. FT-IR absorption spectra of silver containing template <sup>a</sup>

Group number	AgNO <sub>3</sub> / C <sub>12</sub> E <sub>10</sub> :H <sub>2</sub> O(50w/w%):HNO <sub>3</sub>	AgNO <sub>3</sub> / C <sub>12</sub> E <sub>10</sub> :H <sub>2</sub> O:HNO <sub>3</sub> / TMOS
III	<p style="text-align: center;"><b>r &gt; 1.5</b></p> 	<p style="text-align: center;"><b>r ≥ 0.9</b></p> 
	II	<p style="text-align: center;"><b>0.5 ≤ r ≤ 1.5</b></p> 
I		<p style="text-align: center;"><b>0.1 ≤ r &lt; 0.5</b></p> 

<sup>a</sup> Freshly prepared samples **—**, aged samples **- - -**.

Since silver ions can complex with PEO chain of surfactant, the strong sharp peak at  $1384\text{ cm}^{-1}$  due to crystalline  $\text{AgNO}_3$  never appears in the spectra.

The comparison of spectra within the same group reveals that the spectra of freshly prepared surfactant mixtures and the surfactant in confined spaces of silica network are rather different. The spectra of "dried template (surfactant) mixture" and template within aged films resemble one another at corresponding concentrations of silver nitrate present, Table 5 groups I and II. This can be explained by the absence of water in the freshly prepared silica samples compared to the one in the freshly prepared template mixtures. It seems reasonable because some water was consumed during the hydrolysis of TMOS and rest was evaporated during polymerization process. However, in the template mixtures with high silver nitrate content, the amount of water does not play an important role in the formation of supramolecular self-assembly of the surfactant because the system is already saturated. Therefore, no difference in the spectra of both freshly prepared template mixtures and those of films were detected, group III, Table 5. On the other hand, the system with low silver content, group I, have no significant spectral changes. It means that silver nitrate at this concentration range does not disturb surfactant self-assembly and/or LC phase. The presence of sharp characteristic peaks in the frequency range between  $1500\text{-}1220\text{ cm}^{-1}$  in the FT-IR spectra can also be assigned to the formation of  $\text{Ag}^+/\text{C}_{12}\text{E}_{10}/\text{NO}_3^-$  complex. It also means loss of hexagonal LC phase of the template and the collapse of structures which templates the mesoporous silica materials. The evolution of these features in time, group II, Table 5, indicate

phase transition of the template and/or complexation of  $\text{Ag}^+/\text{C}_{12}\text{E}_{10}/\text{NO}_3^-$  during both water evaporation and silica network polymerization process.

The strong and sharp peaks at 1467, 1446, 1427, 1286, and 1256  $\text{cm}^{-1}$  in the FT-IR spectra of freshly prepared template mixtures and mesoporous silica films with high  $\text{AgNO}_3$  content are assigned to the  $\text{Ag}^+/\text{C}_{12}\text{E}_{10}/\text{NO}_3^-$  complex. The absence of changes in the spectra upon aging of already complexed samples also supports this idea.

Figure 23 displays FT-IR spectra of mesoporous silica samples in KBr. Note that the peaks at 1467, 1446, 1427, 1286 and 1256  $\text{cm}^{-1}$  assigned to the  $\text{Ag}^+/\text{C}_{12}\text{E}_{10}/\text{NO}_3^-$  complex were disappeared upon mixing and pressing the silica samples with KBr, but a new sharp relatively intense peak appeared at 1381  $\text{cm}^{-1}$  due to formation of  $\text{KNO}_3$  crystals Figure 23. It is also visible that pressing the samples with KBr causes yellow coloring of the pellets. All these can be explained by a simple ion exchange reaction between  $\text{AgNO}_3$  in mesoporous silica materials and KBr. This exchange process leads to the formation of  $\text{AgBr}$  that accounts for yellowish color of the pellets and the formation of  $\text{KNO}_3$  crystals, which have a sharp intense peak at 1381  $\text{cm}^{-1}$ . The samples of  $\text{KNO}_3/\text{C}_{12}\text{E}_{10}:\text{H}_2\text{O}:\text{HNO}_3/\text{Si}(\text{OCH}_3)_4$  were also synthesized to support the results mentioned above.

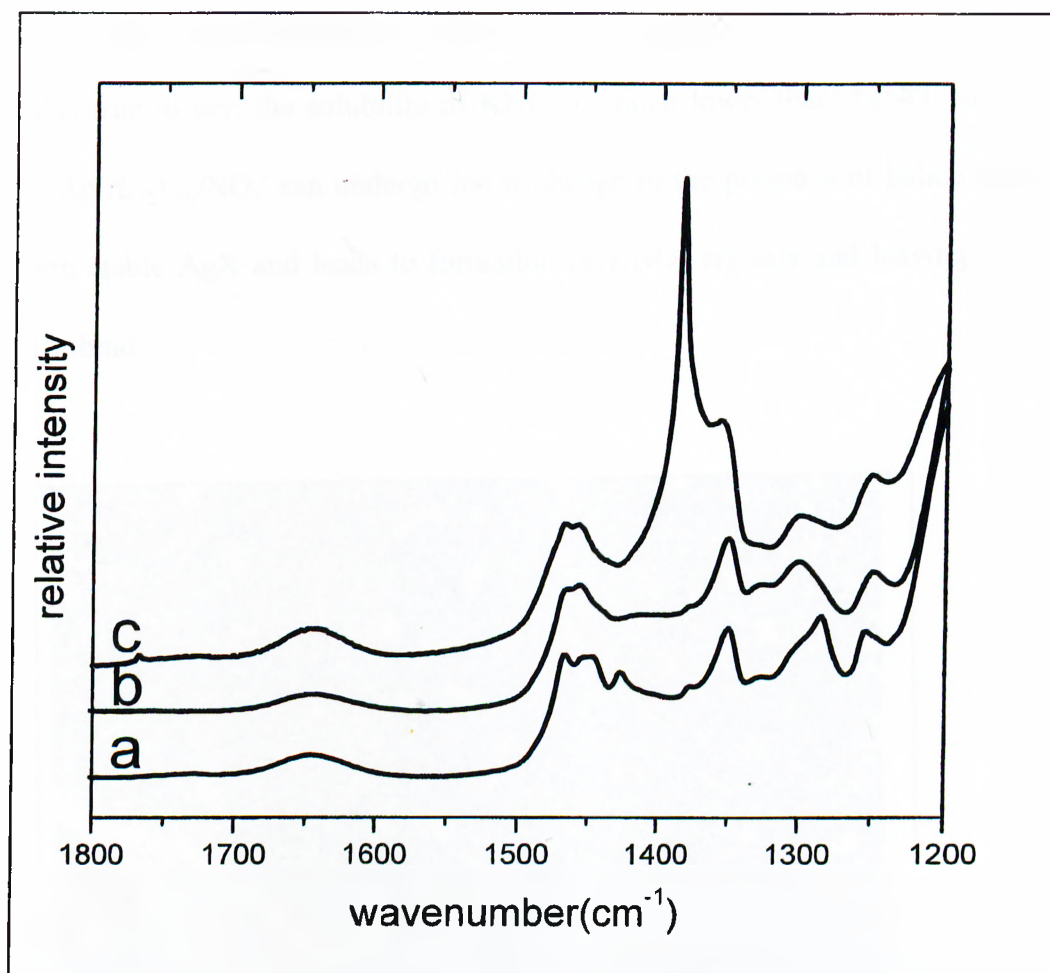


Figure 23. FT-IR spectra of  $\text{AgNO}_3/\text{C}_{12}\text{E}_{10}:\text{H}_2\text{O}:\text{HNO}_3/\text{TMOS}$  at  $r = 0.6$  (a) aged for 3 days, (b) aged for 24 hours, (c) pressed in KBr after 3 days aging; in the frequency range  $1800\text{-}1200\text{ cm}^{-1}$

The samples containing low concentrations of  $\text{KNO}_3$  display fan-like birefringence optical texture while at concentration of  $\text{KNO}_3$  above  $0.5\text{ K}^+/\text{C}_{12}\text{E}_{10}$  molar ratios cubic and hexagon crystals of  $\text{KNO}_3$  were observed over the fan-like texture between crossed polars under POM, Figure 24. The film samples containing potassium nitrate remain transparent independently on salt content, time and conditions of storage. These facts reveal that  $\text{K}^+$  ions do coordinate to the ether

groups of surfactant molecules but have much lower binding capacity than  $\text{Ag}^+$  ions do. It is also true to say, the solubility of  $\text{KNO}_3$  is much lower than  $\text{AgNO}_3$  in the surfactant.  $\text{Ag}^+/\text{C}_{12}\text{E}_{10}/\text{NO}_3^-$  can undergo ion exchange in the presence of halide ions ( $\text{X}^-$ ) to form stable  $\text{AgX}$  and leads to formation of  $\text{KNO}_3$  crystals and leaving free surfactant behind.

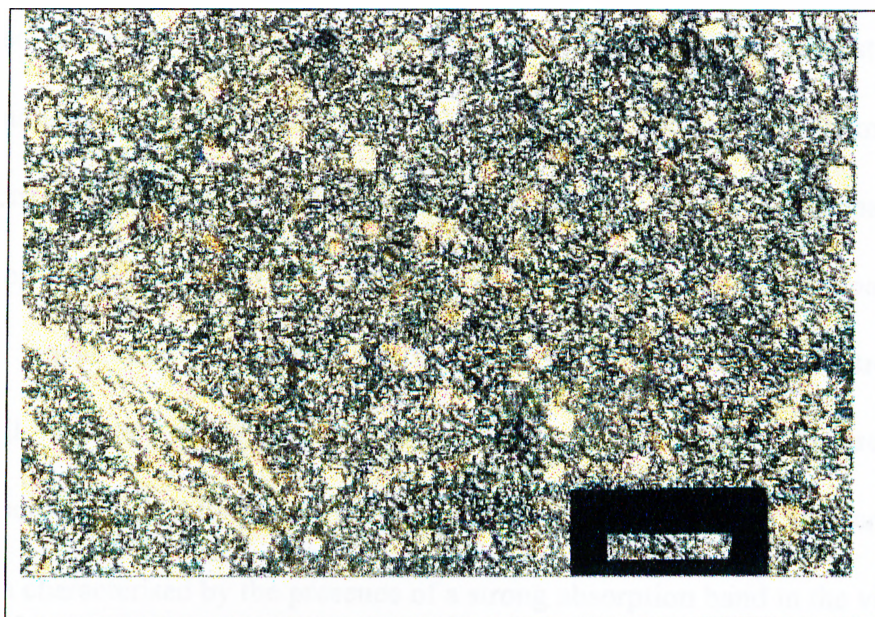


Figure 24. POM image for  $\text{KNO}_3/\text{C}_{12}\text{E}_{10}:\text{H}_2\text{O}:\text{HNO}_3/\text{TMOS}$  of 0.6  $\text{KNO}_3$  to surfactant molar ratio between crossed polars

That is why the sharp peaks due to  $\text{Ag}^+/\text{C}_{12}\text{E}_{10}/\text{NO}_3^-$  complex disappear upon pressing the samples with KBr.

### 3.2.4. UV-Vis Spectral Studies

The numerous applications of metal containing porous materials as well as polymeric composites as catalytic supports, semiconductors, photographic suspensions, polymer ionic electrolytes which require metal particles to possess particular properties have been demonstrated [79]. Some of these properties can be listed as chemical activity, high ionic mobility, stability against coalescence, homogeneity in distribution, ease of accessibility etc. It is well known that the electronic properties of metals are highly dependent on size of the particles. Thus, the optical properties of nanoscaled metal particles are different compare to those of bulk metal. The confinement and quantization of conduction electrons within a small volume enhance optical properties of materials composed of metal nanocrystals [63,130-132]. The optical nature of the noble metal nanoparticles is often characterised by the presence of a strong absorption band in the visible region. This is attributed to the resonance collective motion of conduction electrons in response to an incident electromagnetic field and is called surface plasmon resonance (SPR) [133].

The large silver particles display narrow intense SPR absorption peak at 400 nm. Deviations in UV-Vis absorption band structure can be due to changes in shape, size, and degree of the particle-particle coupling of the nanoparticles, dielectric properties of the metal and the refractive index of surrounding medium [133]. The correlation between structure as well as position of the SPR peak and nature of metal particles to the first approximation can be described as follows:

- Decrease in the particles size leads to band to broaden and intensity to decrease [63, 134]
- The aggregation of colloidal silver particles causes a decrease in peak intensity and results in the long tail at the higher wavelength side of the peak [130].

Table 6. Positions of SPR absorption peak of silver in different reaction medium

stabiliser	Plasmon band	
	$\lambda_{\max}(\text{nm})$	reference
AOT/EtOH	355	109
Brij97/EtOH	430	109
Brij97/cyclohexane	420	109
Tween80/EtOH	430	109
$\text{C}_{12}\text{E}_4/\text{H}_2\text{O}$	420	108
ODA(octadecyl amine)	475	135
CTAB/ $\text{H}_2\text{O}$	410	79
SDS/ $\text{H}_2\text{O}$	392	79
TX-100/ $\text{H}_2\text{O}$	394	79
PVA(polyvinyl alcohol)	385	103
$\text{I}^-/\text{H}^+$	382	63
$\text{SiO}_2$	~403	116
Laponite	~400	79

- Peak shifts toward higher energy with an increase in bandwidth as dielectric constant increases [133].

The experimental data, present in Table 6, show variability of SPR band position of silver nanoparticles in different media. Such deviations of the plasmon band maximum occur even if the particle size distributions are similar.

The silver ion is very sensitive to surroundings and can be easily reduced thermally, photochemically and chemically. In this work, silver in its ionic form introduced in meso-SiO<sub>2</sub> as AgNO<sub>3</sub>, which dissolves in the lyotropic hexagonal LC

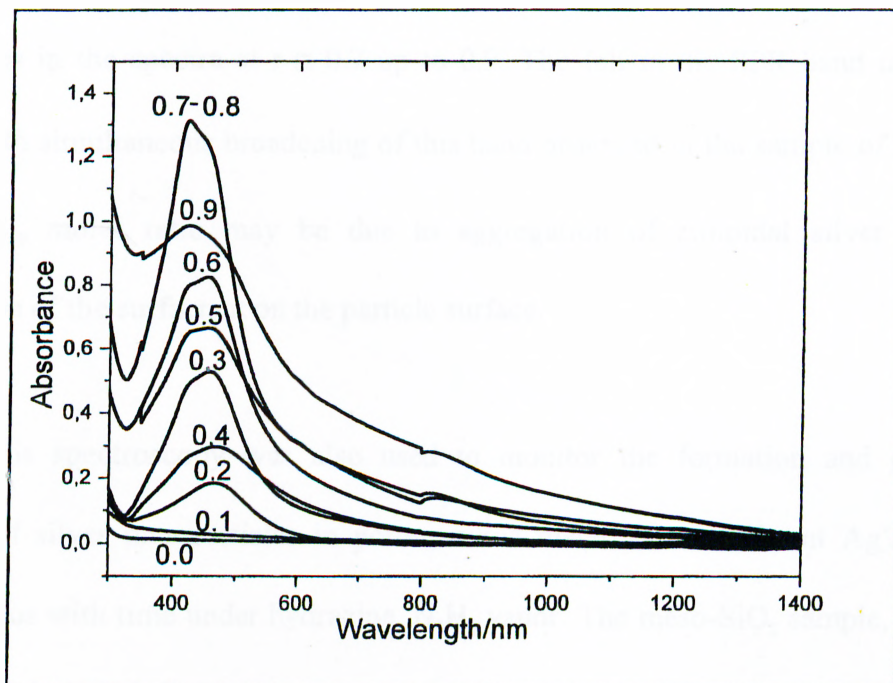


Figure 25. UV-Vis spectra of thin porous silica films containing different amounts of silver before exposure to the reducing agent. Ag<sup>+</sup>/C<sub>12</sub>E<sub>10</sub> molar ratios are indicated along the spectra. Samples were kept in open air in the dark

phase of  $C_{12}E_{10}:H_2O(50 \text{ w/w\%}):HNO_3$  was reduced by direct exposure of the samples to a reducing agent. The samples, used for reduction, were thin films deposited on glass or quartz slides.

The thin films stored in closed containers in the dark remain colorless if the concentration of silver nitrate is low and white at high salt concentrations. It was noticed that color of the samples exposed to air but not to the light changes in the following sequence: colorless  $\rightarrow$  pale  $\rightarrow$  orange  $\rightarrow$  brown as  $Ag^+/C_{12}E_{10}$  molar ratios increases 0.1  $\rightarrow$  0.2  $\rightarrow$  0.3-0.4  $\rightarrow$  0.5-0.9 respectively. The inspection of UV-Vis absorption spectra of colorless and white samples before exposure to the reducing agent show no plasmon band in the vicinity of 400 nm, while the colored samples display a broad band which splits into two at  $\sim 420$  nm and  $\sim 458$  nm, Figure 25. The band at 420 nm becomes sharper as the concentration of silver nitrate increases and dominates in the spectra at  $r \cong 0.7$  up to 0.9. The fall in the SPR band intensity along with simultaneous broadening of this band observed in the sample of  $r = 0.9$   $Ag^+/C_{12}E_{10}$  molar ratio may be due to aggregation of colloidal silver and/or absorption of the surfactant on the particle surface.

UV-Vis spectroscopy was also used to monitor the formation and growth process of silver nanoparticles in porous silica materials of different  $Ag^+/C_{12}E_{10}$  molar ratios with time under hydrazine,  $N_2H_4$  vapor. The meso- $SiO_2$  sample, which contains 0.1  $Ag^+/C_{12}E_{10}$  molar ratio, was subjected to the stepwise reduction by hydrazine and showed development of silver plasmon band centered at  $\sim 423$  nm.

The evolution of surface plasmon resonance (SPR) band for the sample with  $r = 0.2$  is shown in Figure 26. The SPR band increases in intensity and blue shifts at prolonged reduction time. Wiping of the film surface causes an additional blue shift and sharpening of the band and drastic intensity decrease of the shoulder at higher wavelength as well. The color of the film changes in the following sequence, white  $\rightarrow$  pink  $\rightarrow$  orange  $\rightarrow$  yellow  $\rightarrow$  brown  $\rightarrow$  black with increasing reduction time. The UV-Vis absorption spectra of samples with  $\text{Ag}^+/\text{C}_{12}\text{E}_{10}$  molar ratios up to 0.7 resemble overall trend of plasmon absorption peak evolution as successive increase in intensity and blue shift upon elapsed reduction time.

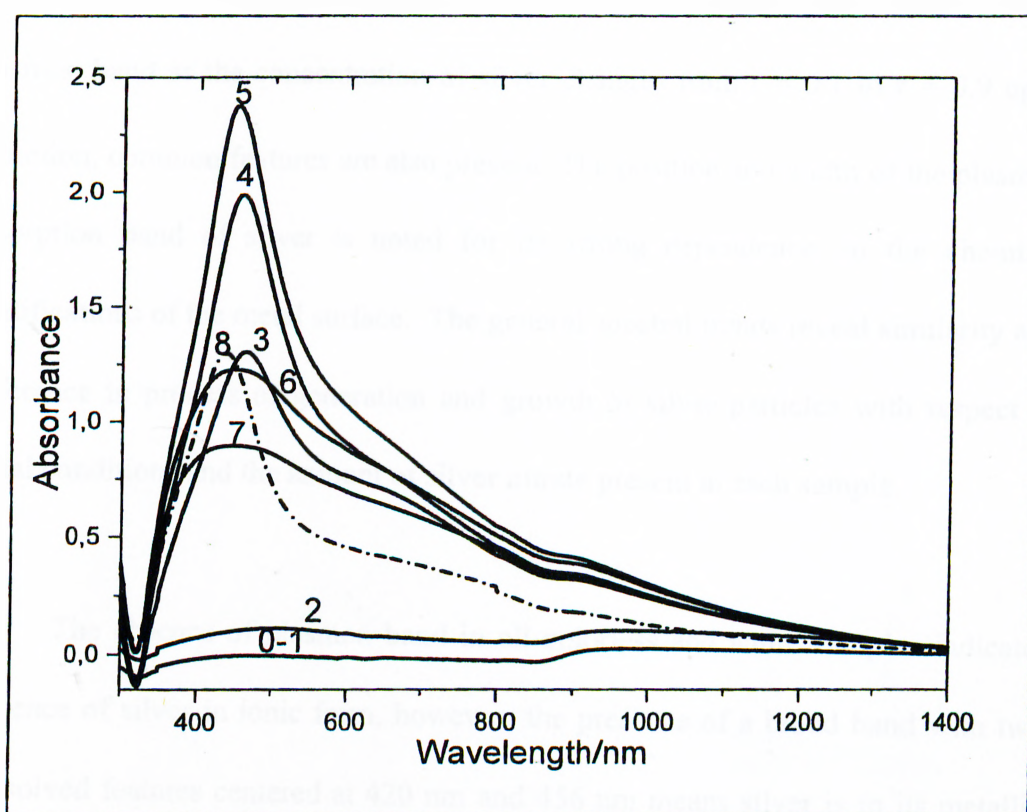


Figure 26. Absorption spectra of silver nanoparticles synthesized in  $\text{C}_{12}\text{E}_{10}:\text{H}_2\text{O}:\text{HNO}_3$  in presence of mase- $\text{SiO}_2$ ,  $\text{Ag}^+/\text{C}_{12}\text{E}_{10}$  molar ratio is 0.2, with elapse expose to  $\text{N}_2\text{H}_4$  0-1) 0-15 min. 2) 30 min. 3) 45 min. 4) 60 min. 5) 90 min. 6) 105 min. 7) 120 min. 8) 120 min, after wiping

However, silver mirror formation was observed in samples with  $r \geq 0.3$ . This thin surface layer can be easily cleaned by wiping, which leaves brown or black film samples behind depending on the reduction time. The plasmon band fades and blue shifts after wiping and remains unchanged when sample surface is seen black with naked eye. The white samples with high silver content  $r \geq 0.8$  display complex spectra at initial steps of reduction, Figure 27(A). However, the evolution of plasmon band of coloured samples resembles those observed for samples with low  $r < 0.8$  silver content, Figure 27(B).

Despite of particular differences in position, intensity, and width of the plasmon band as the concentration of silver changes from  $r = 0.1$  to  $r = 0.9$  upon reduction, common features are also present. The position and width of the plasmon absorption band of silver is noted for its strong dependence on the chemical modifications of the metal surface. The general spectral trends reveal similarity and difference in process of generation and growth of silver particles with respect to initial conditions and the amount of silver nitrate present in each sample.

The absence of plasmon band in all colorless and white samples indicates existence of silver in ionic form, however, the presence of a broad band with two unresolved features centered at 420 nm and 456 nm means silver is in its metallic zero valent form. This is the origin of coloring of the samples before direct expose to the reducing agent.

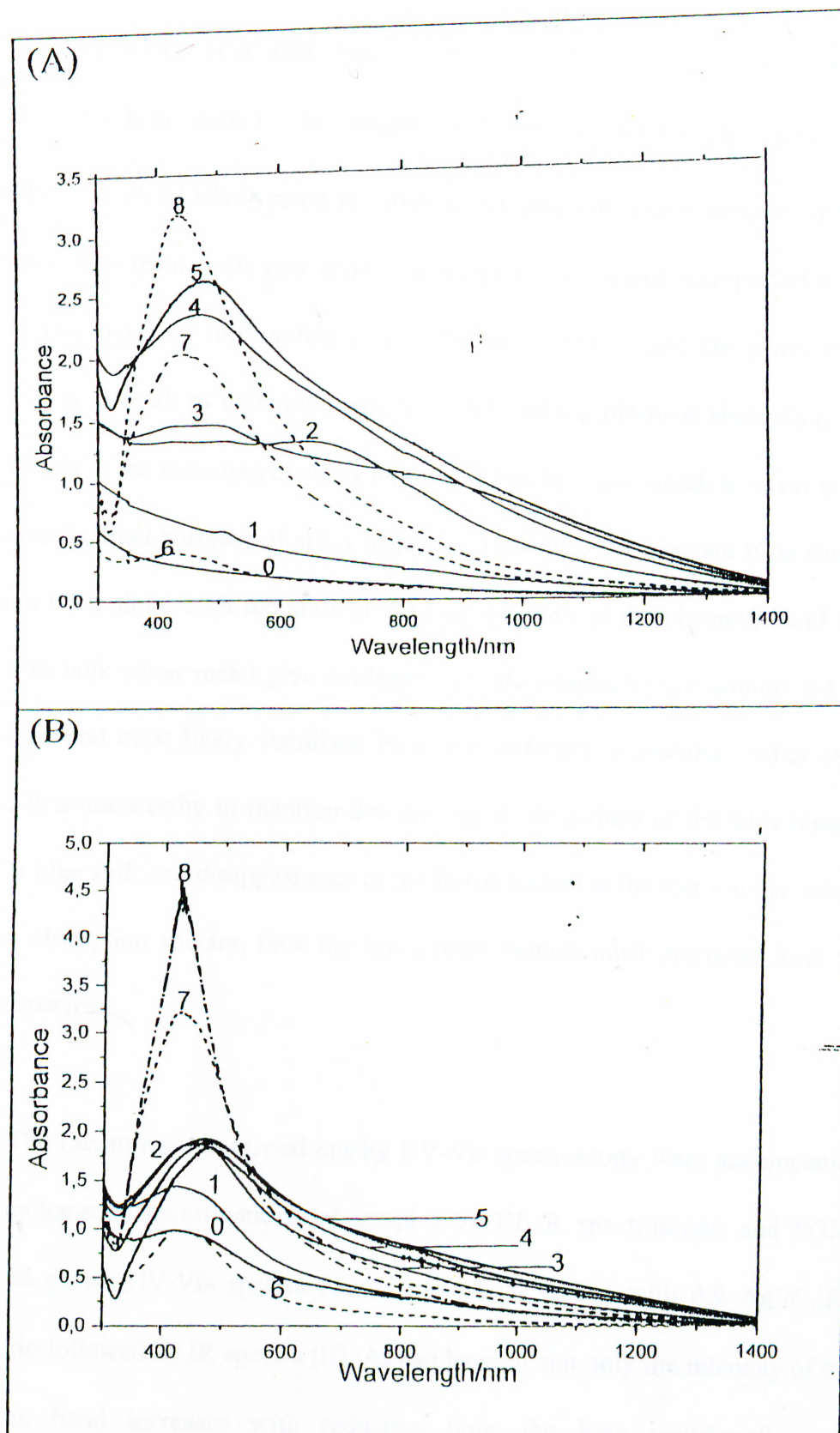


Figure 27. UV-Vis absorption spectra for (A) white and (B) brown meso-SiO<sub>2</sub> containing 0.9 Ag<sup>+</sup>/C<sub>12</sub>E<sub>10</sub> molar ratio upon reduction. Dashed line refers to the prolonged reduction after removing of silvery mirror surface layer

The presence of several peaks in UV-Vis spectra of reduced white samples, especially for films with  $r \geq 0.8$  suggests different rates of reduction which may occur (as a result of silver being in different environment and/or depth of the film samples). The band with two shoulders suggests that silver nanoparticles have mainly two types of surrounding media (the outer surface and the pores of the films). It is difficult to determine which shoulder of the plasmon absorption band corresponds to the reduction of silver on the outer surface and which to silver within the pores (internal surface) of silica materials. However, the constant blue shift of plasmon band along with red shift of the final position of the plasmon band with respect to bulk silver metal give evidence that silver particles are around 2-5 nm size range and most likely stabilized by either surfactant molecules and/or silica matrix. It is noteworthy to mention that wiping of the surface of the film samples causes a blue shift and disappearance of the broad feature at the low energy side of UV-Vis absorption spectra, thus the low energy feature must originate from the surface species.

The measurements carried out by UV-Vis spectroscopy were accompanied with simultaneous investigations of samples by FT-IR spectroscopy and POM. Figure 28 shows UV-Vis spectra (A) of meso-SiO<sub>2</sub> system with 0.9 Ag<sup>+</sup>/C<sub>12</sub>E<sub>10</sub> molar ratio followed by IR spectra (B). As can be seen, not only the intensity of the absorption band increases with reduction time, the long wavelength peak disappearing rather rapidly in UV-Vis absorption spectra, Figure 28(A). A sharp fall in the intensity of the peaks at 1467, 1446, 1427, 1286, 1256, 1234 cm<sup>-1</sup>

corresponding to the surface  $\text{Ag}^+/\text{C}_{12}\text{E}_{10}/\text{NO}_3^-$  complex and appearance of broad bands are revealed by FTIR spectroscopy, Figure 28(B).

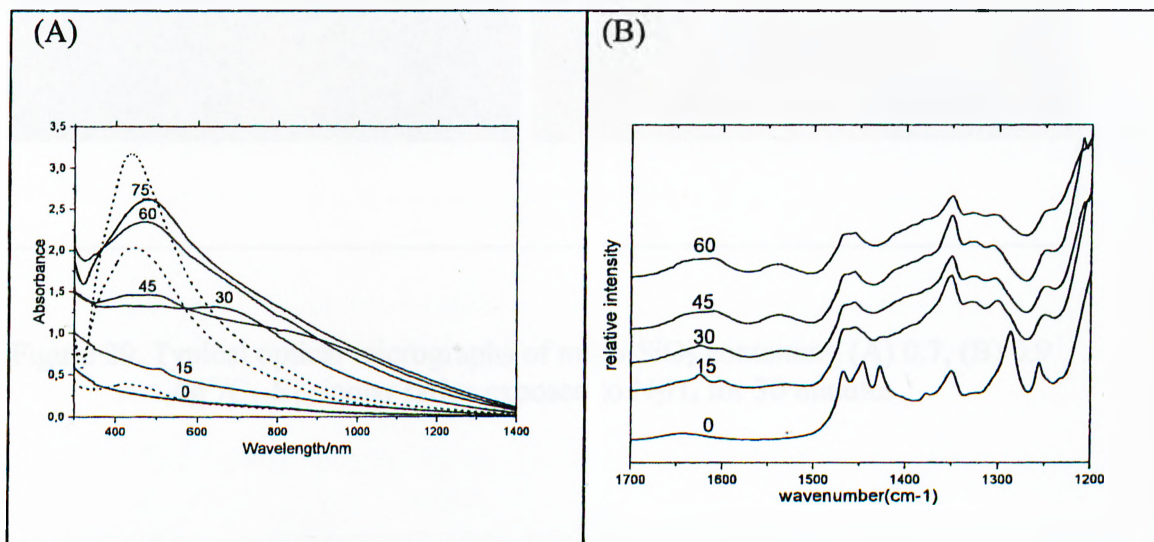


Figure 28. (A) UV-Vis and (B) FT-IR spectra of  $\text{AgNO}_3/\text{C}_{12}\text{E}_{10}:\text{H}_2\text{O}:\text{HNO}_3/\text{TMOS}$  system with  $r = 0.9$  during reduction. Time of reduction is mentioned along the spectra

Note that first the peaks corresponding to  $\text{Ag}^+/\text{C}_{12}\text{E}_{10}/\text{NO}_3^-$  complex at 1467, 1446, 1427, 1286, 1256, 1234  $\text{cm}^{-1}$  in IR spectra disappear. This means that  $\text{Ag}^+/\text{C}_{12}\text{E}_{10}/\text{NO}_3^-$  complex has been reduced into silver metal, leaving behind broad smooth bands of free surfactant. The SPR absorption band centered at 428 nm, detected by UV-Vis spectroscopy, and absence of intense sharp features in the carbon-hydrogen vibration region of IR spectra are evidences for the formation metallic nanosized silver particles.

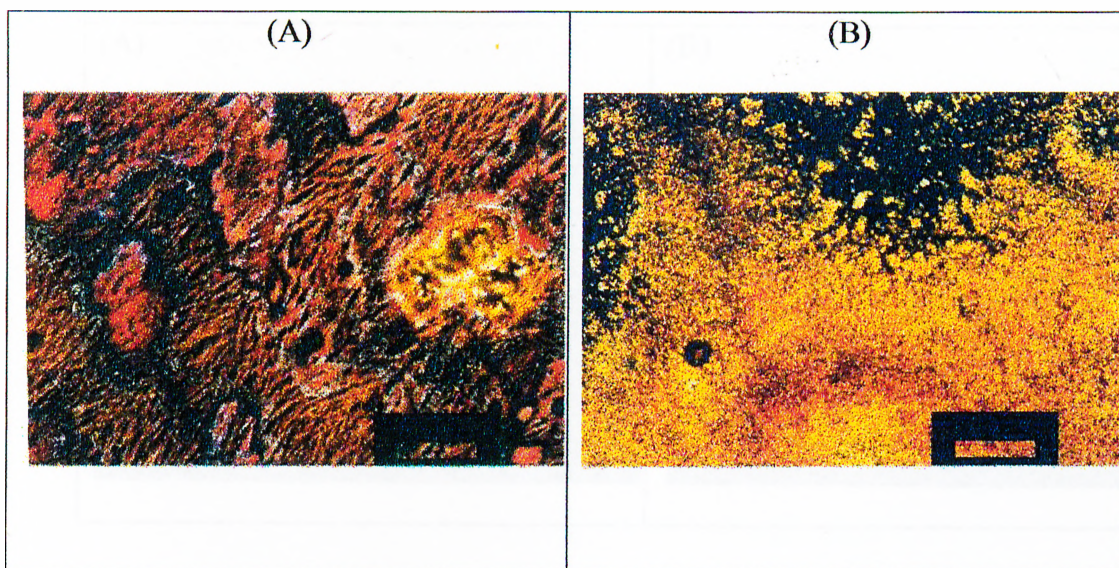


Figure 29. Typical optical micrographs of meso-SiO<sub>2</sub> containing (A) 0.7, (B) 0.9 Ag<sup>+</sup>/C<sub>12</sub>E<sub>10</sub> molar ratios exposed to N<sub>2</sub>H<sub>4</sub> for 30 minutes

The optical microscopy images also reveal formation of filaments of Ag aggregates which is adorned with brushes formed by AgNO<sub>3</sub>/C<sub>12</sub>E<sub>10</sub>:H<sub>2</sub>O:HNO<sub>3</sub> system, as a thin layer on the film external surface in initial stages of reduction, Figure 29. These are most likely originated from the surface species, which are squeezed out during silica polymerization as a result of contraction of the structure.

Figure 30 shows microscopic images of films containing filament-like aggregates of reduced silver when position of SPR peak no longer change with reduction time and wiping of the surface.

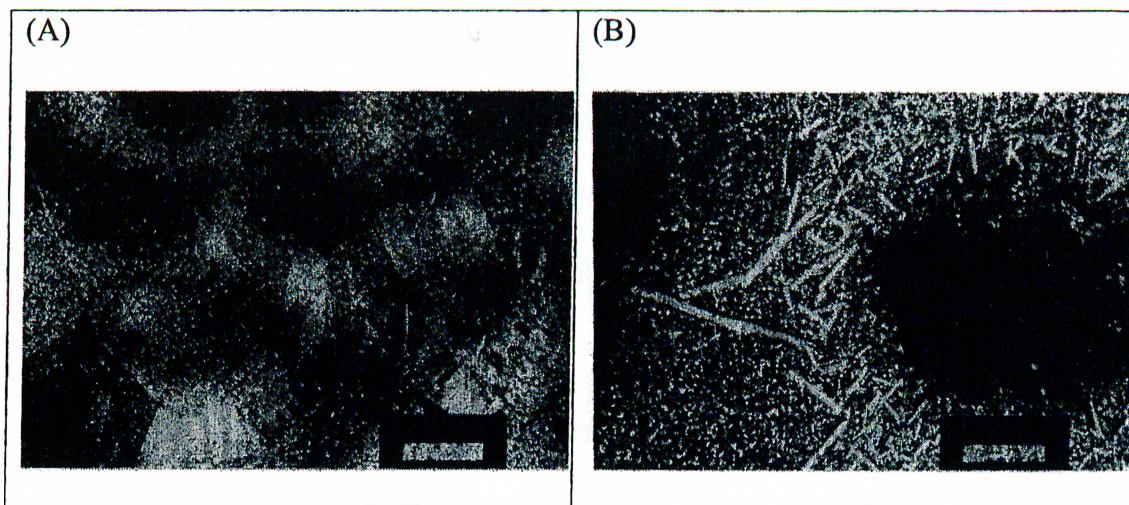


Figure 30. Optical micrographs of meso-SiO<sub>2</sub> containing reduced silver with Ag<sup>+</sup>/C<sub>12</sub>E<sub>10</sub> molar ratio (A) 0.7, (B) 0.8 between crossed polarisers

The optical microscopy images of black sample of  $r = 0.2$  displays fan-like texture when viewed between crossed polarizers, Figure 31.

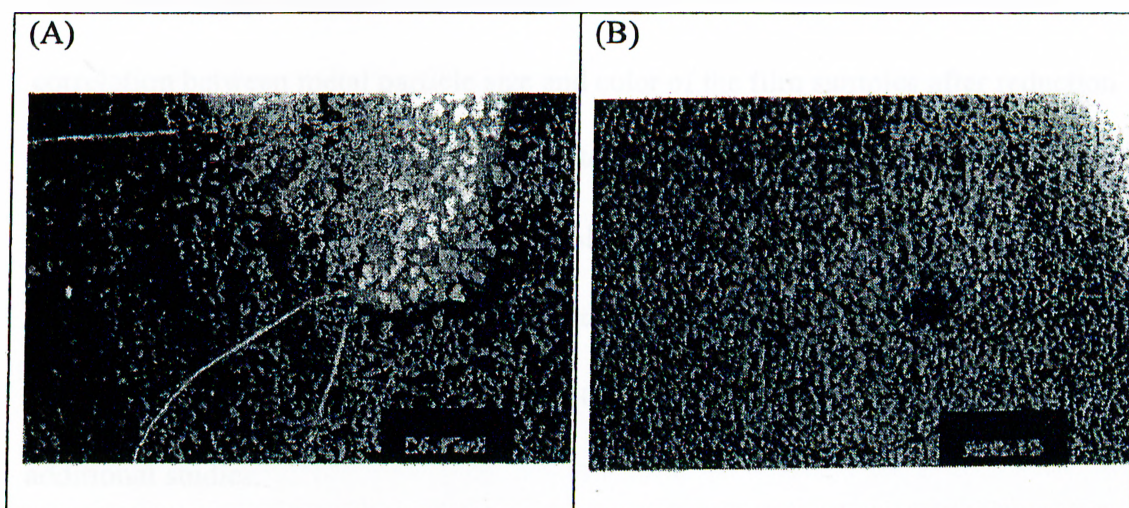
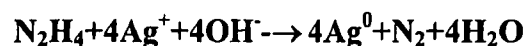


Figure 31. Optical micrographs of meso-SiO<sub>2</sub> containing 0.2 Ag<sup>+</sup>/C<sub>12</sub>E<sub>10</sub> (A) normal, (B) between crossed polarizers

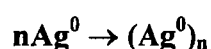
The comparison of microscopic images of any sample (in the range of Ag<sup>+</sup>/C<sub>12</sub>E<sub>10</sub> molar ratios between 0.5 and 0.9 where those were noticed), Figure

29(A) and 30(A), reveals disappearance of surface brushes. This phenomena also correlates with disappearance of strong IR peaks assigned to the  $\text{Ag}^+/\text{C}_{12}\text{E}_{10}/\text{NO}_3$  complex, and with successive blue shift of the plasmon band along with disappearing long wavelength band and tail in the UV-Vis spectra.

The possible reaction between silver ions and hydrazine is given below:



Agglomeration processes of  $\text{Ag}^0$  produce colloidal silver nano-particles according to the reaction:



It is also well known that the color of the metal particles is caused by the sum of the effects of visible light absorption and scattering [130]. Mie's theory has explained the dependence of these factors on the particle size. However, direct correlation between metal particle size and color of the film samples after reduction and wiping fail for such many-particle systems, where the optical absorption is determined by both properties of individual structural units and collective effects due to interaction among particles. Understanding of real processes which take place in the  $\text{AgNO}_3/\text{C}_{12}\text{E}_{10}:\text{H}_2\text{O}:\text{HNO}_3/\text{TMOS}$  during reduction of silver requires additional studies.

#### 4. CONCLUSION

The mesoporous materials tailored through surfactant mediated synthetic pathway find their wide utilization as nanosized reaction vessels or hosts to assemble semiconductors, metals, and other compounds in their pores. It is well known that mesoporous solid due to their large internal surface area, large pore size and pore opening, similarly, nanometer size particles because of their small size and high specific surface area display unique properties. Nanoparticle-loaded porous solid is a new type of composite material and will have properties that neither the nanoparticle nor the mesoporous solid possess. The properties of metal containing nanocomposites can be synthesized by design and preparation methods of materials, which in turn require knowledge about properties of reactant species and their behavior in different stages of synthesis.

The conditions for synthesis of functionalized mesoporous silica materials containing controlled amount of evenly distributed silver in its free ionic form within pores of  $\text{SiO}_2$  were established. The influence of silver nitrate concentration on lyotropic hexagonal mesophase formed by oligo-ethylene oxide surfactant and water in the presence of acid and on the formation of mesoporous silica materials templated by the hexagonal mesophase of the LC mixture of oligo-ethylene oxide surfactant/water/acid and  $\text{AgNO}_3$  was investigated.

It was found out that the hexagonal liquid crystalline phase of  $C_{12}H_{25}(CH_2CH_2O)_{10}OH$  surfactant in water is not disturbed by silver nitrate within the concentration range of 0.0-0.9  $Ag^+$ /surfactant molar ratios. The  $C_{12}E_{10}:H_2O(50 \text{ w/w\%}):HNO_3$  system containing silver salt between 0.9-1.5  $Ag^+/C_{12}E_{10}$  molar ratios has an intermediate phase. The surfactant/water system,  $AgNO_3/C_{12}E_{10}:H_2O(50 \text{ w/w\%}):HNO_3$  is no longer stable and yields white, soft  $Ag^+$ /surfactant/ $NO_3^-$  complex when the  $Ag^+/C_{12}E_{10}$  molar ratio exceeds 1.5. However, even samples with 0.9 and higher  $Ag^+/C_{12}E_{10}$  ratios give soft solid complex out and undergo phase separation with time.

On the basis of PXRD data, the  $AgNO_3/C_{12}E_{10}:H_2O(50 \text{ w/w\%}):HNO_3$  template yields 3D-hexagonal mesoporous silica framework up to 0.7  $Ag^+/C_{12}E_{10}$  molar ratio while amorphous silica oxide is formed in the samples of higher  $AgNO_3$  concentration. During the silica polymerization and drying process,  $Ag^+$  ions undergo phase separation and form  $Ag^+$ /surfactant/ $NO_3^-$  complex and break the LC structure of the template. The complex formation and phase separation yield collapse of the structure, as a result, the formation of disordered materials upon polymerization of silica in the mixtures with higher  $AgNO_3$ /surfactant ratios take place.

It is worth to mention that the homogeneity of the mixture in every stage of "one-pot" synthesis and handling condensation polymerization reaction of TMOS in first 2 hours of synthesis at 18-20 °C are important to attain nanoscaled silica materials.

The  $\text{Ag}^+$  ions in mesoporous silica materials can be reduced by gas phase hydrazine into metallic Ag to yield Ag nano-particles embedded in the pores and external surface of ordered silica materials. Further study is required to understand the Ag nano-particle formation and growth and to elucidate the electronic properties with respect to particle size, shape and the effect of the dielectric media.

## 5. REFERENCES

- (1) J.Y. Yang, C.P. Mehnert and M.S. Wong, "Synthesis and Applications of Supramolecular-Templated Mesoporous Materials," *Angew. Chem. Int. Ed.*, vol. 38, pp. 56-77, 1999.
- (2) S. Iijima and T. Ichihashi, "Single-Shell Carbon Nanotubes 1nm Diameter," *Nature*, vol. 363, pp. 603-605, 1993
- (3) S. Amelinck, X.B. Zhang, D. Braerts, X.F. Zhang, V. Ivanov, J.B. Nagy, "A Formation Mechanism of Catalitically Grown Helix-Shaped Graphite Nanotubes," *Science*, vol. 265, pp. 635-637, 1994.
- (4) E.J.M. Hamilton, S.E. Dolan, C.E. Mann, H.O. Colijm, C.A. McDonald, S.G. Shore, "Preparation of Amorphous Boron Nitride and its Conversion to a Tubostratic," *Science*, vol. 260, pp.659-661, 1993.
- (5) H.J. Muhr, F. Krymeich, U.P. Schönholzer, F. Bieri, M. Neiderberger, L.J. Gauckler, R. Nesper, " Vanadium Oxide Nanotubes - A New Flexible Vanadate Nanophase," *Adv. Mater.*, vol.12, pp. 231-234, 2000.
- (6) M. Harada, M. Adachi, "Surfactant Mediated Fabrication of Silica Nanotubes," *Adv. Mater.*, vol. 12, pp. 839-841, 2000.
- (7) S. Mann, "Molecular Techtonics in Biomineralization and Biomimetic Material Chemistry", *Nature*, vol. 365, pp. 499-505, 1993.
- (8) A. Heuer, D. Fink, V. Laraia, J. Arias, P. Calvert, P. Kendall, G. Messing, J. Bleckwell, P. Rieke, D. Thompson, A. Whiller, A. Veils, A. Caplan, "Innovative Materials Strategies: A Biomimetic Approach", *Science*, vol. 255, pp. 1098-1105, 1992.
- (9) I. Aksay, M. Tray, S. Mann, I. Honma, N. Yao, L. Zhou, P. Eisenberg, S. Gruner, "Biomimetic Pathways for Assembling Inorganic Thin Films," *Science*, vol. 273, pp. 892-898, 1996.

- [10] C. Kresge, M. Leonowicz, W. Roth, C. Vartuli, J. Beck, "Ordered Mesoporous Molecular Sieves Synthesized by a Liquid Crystal Template Mechanism," *Nature*, vol. 359, pp. 710-712, 1992.
- [11] T. Thurn-Alreched, R. Stainer, J. DeRouchey, C.M. Stafford, E. Huang, M. Tuominen, C.J. Hawker, T.P. Russell, "Nanosopic Templates from Oriented Block Copolymer Films," *Adv. Mater.*, vol. 12, pp. 787-791, 2000.
- [12] Y. Yang, A. Sayary, "Highly Ordered MCM-41 Silica Prepared in the Presence of Dethyltrimethylammonium Bromide," *J. Phys. Chem. B*, vol.104, pp. 3651-3656, 2000.
- [13] D. Khushalani, A. Kuperman, N. Coombs, G.A. Ozin, "Mixed Surfactant Assemblies in the Synthesis of Mesoporous Silicas," *Chem. Mater.*, vol. 8, pp. 1234-1240, 1996.
- [14] D. Khushalani, G. Ozin, A. Kupermann, "Glycometallate Surfactants Part 2: Non-Aqueous Synthesis of Mesoporous Titanium, Zirconium, and Niobium Oxides," *J. Mater. Chem.*, vol. 9, pp.1491-1500, 1999.
- [15] M.J. MacLachlan, I. Manners, G. Ozin, "New (Inter) Faces: Polymers and Inorganic Materials," *Adv. Mater.*, vol.12, pp. 675-681, 2000.
- [16] Q. Huo, D.I. Margulese, G.D. Stucky, "Surfactant Control of Phases in the Synthesis of Mesoporous Silica-Based Materials," *Chem. Mater.*, vol. 8, pp. 1147-1160, 1996.
- [17] X.S. Zhao, G.Q. (Max) Lu, G.J. Millar, "Advances in Mesoporous Molecular Sieve MCM-41," *Ind.&Engeneer. Chem. Res.*, vol. 3(7), pp.2075-2090, 1996.
- [18] V.Y. Gusev, X. Feng, Z. Bu, G.L Haller, J.A. O'Brien, "Mechanical Stability of Pure Silica Mesoporous MCM-41 by Nitrogen Absorption and Small Angle X-Ray Diffraction Measurements," *J. Phys. Chem.*, vol. 100, pp. 1-4, 1996.

- (19) X.S. Zhao, Q.X. Wang, L.Y. Hu, X.S. Li, "Direct Synthesis of Mesoporous Molecular Sieve MCM-41," Unpublished results, 1994.
- (20) A. Corma, V. Fornes, M.T. Navarro, J. Perez-Pariente, "Acidity and Stability of MCM-41 Crystalline Aluminosilicates," *J. Catal.*, vol.148, pp. 549-564, 1994.
- (21) T.J. Barton, L.M. Bull, W.G. Klemper, D.A. Koy, M. Misono, P.A. Monson, J.W. Scherer, J.C. Vartuli, O.M. Yaghi, "Tailoring Porous Materials," *Chem. Mater.*, vol. 11, pp.2633-2656, 1999.
- (22) D. Zhao, D. Goldfanz, "Synthesis of Manganosilicates: Mn-MCM-41, Mn-MCM-48, Mn-MCM-L," *J. Chem. Soc., Chem. Commun.*, pp. 875-876, 1995.
- (23) A. Tuel, S. Gontier, "Synthesis and Characterization of Trivalent Metal Containing Mesoporous Silicas Obtained by a Neutral Templating Route," *Chem. Mater.*, vol. 8, pp. 114-122, 1995.
- (24) B. Echahed, A. Moen, D. Nicholson, L. Bonneviot, "Iron Modified MCM-48 Mesoporous Molecular Sieves," *Chem. Mater.*, vol. 9, pp. 1716-1719, 1997.
- (25) D. Yang, D. Zhao, D.I. Margolese, B.F. Chmelka, G.D. Stucky, "Generalized Synthesis of Large-Pore Mesoporous Metal Oxides with Semicrystalline Frameworks," *Nature*, vol. 396, pp. 152-155, 1998.
- (26) X.S. Zhao, G.Q. Lu, A.K. Whittaker, G.J. Millar, H.Y. Zhu, "Comprehensive Study of Surface Chemistry of MCM-41 Using  $^{29}\text{Si}$  CP/MASNMR, FTIR, Pyridine-TPD, and TGA," *J. Phys. Chem. B*, vol. 101(33), pp.6525-6531, 1997.
- (27) R.K. Iller, *The Chemistry of Silica*, John Wiley&Sons: New York, 1979.
- (28) X. Feng, G.E. Fruxell, L.Q. Wang, A.Y. Kim, J. Liu, K.M. Kemner, "Functionalized Monolayers on Ordered Mesoporous Supports," *Science*, vol. 276, pp. 923-926, 1997.

- (29) J.Wen, G.L.Wilkes, "Organic/Inorganic Hybrid Network Materials by the Sol-Gel Approach," *Chem. Mater.*, vol. 18, pp. 1667-1681, 1996.
- (30) D.A. Lou, K.J. Shea, "Bridged Polysilsesquioxanes. Highly Porous Hybrid Organic-Inorganic Materials," *Chem. Rev.*, vol. 95, pp. 1431-1442, 1995.
- (31) R.H. Baney, M. Itoh, A. Sakakibara, T. Suzuki, "Selsesquioxanes," *Chem. Rev.*, vol.95, pp. 1410-1430, 1995.
- (32) B. Boury, R. Chevalier, R.P.J. Corriu, P. Delord, M. Wong, "Hybrid Organic/Inorganic Xerogel Access to Meso and Microporous Silica by Thermal and Chemical Treatment," *Chem. Mater.*, vol. 11, pp. 281-291, 1999.
- (33) T. Asefa, M.J. MacLachian, Niel Coombs, G.A. Ozin, "Periodic Mesoporous Organosilicas with Organic Groups Inside the Channel Walls," *Nature*, vol.402, pp. 867-871, 1999.
- (34) S. Inagaki, S. Guan, Y. Fuckuchima, T. Ohsuna, O. Terasaki, "Novel Mesoporous Materials with a Uniform Distribution of Organic Groups and Inorganic Oxide in their Framework," *J. Am. Chem. Soc.*, vol. 121, pp. 9611-9614, 1999.
- (35) T. Asefa, N. Coonts, Ö. Dag, M.J.MackLachlan, C. Yoshina-Ishii, G.A. Ozin, "New Nanocomposites: Putting Organic Function "Inside" the Channel Walls of Periodic Mesoporous Silica," Submitted to *Adv. Mater.*
- (36) J.S. Beck, C. Vartuli, W.J. Roth, M.E. Leonowicz, C.T. Kresge, D.H. Olson, E.W.Sheppard, J.B. Higgins, J.L. Schlenker, "New Family of Mesoporous Molecular Sieves Prepared with Liquid Crystal Templates," *J. Am. Chem. Soc.*, vol.114, pp. 10834-10843, 1992.
- (37) N.K. Raman, M.T. Anderson, C.J. Brinker, "Template-Based Approaches to the Preparation of Amorphous Nanoporous Silicas," *Chem. Mater.*, vol. 8, pp. 1682-1701, 1996.

- (38) C.Y. Chen, H.Y. Li, M.E. Davis, "Studies on Mesoporous Materials II. Synthesis Mechanism of MCM-41," *Microporous. Mater.*, vol.2, pp. 27-34, 1993.
- (39) A. Steel, S.W. Carr, M.W. Anderson, "<sup>14</sup>N NMR Study of Surfactant Mesophases in the Synthesis of Mesoporous Silicates," *J. Chem. Soc., Chem. Commun.*, pp. 1571-1572, 1994.
- (40) A. Monnier, F. Shuth, Q. Huo, D. Kumar, D. Margolese, R.S. Maxwell, G.D. Stucky, M. Krishnamurty, P. Petroff, A. Firrouzi, M. Junicke, B.F. Chmelka, "Cooperative Formation of Inorganic-Organic Interfaces in the Synthesis of Silicate Mesostructures," *Science*, vol. 261, pp. 1299-1303, 1993.
- (41) A. Firrouzi, D. Kumar, L.M. Bull, T. Besier, P. Sieger, Q. Huo, S.A. Walker, J.A. Zasadzinski, C. Glinca, S. Nickol, D. Margolese, G.D. Stucky, B.F. Chmelka, "Cooperative Organization of Inorganic Surfactant and Biomimetic Assemblies," *Science*, vol. 267, pp. 1138-1143, 1995.
- (42) Q. Huo, D.I. Margolese, U. Ciesla, D.G. Demuth, P. Feng, P. Sieger, A. Firrouzi, B.F. Chmelka, G.D. Stucky, "Organization of Organic Molecules with Inorganic Molecular Species into Nanocomposite Biphase Arrays," *Chem. Mater.*, vol. 6, pp.1176-1191, 1994.
- (43) C.J. Brinker, I. Lu, A. Sellinger, H. Fan, "Evaporation-Induced Self-Assembly: Nanostructures made Easy," *Adv. Mater.*, vol. 11, pp. 579-585, 1999.
- (44) J.S. Beck, J.C. Vartuli, G.J. Kennedy, C.T. Kresge, W.J. Roth, S.E. Schramm, "Molecular or Supramolecular Templating: Depending the Role of Surfactant Chemistry in the Formation of Microporous and Mesoporous Molecular Sieves," *Chem. Mater.*, vol. 6, pp. 1816-1821, 1994.
- (45) R.G. Collings, M. Hird, *Introduction to Liquid Crystals. Chemistry and Physics*, Taylor&Francis Ltd. 1997.
- (46) D.F. Evans, H. Wennerström, *The Colloidal Domain*, Wiley-VCH, 1999.

- (47) P. Yang, D. Zhao, B.F. Chmelka, G.D. Stucky, "Triblock-Copolymer-Directed Synthesis of Large-Pore Mesoporous Silica Fibers," *Chem. Mater.*, vol.10, pp. 2033-2036, 1998.
- (48) Q. Huo, D.I. Margolese, U. Ciesla, P. Feng, T.E. Gier, P. Sieger, R. Leon, P.M. Petroff, F. Schuth, G.D. Stucky, "Generalized Synthesis of Periodic Surfactant/Inorganic Composite Materials," *Nature*, vol. 368, pp. 317-321, 1994.
- (49) D.M. Antonetti, J.V. Ying, "Synthesis and Characterization of Hexagonally Packed Mesoporous Tantalum Oxide Sieves," *Chem Mater.*, vol. 8, pp.874-881, 1996.
- (50) G.S. Attard, G.C. Glude, C.G. Golther, "Liquid Crystalline Phases as Templates for the Synthesis of Mesoporous Silica," *Nature*, vol. 378, pp. 366-368, 1995.
- (51) W. Zhang, T.R. Pauly, T.G. Pinnavaia, "Tailoring the Framework and Textural Mesopores of HMS Molecular Sieve through an Electrically Neutral ( $S^{0T^0}$ ) Assembly Pathway," *Chem Mater.*, vol 9, pp. 2491-2498, 1997.
- (52) S.A. Bagshav, E. Prouzet, T.G. Pinnavaia, "Templating of Mesoporous Molecular Sieves by Nonionic Polyethylene Oxide Surfactant," *Science*, vol. 269, pp. 1242-1244, 1995.
- (53) C. Boissiere, A. Larbort, E. Prouzet, "Synthesis of Mesoporous MSU-X Materials Using Inexpensive Silica Sources," *Chem. Mater.*, vol. 12, pp. 1937-1940, 2000.
- (54) E. Prouzet, F. Cot, G. Nabias, A. Larbort, P. Kooyman, T. Pinnavaia, "Assembly of Mesoporous Molecular Sieves Based on Nonionic Ethoxylated Sorbitan Esters as Structure Directors," *Chem. Mater.*, vol.11, pp. 1498-1503, 1999.
- (55) D.H. Gray, D.L. Gin, "Polymerizable Lyotropic Liquid Crystals Containing Transition Metal Ions as Building Blocks for Nanostructured Polymers and Composites," *Chem. Mater.*, vol. 10, pp.1827-1832, 1998.

- (56) H. Schmidt, "New Type of Noncrystalline Solides between Inorganic and Organic Materials," *J. Non-Cryst. Solids*, vol. 73, pp. 681-691, 1985.
- (57) H. Schmidt, G. Philipp, "New Materials for Contact Lenses Prepared from Si- and Ti-Alkoxides by the Sol-Gel Process," *J. Non-Cryst. Solids*, vol. 63, pp. 283-292, 1984.
- (58) G.L. Wilkes, H. Huang, R.H. Glaser, *Silicon-Based Polymer Science: A Comprehensive Resource*, Am. Chem. Soc.: Washington, DC, 1990.
- (59) J.E. Mark, C. Jiang, M.-Y. Tang, "Semultaneous Curing and Filling of Elastomers," *Macromoleules*, vol. 17, pp. 2613-2616, 1984.
- (60) J.E. Mark, *In Frontiers of Macromolecular Science*, Oxford, 1989.
- (61) M. Yoshida, P.N. Prasad, "Sol-Gel Processed  $\text{SiO}_2/\text{TiO}_2$ /Polyvinylpyrrolidone Composite Materials for Optical Waveguides," *Chem. Mater.*, vol. 8, pp. 235-241, 1996.
- (62) Y. Pong, H. Samoc, P.N. Prasad, "Thirol-Order Nonlinearity and Two-Photon-Induced Molecular Dynamics: Femtosecond Time-Resolved Transient Absorption, Kerr Gate, and Degenerate Four-Wave Mixing Studies in Poly(p-phenylene vinylene)/Sol-Gel Silica Film," *J. Chem. Phys.*, vol. 94, pp. 5282-5290, 1991
- (63) P. Mulvaney, "Surface Plasmon Spectroscopy of Nanosized Metal Particles," *Langmuir*, vol. 12, pp. 788-101, 1996.
- (64) H. Schmidt, H. Walter, "Organically Modified Ceramics and their Applications," *J. Non-Cryst. Solids*, vol. 121, pp. 428-435, 1990.
- (65) R.L. Ballard, S.J. Tuman, D.J. Foguelette, W. Siegmeler, M.D. Socek, "Affect of an Acid Catalyst on the Inorganic Domain of Inorganic-Organic Hybrid Materials," *Chem. Mater.*, vol. 11, pp. 726-735, 1999.

- (66) B. Dunn, J.I. Zink, "Probes of Pore Environment and Molecule-Matrix Interactions in Sol-Gel Materials," *Chem. Mater.*, vol. 9, pp. 1575-1586, 1997.
- (67) K.C. Chen, T. Tsuchiya, I.D. Makenzie, "Sol-Gel Processing of Silica," *J. Non-Cryst. Solids*, vol.21, pp. 227-237, 1986.
- (68) J.D. Mitchell, G.J.T. Tiddy, L. Waring, T. Bostock, M.P. McDonald, "Phase Behavior of the Polyethylene Surfactants with Water," *J. Chem. Soc., Faraday Trans.*, vol. 79, pp. 975-100, 1983.
- (69) P.A. Winson, "Binary and Multicomponent Solutions of Amphiphilic Compounds. Solubilization and Formation, Structure and Theoretical Significance of Liquid Crystalline Solutions," *Chem. Rev.*, vol. 68, pp. 1-40, 1968.
- (70) M.E. Fragala, G. Malandiro, O. Puglisi, "Synthesis, X-ray structure and characterization of Ag(hfa)Tetraglume [hfa-Hexafluoroacetylacetonate]: A Novel Adduct for the Fabrication of Metallic Silver Based Films via in Situ Self Reduction," *Cem. Mater., Communications*, vol. 12, pp. 290-293, 2000.
- (71) T. Sreekanth, M.J. Reddy, S. Subramanyam, U.V. Subba Rao, "Ion Conducting Polymer Electrolyte Films Based on (PEO+KNO<sub>3</sub>) System and its Application as an Electrochemical Cell," *Mater. Sci.&Eng.*, vol. 64, pp. 107-112, 1999.
- (72) T. Sreekanth, M.J. Reddy, S. Subramanyam, U.V. Subba Rao, "Ion-Conducting Polymer electrolyte Based on Poly(ethylene oxide) Complexed with NaNO<sub>3</sub> Salt-Application as an Electrochemical Cell," *J. Power Sources*, vol. 79, pp.105-110, 1999.
- (73) H. Schott, "Lyotropic Numbers of Anions from Cloud Point Changes of Nonionic Surfactants," *Coll. Surface*, vol.11, pp. 51-54, 1984.
- (74) H. Schott, "Effect of Inorganic Additives on Solution of Nonionic Surfactants. XV. Effect of Transition Metal Salt on the Cloud Point of Oxtoxynol 9 (TritonX-100)," *J. Coll. Interf. Sci.*, vol. 192, pp. 458-462, 1997.

- [75] C.J. Brinker, "Oriented Inorganic Films," *Curr. Opinion in Coll. & Interf. Sci.*, vol.3, pp. 166-173, 1998.
- [76] H. Yang, A. Kuperman, N. Coombs, S. Mamiche-Atara, G. Ozin, "Synthesis of Oriented Films of Mesoporous Silica on Mica," *Nature*, vol. 379, pp. 703-705, 1996.
- [77] H. Yang, N. Coombs, I. Sokolov, G. Ozin, "Free Standing and Oriented Mesoporous Silica Films Grown at the Air-Matter Interface," *Nature*, vol. 381, pp. 589-592, 1996.
- [78] Ö. Dag, A. Verma, G. Ozin, C. Kresge, "Salted Mesostructures: Salt Liquid Crystal Templating of Lithium Triflate-Oligo(ethylene oxide) Surfactant Mesoporous Silica Nanocomposite Films and Monolith," *J. Mater. Chem.*, vol. 9, pp. 1475-1482, 1999.
- [79] T. Pal, K. Sau, S.R. Jana, "Reversible Formation and Dissolution of Silver Nanoparticles in Aqueous Surfactant Media," *Langmuir*, vol. 13, pp. 1481-1485, 1997.
- [80] K. Moller, T. Bein, "Inclusion Chemistry in Periodic Mesoporous Hosts," *Chem. Mater.*, vol.10, pp. 2950-2963, 1998.
- [81] J.M. Baker, J.C. Dore, P.J. Behrens, "Nucleation of Ice in Confined Geometry," *Phys. Chem. B.*, vol. 101, pp. 6226-6229, 1997.
- [82] K. Marisige, H. Fujii, M. Uga, D. Kinukawa, "Capillary Crystal Point of Argon, Nitrogen, Oxygen, Ethylene, and Carbon Dioxide in MCM-41," *Langmuir*, vol. 13, pp. 3494-3498, 1997.
- [83] M. Yonemitsu, Y. Tanaka, M. Ivamoto, "Metal Ion-Planted MCM-41. 1. Planting of Mn (II) Ion into MCM-41 by Newly Developed Template Ion Exchange Method," *Chem. Mater.*, vol. 9, pp. 2679-2681, 1997.
- [84] S. Dai, Y. Shin, Y.Lu, M.C. Burleigh, J.S. Lin, G.E. Barnes, Z. Xue, "A New Methodology to Functionalize Surfaces of Ordered Mesoporous

Materials Based on Ion Exchange Reactions," *Adv. Mater.*, vol. 11, pp. 1226-1230, 1999.

- (85) R. Ryoo, J.M.Kim, C.H.Ko, C.H. Shin, "Disordered Molecular Sieve with Branched Mesoporous Channel Network," *J. Phys. Chem.*, vol. 100, pp. 17718-17721, 1996.
- (86) R. Leon, D. Margulese, G. Stucky, P.M. Petroff, "Nanocrystalline Ge Filaments in the Pores of Mesosilicate," *Phys. Rev. B: Condens. Matter*, vol. 50, pp. 2285-2288, 1995.
- (87) J. Chen, Q. Li, H. Ding, W. Pang, R. Xu, "Infrared Study on the Deydroxilation of C<sub>60</sub>-Loaded MCM-41," *Langmuir*, vol.13, pp.2050-2054, 1997.
- (88) H.L. Frisch, J.E. Mark, "Nanocomposites Prepared by Threading Polymer Chains through Zeolites, Mesoporous Silica or Silica Nanotubes," *Chem. Mater.*, vol. 8, pp.1735-1738, 1996.
- (89) C.G. Wu, T. Bein, "Conducting Carbon Wires in Ordered Nanometer-Sized Channels," *Science*, vol.264, pp. 1757-1758, 1994.
- (90) K. Moller, T. Bein, R.X. Fischer, "Synthesis of Ordered Mesoporous Methacrylate Hybride Systems: Hosts for Molecular Polymer Compositis," *Chem. Mater.*, vol. 11, pp. 665-673, 1999.
- (91) M.T. Janicke, C.C. Lundry, S.C. Christiansen, S. Birtalan, G.D. Stucky, B.F. Chmelka, "Low Silica MCM-41 Composites and Mesoporous Solids," *Chem. Mater.*, vol.11, pp. 1342-1351, 1999.
- (92) A. Sayari, "Catalysis by Crystalline Mesoporous Molecular Seives," *Chem. Mater.*, vol.8, pp. 1840-1852, 1996.
- (93) R.Q. Long, R.T. Yang, "In Situ FT-IR Study of Rh-Al-MCM-41 Catalyst for the Selective Catalytic Reduction of Nitric Oxide with Propylene in the Presence of Excess Oxygen," *J. Phys.Chem. B*, vol. 102, pp. 3840-3847, 1999.

- [94] A. Corma, "From Microporous to Mesoporous Molecular Sieve Materials and their Use in Catalysis," *Chem. Rev.*, vol.97, pp. 2373-2419, 1997.
- [95] D. Zhao, P. Yang, B.F. Chmelka, G.D. Stucky, "Multiphase Assemblies of Mesoporous-Microporous Membranes," *Chem. Mater.*, vol. 11, pp. 1174-1178, 1999.
- [96] Q. Huo, R. Leon, P. Petroff, G.D. Stucky, "Mesostructure Design with Gemini Surfactants: Supercage formation in Three-Dimensional Hexagonal Array," *Science*, vol. 268, pp. 1324-1326, 1995.
- [97] W. Cai, L. Zhang, "Synthesis and Structural and Optical Properties of Mesoporous Silica Containing Silver Nanoparticles," *J. Phys. Condens. Matter.*, vol. 9, pp. 7257-7267, 1997.
- [98] J.H. Fendler, "Self Assembled Nanostructured Materials," *Chem. Mater.*, vol. 8, pp. 1616-1624, 1996.
- [99] T. Ung, L.M. Liz-Marzan, P. Mulvaney, "Controlled Method for Silica Coating of Silver Colloids. Influence of Coating on the Rate of Chemical Reactions," *Langmuir*, vol. 14, pp. 3740-3748, 1998.
- [100] L.M. Lewis, "Chemical Catalysis by Colloids and Clusters," *Chem. Rev.*, vol. 93, pp. 2693-2730, 1993.
- [101] L-Z. Whang, J.L. Shi, W-H. Zhang, M-L. Ruan, J. Yu, D-S. Yang, "Self-organization of Ordered Silver Nanocrystal Arrays on Cubic Mesoporous Silica Surfaces," *J. Chem. Mater.*, vol. 11, pp. 3015-3017, 1999.
- [102] B.A. Korgel, S. Fullam, S. Connolly, D. Fitzmaurice, "Assembly and Self-Organization of Silver Nanocrystal Superlattices: Ordered Soft Spheres," *J. Chem. Phys. B*, vol. 102, pp. 8379-8388, 1998.
- [103] A.L. Rogach, G.P. Shevchenko, Z.M. Afanas'eva, V.V. Sviridov, "Changes in the Morphology and Optical Absorption of Colloidal Silver Reduced with Formic Acid in the Polymer Matrix under UV Irradiation," *J. Phys. Chem. B*, vol. 101, pp. 8129-8132, 1997.

- (104) W.P. Halperin, "Quantum Size Effects in Metal Particles," *Rev Mod. Phys.*, vol. 58, pp. 533-606, 1986.
- (105) G. Schmidt, H. Harms, J.-O. Malm, J. vanRuitenbeck, H.V. Zandbergen, W.T. Fu, "Ligand Stabilized Giant Palladium Clusters: Promising Candidates in Heterogeneous Catalysis," *J. Am. Chem. Soc.*, vol. 115, pp. 2046-2048, 1993
- (106) M. Brust, M. Walker, D. Bethell, D.J. Schiffrin, R.G. Whyman, "Synthesis of Thiol-derivatised Gold Nanoparticles in a Two Phase Liquid-Liquid System," *J. Chem. Soc., Chem. Commun.*, pp. 801-804, 1994.
- (107) Y. Lin, R.J. Finke, "Novel Polyoxoanion- and  $\text{Bu}_4\text{N}^+$ -stabilized, Isolable, and Redissolvable, 20-30 Å  $\text{Ir}_{-300-800}$  Nanoclusters: The Kinetically Controlled Synthesis, Characterization and Mechanism of Formation of Organic Solvent-Soluble, Reproducible Size, and Reproducible Catalytic Activity Metal Nanoclusters," *J. Amer. Chem. Soc.*, vol. 116, pp. 8335-8353, 1994.
- (108) L. Qi, Y. Gao, J. Ma, "Synthesis of Ribbons of Silver Nanoparticles in Lamellar Liquid Crystals," *Coll. Surf. Sci.*, vol. 157, pp. 285-294, 1999.
- (109) L.M. Liz-Marzan, I. Lado-Taurino, "Reduction and Stabilization of Silver Nanoparticles in Ethanol by Nonionic Surfactants," *Langmuir*, vol. 12, pp. 3585-3589, 1996.
- (110) C.K. Yee, R. Jordan, A. Ulman, H. White, A. King, M. Rafeilovich, J. Sokolov, "Novel One-Phase Synthesis of Thiol-Functionalized Gold, Palladium and Iridium Nanoparticles Using Superhydride," *Langmuir*, vol. 15, pp. 3486- 3491, 1999.
- (111) Y.J. Nakao, "Preparation and Characterization of Nobel Metal Solid Sols in Poly(methyl methacrylate)," *J. Chem. Soc., Chem. Commun.*, pp. 826-828, 1993.
- (112) W. Cai, G. Wang, L. Zhang, "Reversible Transition between Transparency and Opacity for the Porous Silica Host Dispersed with Silver Nanometer Particles within its Pores," *J. Appl. Phys. Lett.*, vol. 69, pp.2980-2982, 1996.

- (113) C.R. Martin, "Membrane-Based Synthesis of Nanomaterials," *Chem. Mater.*, vol. 8, pp. 1534-1542, 1996.
- (114) W. Cai, H. Zhong, L. Zhong, "Optical Measurements of Oxidation Behavior of Silver Nanometer Nanoparticle within Pores of Silica Host," *J. Appl. Phys.*, vol. 83(3), pp. 1705-1710, 1998.
- (115) M. Shi, L. Zhang, W. Cai, "Composition Modulation of Optical Absorption in  $Ag_xAu_{1-x}$  Alloy Nanocrystals in situ Formed within Pores of Mesoporous Silica," *J. Appl. Phys.*, vol. 87, pp. 1572-1574, 2000.
- (116) N. Aihara, K. Torigoe, K. Esumi, "Preparation and Stabilization of Gold and Silver Nanoparticles in Layered Laponite Suspensions," *Langmuir*, vol. 14, pp. 4945-4949, 1998.
- (117) V.V. Hardicar, E. Matievich, "Coating of Nanosized Silver Particles with Silica," *J. Coll.&Inter. Sci.*, vol. 221, pp. 133-136, 2000.
- (118) J.P. Carpinter, C.M. Lukehart, S.B. Milne, D.O. Hendersoh, R. Mu, S.R. Stock, "Formation of Crystalline Nanoclusters of Ag, Cu, Pd, Pt, Re or Ru in a Silica Xerogel Matrix from Single Source Molecular Precursor," *Chem. Mater.*, vol. 9, pp. 3164-3170, 1997.
- (119) W. Wiecek, D. Raducha, A. Zalewska, J.R. Stevens, "Effect of Salt Concentration on the Conductivity of PEO-Based Composite Polymeric Electrolyts," *J. Phys. Chem. B*, vol. 102, pp. 1458-1465, 1998.
- (120) B. Scrosati, *Applications of Electroactive Polymers*, Chapman and Hall, London, 1993.
- (121) V.D. Noto, D. Longo, V. Münchow, "Ion-Oligomer Interactions in Polyethylene Glycol400/(LiCl)<sub>x</sub> Electrolyte Complexes," *J. Phys. Chem. B*, vol. 101, pp. 2636-2646, 1991.
- (122) Y. Nibu, T. Inoue, "Phase Behavior of Aqueous Mixtures of Some Polyethelene Glycol Decyl Ethers Revealed by DSC and FT-IR Measurements," *J. Coll. Interf. Sci.*, vol. 205, pp. 305-315, 1998.

- (123) Y. Nibu, T. Inoue, "Solid-Liquid Phase Behavior of Binary Mixture of Tetraethylene Glycol Decyl Ether and Water," *J. Coll. Interf. Scie.*, vol. 205, pp. 231-240, 1998.
- (124) K. Beyer, "Phase Structures, Water Binding and Molecular Dynamics in Liquid Crystalline and Frozen States of the System TritonX-100-D<sub>2</sub>O: A Deuteron and Carbon NMR Study," *J. Coll. Interf. Sci.*, vol. 86, pp. 73-89, 1982.
- (125) H. Matura, K. Fukuhara, K. Takashima, M. Sakokibara, "Conformational States of Nonionic Surfactants," *J. Phys. Chem.*, vol. 95, pp. 10800-10810, 1991.
- (126) N. Kimura, J. Umemura, S. Hayashi, "Polarized FT-IR Spectra of Water in the Middle Phase of Triton X100-Water System," *J. Coll.&Interf. Sci.*, vol. 182, pp. 356-364, 1996.
- (127) G. Göltner, S. Menke, M.S. Wiczenbergerr, M. Antonietti, "Mesoporous Silica from Lyotropic Liquid Crystal Polymer Templates," *Angew. Chem. Int. Ed.*, vol. 37, pp. 613-616, 1998.
- (128) M.A. Aramendia, V. Barau, C. Jimëniz, J.M. Marinas, F.G. Romero, "Supramolecular Templated Synthesis of Platinum-Supported Silica," *Chem. Com.*, vol. 6, pp. 1239-1240, 1999.
- (129) M.J. Kim, R. Ryoo, "Synthesis and Pore Size Control of Cubic Mesoporous Silica SBA-1," *Chem. Mater.*, vol. 11, pp. 487-491, 1999.
- (130) S. Kapoor, "Preparation, Characterization, and Surface Modification of Silver Particles," *Langmuir*, vol. 14, pp. 1021-1025, 1998.
- (131) A. Hengleim, "Physicochemical Properties of Small Metall Particles in Solution: Microelectrode Reactions, Chemisorption, Composite Metal Particles, and the Atom to Metal Transition," *J. Phys. Chem.*, vol. 97, pp. 5457-5471, 1993.

- (132) T.R. Jensen, M.L. Duval, K.L. Kelly, A.A. Lazarides, G.C. Schatz, R.P. Van Duyne, "Nanosphere Lithography: Effect of the External Dielectric Medium on the Surface Plasmon Resonance Spectrum of a Periodic Array of Silver Nanoparticles," *J. Phys. Chem. B*, vol. 103, pp. 9846-9853, 1999.
- (133) J.C. Hulteen, D.A. Triechel, M.T. Smith, M.L. Duval, T.R. Jensen, R.P. Van Duyne, "Nanosphere Lithography: Size-Tunable Silver Nanoparticle and Surface Cluster Arrays," *J. Phys. Chem. B*, vol. 103, pp. 3854-3863, 1999.
- (134) A. Taleb, C. Petit, P. Pileni, "Optical Properties of Self-Assembled 2D and 3D Superlattices of Silver Nanoparticles," *J. Phys. Chem. B*, vol. 102, pp. 2214-2220, 1998.
- (135) V. Patil, M. Sastry, "Formation of Closed Packed Silver Nanoparticle Multilayers from Electrostatically Grown Octodecylamine/Colloid Nanocomposite Precursors," *Langmuir*, vol. 16, pp. 2207-2212, 2000.
- (136) M.C. Morey, S. O'Brien, S. Schwarz, G.D. Stucky, "Hydrothermal and Postsynthesis Surface Modification of Cubic, MCM-48, and Ultralarge Pore SBA-15 Mesoporous Silica with Titanium," *Chem. Mater.*, vol.12, pp. 898-911, 2000.